ABSTRACT

ACOUSTICAL CHARACTERIZATION AND PARAMETER OPTIMIZATION OF POLYMERIC NOISE CONTROL MATERIALS

by
Emile N. Homsi

The sound transmission loss (STL) characteristics of polymer-based materials are considered. Analytical models that predict, characterize and optimize the STL of polymeric materials, with respect to physical parameters that affect performance, are developed for single layer panel configuration and adapted for layered panel construction with homogenous core. An optimum set of material parameters is selected and translated into practical applications for validation.

Sound attenuating thermoplastic materials designed to be used as barrier systems in the automotive and consumer industries have certain acoustical characteristics that vary in function of the stiffness and density of the selected material. The validity and applicability of existing theory is explored, and since STL is influenced by factors such as the surface mass density of the panel's material, a method is modified to improve STL performance and optimize load-bearing attributes. An experimentally derived function is applied to the model for better correlation. In-phase and out-of-phase motion of top and bottom layers are considered. It was found that the layered construction of the co-injection type would exhibit fused planes at the interface and move in-phase. The model for the single layer case is adapted to the layered case where it would behave as a single panel.

Primary physical parameters that affect STL are identified and manipulated. Theoretical analysis is linked to the resin's matrix attribute. High STL material with

representative characteristics is evaluated versus standard resins. It was found that high STL could be achieved by altering materials' matrix and by integrating design solution in the low frequency range.

A suggested numerical approach is described for STL evaluation of simple and complex geometries. In practice, validation on actual vehicle systems proved the adequacy of the acoustical characterization process.

ACOUSTICAL CHARACTERIZATION AND PARAMETER OPTIMIZATION OF POLYMERIC NOISE CONTROL MATERIALS

by
Emile N. Homsi

A Dissertation
Submitted to the Faculty of
New Jersey Institute of Technology
In Partial Fulfillment of the Requirements for the Degree of
Doctor of Philosophy in Mechanical Engineering

Department of Mechanical Engineering

January 2003

APPROVAL PAGE

ACOUSTICAL CHARACTERIZATION AND PARAMETER OPTIMIZATION OF POLYMERIC NOISE CONTROL MATERIALS

Emile N. Homsi

Dr. Nadine Aubry, Dissertation Advisor — Date
Distinguished Professor and Chair of Mechanical Engineering, NJIT

Dr. Pushpendra Singh, Committee Member — Date
Associate Professor of Mechanical Engineering, NJIT

Dr. Ernest Geskin, Committee Member — Date
Professor of Mechanical Engineering, NJIT

Dr. Chul Lee, Committee Member — Date
Application Development Engineering Manager, Honeywell Int.

Dr. Nanying Jia, Committee Member — Date
Principal Scientist, Honeywell Int.

BIOGRAPHICAL SKETCH

Author: Emile N. Homsi

Degree: Doctor of Philosophy

Date: December 2002

Undergraduate and Graduate Education:

- Doctor of Philosophy in Mechanical Engineering
  New Jersey Institute of Technology
  Newark, New Jersey, 2002

- Master of Science in Technology Management
  Stevens Institute of Technology
  Hoboken, New Jersey, 2001

- Master of Science in Mechanical Engineering
  Louisiana Sate University in New Orleans
  New Orleans, Louisiana, 1984

- Bachelor of Science in Mechanical Engineering
  University of Louisiana
  Lafayette, Louisiana, 1982

Major: Mechanical Engineering

Publications and Presentations:

E. Homsi, C. Lee, K. Hu, "Acoustic modeling and radiated noise prediction for plastic air –intake manifold", 2003 SAE Noise and Vibration Conference 12, number 1, 711-714, January 2003.

E. Homsi, "Acoustic characterization and optimization of sound transmission loss in polymer-based materials", Proceedings of the 2002 INCE, Dearborn, Michigan, Paper N418, August 2002.

E. Homsi, C. Lee, K. Hu, D. Moenssen, "A practical approach for computing air-intake manifold radiated noise", Proceedings of the 2002 LMS Conference for Physical and Virtual Prototyping, Troy, Michigan, June 2002.

Dedicated to Honeywell Plastics and to my beloved family

ACKNOWLEDGMENT

The author would like to express his sincere appreciation to his advisor, Dr. Nadine Aubry, for her commitment in enabling this successful collaborative research program with Honeywell International, and for her guidance and insight toward the fulfillment of all the requirements of the research. This work would have never been possible without her help and advice.

More specifically, many thanks to Dr. Ernest Geskin, Dr. Pushpendra Singh, Dr. Chul Lee and Dr. Nanying Jia for accepting and serving as members of the Dissertation Committee. The author would like to thank Dr. Peter Han and all of his colleagues at Honeywell Plastics, GM NVH Laboratories, Battenfeld Co-Injection Molding, Kolano and Saha Laboratories, Noise Unlimited Laboratories and Great Lakes Sound and Vibration Laboratories, for their support, cooperation and resource contributions during the critical phases of this study.

The author also would like to acknowledge and extend his appreciation to the management staff at Honeywell Plastics, especially Mark Minnichelli, for their continued financial support, help and encouragement throughout all phases of this process.

TABLE OF CONTENTS

TABLE OF CONTENTS
(Continued)

Chapter **Page**

LIST OF TABLES

LIST OF FIGURES

LIST OF FIGURES
(Continued)

LIST OF FIGURES
(Continued)

LIST OF FIGURES
(Continued)

LIST OF FIGURES
(Continued)

CHAPTER 1

INTRODUCTION

1.1 Overview

Numerous methods exist for the control of noise, vibration and harshness (NVH) within a certain environment. These can range from simple barrier and damping systems to more sophisticated electronic noise canceling techniques not covered in this study (see Figure 1.1). In some applications, these methods are implemented in combination. Absorptive techniques are typically utilized to prevent or reduce airborne acoustic energy from reaching a receiving site. Similarly, vibration-damping techniques are usually applied in close contact with the vibrating structure to prevent or reduce structure-borne energy from propagating to the protected area. Both techniques utilize internal damping for reducing sound energy levels. For lower frequency attenuation, absorptive materials are usually combined with a rigid material separated by a decoupling air space, which may increase the overall weight and thickness of the resulting sound attenuating structure. Another approach embodies the "mass law" [15], which states that the loss of energy as it transmits through an attenuating barrier is a function of the surface density of the barrier material and the frequency in question.

The main goal of this thesis is to describe a new approach for predicting STL, and to illustrate how analytical and numerical predictive techniques can be used as material property characterization tools, and to effectively understand their relationship and effect on sound transmission control when developing polymer-based materials with superior sound insulation characteristic. Optimal sound reduction or insulation can be achieved

with minimal weight penalty and adequate structural integrity. The focus of this study revolves around the optimum sound transmission criteria as it relates to the macroscopic physical parameters of polymer-based materials such as the thermoplastic Nylon 6. In many applications, the current interest is to improve the barrier properties of thermoplastic materials, especially those targeted for replacing the incumbent metal counterparts. In the context of this study, the increase in sound energy emission stems primarily from structural differences inherent of plastic materials when compared to metals. For corresponding practical applications, the passenger-vehicle manufacturing industry is the target field for validation studies.

In this case, the use of analytical and numerical techniques for acoustic characterization of plastics is tailored initially around the STL properties of finite homogenous and heterogeneous panels. These techniques can facilitate the simulation of an infinite plate behavior in predicting trends for a finite size plate. Results may be backward integrated into the chemical formulation stage of a material and linked to parameters at the microscopic level. Depending on the application, this approach can permit STL gain without the added weight, which has been a significant limitation to-date. The real life systems of interest are numerous and can be classified into open and closed systems. Here, open systems are related to barrier-type panels, and closed systems to enclosures. Overall, the study concentrates on the application and expansion of existing theories for predicting sound transmission loss, and employing the experimental "mass law" approach, which applies to relatively thin, homogenous, single layer panels, but modified for multi-layered panel systems. This experimental approach can be used to validate analytical STL parameter estimation for various heterogeneous systems. Based

on the findings from this study, it is shown that materials formulated from a set of characterized parameters can also be evaluated via measurements on actual closed systems, and thus optimized right from the onset of the conceptualization process.

1.2 Background

1.2.1 Prediction of STL

While the STL of single, double and multi-layered panels can be measured experimentally, it is often time consuming and costly to go through the process, since STL international testing standards require it be done in laboratories approved for such purpose [9], [10]. In a nutshell, STL is a measure of the ability of a structure to serve as a mechanism for acoustic isolation. As a guideline, good STL performance can be achieved using analytical predictive techniques. Typically, an STL-efficient panel would exhibit effective reflection of incident acoustical energy and sound energy dissipation through it with little or no transmission across. When the design of a certain component is finalized, STL can be used as one of the key parameters for material selection among candidate materials that meet the structural and acoustical requirements of that component. In order to select a material from a group of candidates, it is sufficient to understand the acoustical behavior of the material with respect to traveling sound waves, and to use analytical predictive techniques to characterize the STL capacity of the materials in consideration.

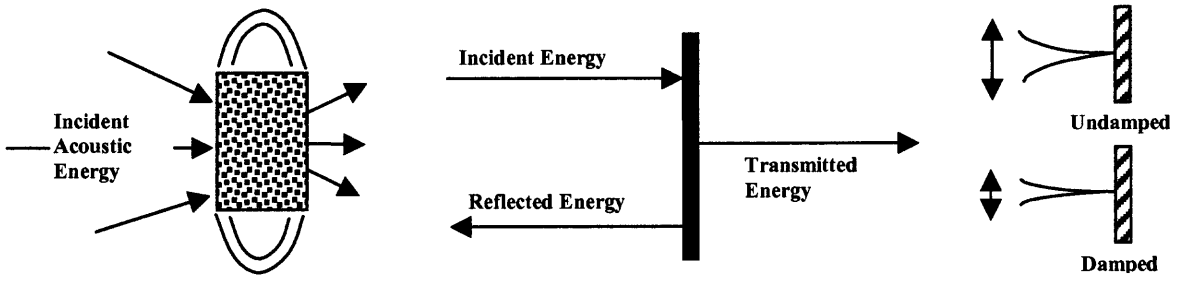

Figure 1.1 Absorption, transmission and damping are common methods of acoustic control often used in combination as one system package. Noise cancellation is not covered in this study.

1.2.2 Sound Reduction STL Prediction Models in Panels

In this section a general overview of the prediction models of sound transmission will be presented. The words "panels," "barriers" and "partitions" are used interchangeably throughout the text and each refers to the same. The STL and transmission loss (TL) are also used interchangeably to mean the same. STL is a laboratory measure of a barrier's ability to reduce the noise level resulting from passage through it, and does not include diffracted sound that bends around the top or ends of a freestanding barrier. A typical polymeric barrier is shown in Figure 1.2.

Cremer [1] presented the most referred to STL prediction model for thin infinite panels in 1942. In his theory, Cremer included the effect of bending stiffness and the sound incidence angle ϕ on STL. This model has been incorporated in several other models dealing with more complex structures; however, one important limitation was its non-applicability to finite panels. According to Guy (1981) [17], the limitation of Cremer's model was its lack of direct applicability to finite panels. Indeed, freely propagating flexural waves do not exist in finite panels, because their dimensions and boundary conditions define the wavenumbers of such panels. In general, the theory for infinite panels has been regarded as being capable of approximating the finite one, but it has been also a matter of concern what special features of finite panels influence the sound transmission characteristics.

The STL performance of a sound partition or panel can be predicted by several methods [11], such as mass law-Cremer model [1], mass law-Sharp-Cremer model [2], and Sewell-sharp-Cremer model [3]. STL is usually referred to as the single most important sound reduction measure, and is defined as ten times the log (to the base ten) of

the ratio of the sound power incident on one side of a partition, wall or a panel obstruction, to the sound power transmitted through the partition, wall or panel obstruction, to a space on the other side. The STL measured in the two-reverberation rooms is conveniently represented as a function of frequency in accordance with international standards [4], [9], [10]. The predicted STL of a sound insulation or sound reduction panel is calculated by the theoretical mass law equation $STL = 10\log_{10}\left[1+(\omega\rho_s/3.61\rho_0 c)^2\right]$, where $\rho_0 c$ is the characteristic impedance of air, ω and ρ_s are angular frequency and surface density of panel material, respectively [5]. The theoretical mass law can be rewritten in the familiar form, $STL \cong 20\log_{10} f\rho_s - 47.4$ for $\omega\rho_s >> 3.61\rho_0 c$ [6], where f is the frequency of the panel. This indicates that STL for a single panel increases with the thickness of the panel and frequency [8], [13]. However, STL decreases drastically at a given frequency, which coincides with the frequency of bending resonance. This is commonly referred to as the critical frequency. The concept of coincidence theory for a single panel can also be restated, as that the occurrence where the mechanical impedance of the panel equals the bending impedance [8]. The STL dip at coincidence frequency is a result of the bending resonance, and the resulting vibration radiates the acoustic wave in phase with the transmitted sound wave [1], [11], [12], [13]. The coincidence is also referred to in later text.

STL often disagrees with the prediction made by mass law and explicit prediction of STL is not possible because of the coincidence effect [5], [11], [14]. Many published results of STL lack close agreement in magnitude as well. This is affected by different measurement conditions, such as volumes of sound and receiving room, opening size, sample size, and room shape, etc. [14], and the customary assumption of incident energy

uniformity over all angles of incidence [14], [15], used to represent a perfectly diffuse field. It has also been usual to estimate forced vibration transmission by using the formula for an infinite partition and placing an empirical upper limit on the angles of incidence field in order to produce closer agreement with experiments [14], [15]. Sewel [3] derived a formula for forced vibration transmission that did not need the arbitrary assumption required with the infinite panel formula. His equation led to better agreement with experimental data than the mass law at low frequencies below half of the critical frequency, however, it was limited to specific panel mass densities exceeding 10 kg/m^2. To bridge the gap between the mass law prediction and the coincidence dip, Sharp suggested an empirical linear interpolation scheme that worked well only between the mass law and one half the coincidence frequency [2], [11]. Callister et al. [11] suggested a prediction scheme combining the three equations of Sewel, Sharp and Cremer, and devised a scheme for single layers. They claimed its usefulness for multi-layers, but no corresponding specific examples were given. A. D. Bruijn [23] used a modified spatial correlation function by introducing experimentally scaled coefficients to study the influence of diffusivity on STL through a single-leaf finite size panel. He was able to describe the diffusivity near the panel of a reverberant chamber and obtained excellent correlation with experiments in the mass law region, however, his model was not extended to layered panels [14]. In this case, the transmission coefficient for an unbounded flexible panel is derived by adopting a directional distribution of incident energy weighting function to better approximate the actual sound field impinging on panel fitted on a common wall to two reverberation chambers.

For double and multi-layered panels, several studies have dealt with such a construction including air cavities and sandwiched cores. Since the focus here is to adapt the formulation for single panels to layered plastic panels with fused interphase at the interface planes (co-injection processed panel types), only the relevant background is noted. Price and Crocker [16] used the statistical energy techniques for predicting the STL, but the technique is valid for frequency bands with fairly high modal densities, which inherently excludes low frequencies and/or small model consideration [17]. Disagreement between the measured and the predicted STL of a double wall with air cavity were inherent within the earlier work by London [18]. His model assumed the diffuse field and accounted for the effects of incident angle, however, it was restricted to double panels with empty cavities. He also introduced an empirically determined term into the panel impedance in order to achieve better agreement with measurements. Mulholland et al. [19] followed London's work and used a more physically meaningful term. They used the empirical limit angle approach and accounted for cavity absorption based on unrealistic values for the coefficients to obtain a good fit to the experiment. The cavity edge absorption corrections made later by Cummings and Mulholland [20] proved to be of limited use because of the high absorption value required for a good match. Guy [17] used the mode coupling between two rooms of common double wall to describe that the angle of incidence was related to the excitation term only, however, his model was applicable to small panels. Tillery et al. [59] showed that a significant increase of STL could be achieved by careful choice of a distributed coupling material within a double leaf construction. Their work, which was based on Fahy's [12] maximum pressure transmission ratio, was predominantly experimental and no clear link to the accuracy of a

model was presented. Several impedance formulations were developed and some were used to address coating materials in layer systems [21], [22], which present some relevance to the approach adapted in this study.

Many researchers have investigated the STL of single, double and triple panels (multi-layered) systems, and various analytical prediction formulations have been devised over the years, some of which have been described above. However, no serious attempts by practical users have been made to control the STL over the frequency range with respect to "real-life" noise control material applications. The analytical predictions of STL gained little focus as a potential tool to characterize the mechanical properties of injection and co-injection molded polymers for best acoustic control, starting at the formulation phase. In this work, an attempt is made to demonstrate the significance of such an analytical tool and its usefulness in tuning polymer-based material properties.

In this chapter a general overview on the motive of this study and on the background of STL prediction was presented for single and layered panels. While the concepts of STL for single and layered panels is quite related, there have been numerous and distinct models for both aspects throughout the literature [8], [11], [12], [14], [15], [63], etc. The main concern here is the application and expansion of existing models for predicting and measuring sound transmission. In Chapter 2, the theory behind a suggested STL prediction model is explored based on existing theories for mass law and coincidence effects. The formulation presented is limited to homogenous flat and thin panels. The random diffuse field approach, which is based on the uniform distribution of incident energy, is adopted, and a weighting function for the directional distribution of incident energy is employed in the calculation of the transmission coefficient. The

formulation is extended to the layered case, which represents a practical co-injection type layered construction with homogenous core. It is demonstrated that the basis of the model for the single case is adequate for the specific layered case, since the layers tend to behave as a single layered panel due to their fused regions at each layer's interface. Fahy's [12] suggested transmission coefficient for infinite, unbounded, and flexible panel is used as the baseline in the model. In Chapter 3, an analytically driven STL characterization approach is discussed. The focus is on presenting how the optimization and knowledge of important physical properties that directly affect the acoustical characteristics of a certain compound, such as stiffness and mass density, can be directly linked to a material's microstructure and microscopic properties, thus enabling the attainment of the end-use criteria. Selected sets of properties, which can induce high STL performance are identified and used to fabricate a polymeric material that is later used as the subject of validation studies. Chapter 4 gives a brief description of the computational boundary element approach as it relates to an integrated FEM-BEM analysis for structural acoustic characterizations. The indirect baffled BEM technique is reviewed and adopted by introducing acoustic transparency for quick evaluations of STL through finite size panels of different materials. Chapter 5 gives a highlight of some of the materials and experimental procedures employed throughout the study.

All measurement methods used in this study are standardized. The STL laboratory measurements were done using the sound reduction method as outlined in SAE J1400 [9]. Most measurements were done in third octave bands. The frequency range of interest for practical purposes was 100 to 5000 Hz. Field system measurements were done primarily using pressure or sound intensity methods. In Chapter 6, panels of

different thickness and parameter configurations are evaluated and it is confirmed that high STL performance materials can be analytically tuned using simple shape panels. More importantly, actual system validations on vehicle engine covers and the more complex geometries such as vehicle air intake manifold, exhibit a promising trend for progressive sound insulation against phenomena like noise transmission and noise radiation.

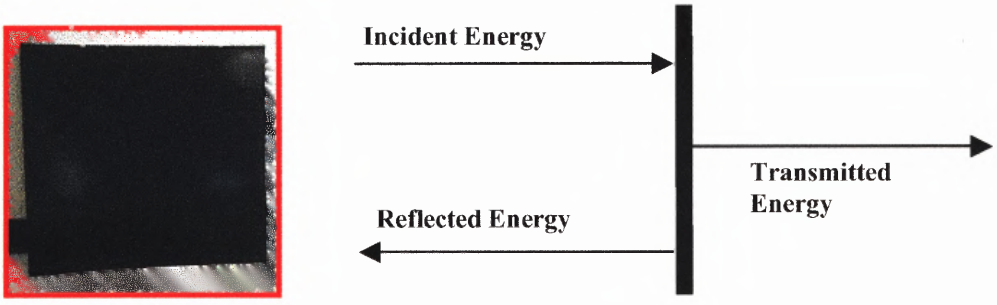

Figure 1.2 A typical panel barrier sheet (3mm thick) made by extruding thermoplastic resin.

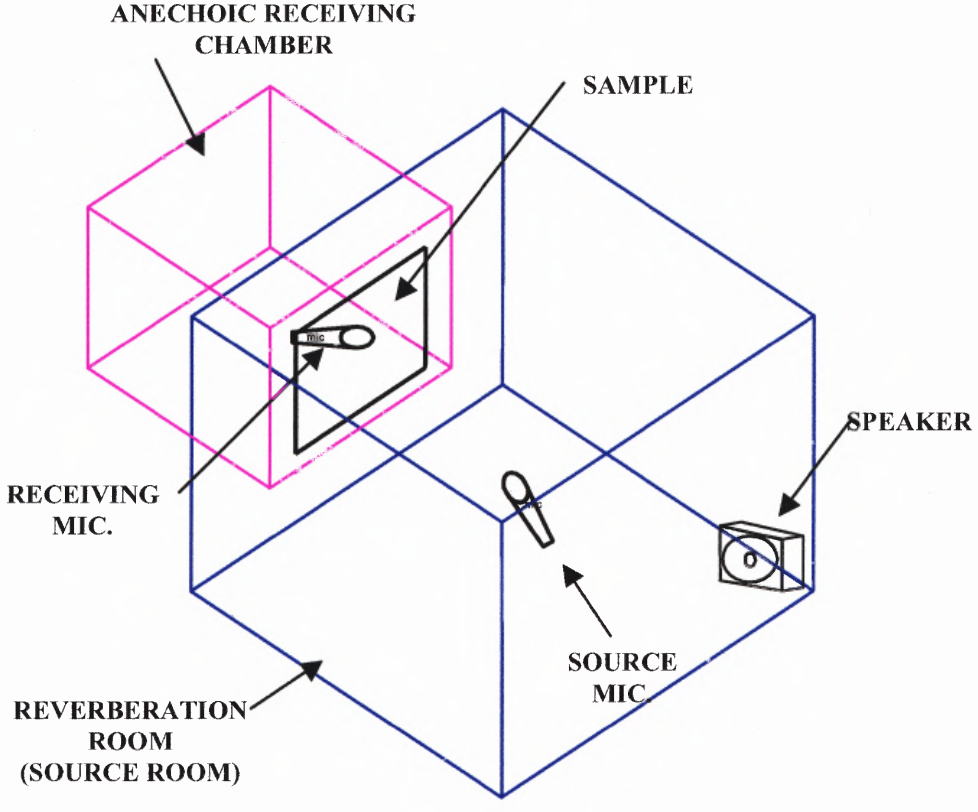

Figure 1.3 Typical reverberation/anechoic room set-ups for measuring STL of panels.

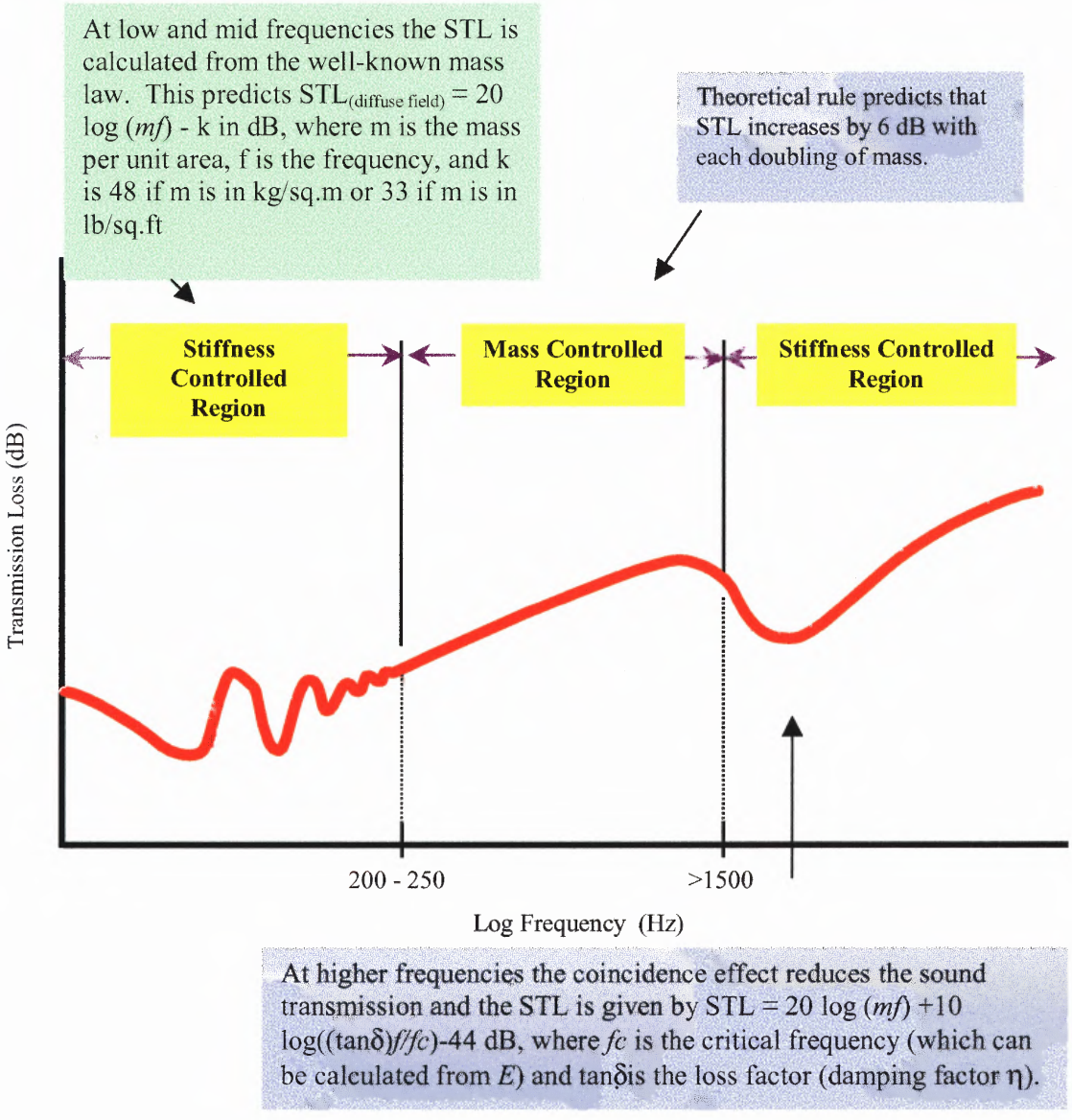

Figure 1.4 Typical STL curve over frequency. "Mass Law" is bounded by the low frequency resonance and the high frequency coincidence.

CHAPTER 2

THEORETICAL ACOUSTICAL CHARACTERIZATION OF NYLON BASED POLYMER IN SIMPLE FLAT SHAPE

2.1 Introduction

In general, the transmission loss increases by 6 dB for each octave increase in frequency and for each doubling of material mass. This gain in transmission loss is at the cost of added barrier weight. As a guideline, good STL performance can be achieved using analytical predictive techniques. STL gain can exceed that obtained using costly systems in various practical applications. It follows that an empirical technique to obtain predictive measures of STL for an infinite panel is described over the frequency range of interest. This method suggests good agreement with experiments [62]. A modified method is proposed and validated by good correlation with measurements conducted on finite size panels. Applied analytical models can be used to predict the physical acoustical parameters of an infinite single or multi-layered panel. Indeed, the behavior of noise control materials in simple shapes, such as flat panels, may be estimated using analytical methods without the use of conventional modeling associated with numerical techniques such as finite element and boundary element methods. Physical parameters can be varied to obtain the best characteristics that meet the target criteria. This allows the rapid evaluation of the acoustical performance since no modeling is required.

STL is measured using ASTM E90-90 (building partitions) [10], ISO140-III (building elements) [4], and SAE J1400 (automotive materials and assembly) [9], which

utilize a sealed opening fitted with the test panel, described in more detail in Chapter 5. The primary factors that control the sound transmission through single panels are:

- The surface mass density associated with forced vibration,
- The panel's bending stiffness which acts with the surface mass density to determine the critical frequency of the panel,
- The panel's physical dimensions, which act with bending stiffness and surface mass density to determine the lowest natural frequencies of the panel,
- The loss factor (damping factor), which controls the amplitude of resonance,
- The sound incidence angle, and
- Leaks (air paths through the barrier).

Critical frequency is denoted as the coincidence frequency of a single panel, and it occurs when the wavelength of sound in air and the bending wave of the panel coincide. This happens when the panel becomes fairly flexible and its STL performance is significantly diminished. At this point, the structural damping of the panel is an important factor affecting the extent of the sound transmission through it. Forced vibration is mainly the characteristic STL behavior below the critical frequency [60]. The region where this occurs is denoted as the mass-controlled region where the slope of the STL curve is 6 dB/octave.

Resonant vibration, on the other hand, is characteristic of the region at and above the critical frequency, which is denoted as the stiffness-controlled region where the slope of the STL curve is 9 dB/octave. In this region, STL values greater than mass law values are achievable when the panel is heavily damped. However, resonant vibration may

occur as well below the critical frequency, but the sound radiation efficiency is only significant at the lowest normal modes.

For single panels or partitions, previous work has shown that results of infinite theory possibly differ from those of the finite one [63]; however, this study shows that good agreement between the analytical prediction of STL for infinite panels and the experimental STL for finite panels can be achieved up to the critical frequency region, depending on the following factors: the analytical theory considered, the angle of incidence, and the experimental set-up. Thus, despite the fact that STL depends on the angle of incidence, perfect coincidence will only occur at the critical frequency, which is independent of the latter.

2.2 Formulation of The Transmission of Sound Through an Infinite Plate

The sound transmission loss through infinite panels has been studied extensively, and analytical predictions have commonly been based on the assumption of random sound incidence which was based in turn on a perfectly diffused sound field, with uniform incident energy at all incidence angles.

The actual sound field around a panel is better depicted by the filed incidence (diffuse-field) approach, which takes into account the directional distribution of incident energy, and which suggests truncating the angle of incidence up to a limit angle ϕ_{lim}. An empirically-determined limit angle of 78° for single panels was suggested by Beranek [15], who chose it to yield best agreement with measurements and laboratory settings. The sound field is thus, better modeled as a diffuse field. In general, the angle dependent transmission coefficient $\tau(\phi, f)$ is smallest at normal sound incidence and approaches

unity at grazing sound incidence. Cremer [1] applied the Paris equation to calculate the diffuse field transmission coefficient using $\tau(\phi, f)$.

$$\tau(f) = \frac{\int_0^{\phi_{\lim}} \tau(\phi, f)\cos\phi \sin\phi d\phi}{\int_0^{\phi_{\lim}} \cos\phi \sin\phi d\phi}$$

Here, $\phi_{\lim}$ is the maximum sound field incidence angle and commonly limited to approximately 78°...85°, and f is the frequency in Hz..

The average sound transmission coefficient $\tau(f)$ can be obtained by weighting the directional energy density $D(\xi)$ per unit solid angle Ψ, where θ and ϕ are the azimuth and cone angles, respectively (see Figure 2.2), in the direction of propagation as follows [14]:

$$\tau(f) = \frac{\iint \tau(f,\xi) D(\xi) \xi \cdot n d\Psi}{\iint D(\xi) \xi \cdot n d\Psi}$$

Here, ξ and n represent the unit directional and normal vectors incident on the wall of the panel under consideration, respectively. The directional energy density on a wall has usually been assumed to be independent of ξ for a perfectly diffuse field with equal probability of plane incident waves from all directions. In this case, D (ξ) is equal to $E/4\pi$, where E is the energy density [14]. Thus, the average transmission coefficient reduces to

$$\tau(f) = \frac{\int_0^{2\pi} \int_0^{\pi/2} \tau(f,\phi)\cos\phi \sin\phi d\phi d\theta}{\int_0^{2\pi} \int_0^{\pi/2} \cos\phi \sin\phi d\phi d\theta}$$

$$= \bar{\tau} = \frac{\int_0^{\phi_{lim}} \tau(f,\phi)\cos\phi \sin\phi d\phi}{\int_0^{\phi_{lim}} \cos\phi \sin\phi d\phi}$$

The diffuse field sound transmission loss is given by

$$STL_d = 10\log\frac{1}{\bar{\tau}} \quad \text{in dB} \tag{2.1}$$

Following the derivation of the equations of motion presented by Fahy [12], the expression for the sound power transmission coefficient through an unbounded, flexible partition is given by

$$\tau(f) = \frac{(\rho_o c/\pi f m)^2 \sec(\phi)^2}{[(\rho_o c/\pi f m)\sec(\phi) + (k/k_b)^4 \eta \sin(\phi)^4]^2 + [1-(k/k_b)^4 \sin(\phi)^4]^2} \tag{2.2}$$

where ρ_o is the density of air, c is the speed of sound in air, f is the frequency, m is the mass density of the partition material/unit-area, k is the wavenumber in air, k_b is wavenumber in the partition, η is the structural loss factor (damping factor), and ϕ is the angle of incidence as shown in Figure 2.1.

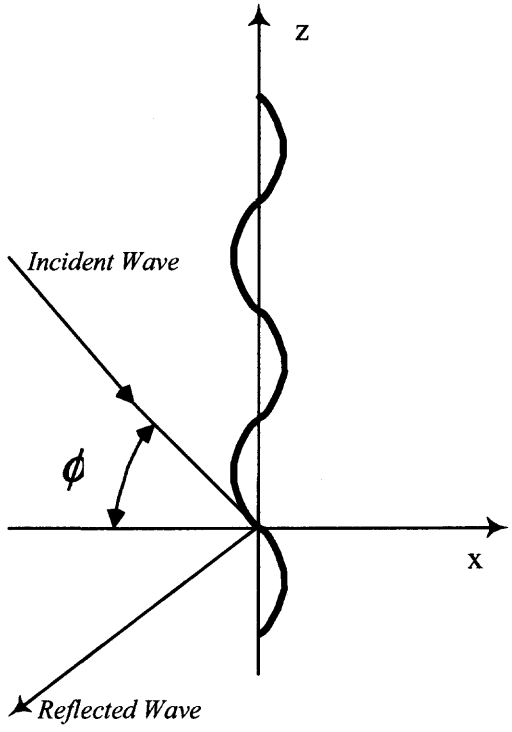

Figure 2.1 Transmission of obliquely incident sound through an unbounded flexible barrier [12].

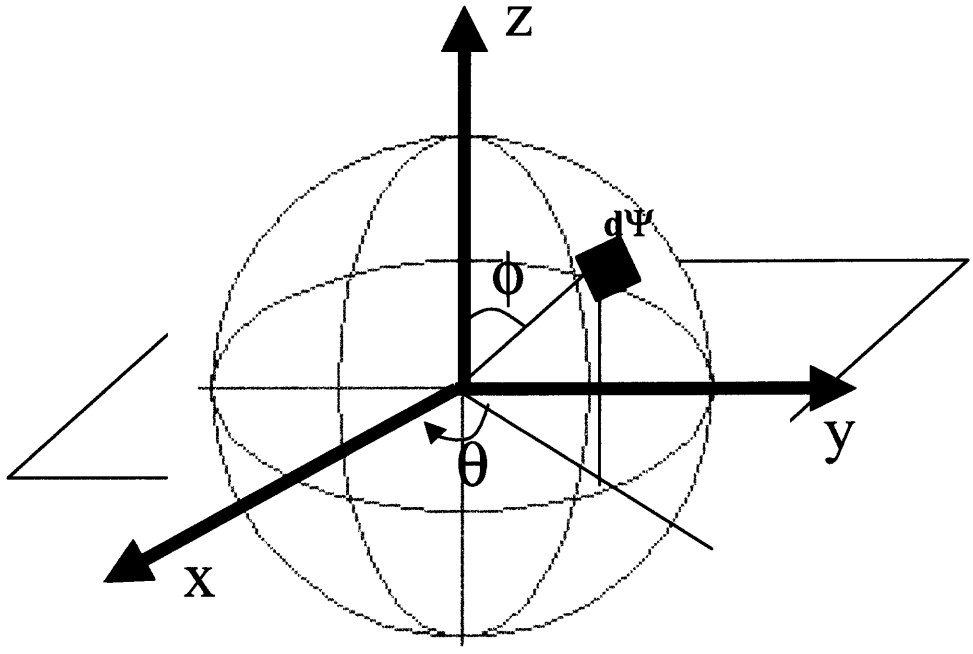

Figure 2.2 Description of angles in the formulation of the transmission coefficient (after ref. 14).

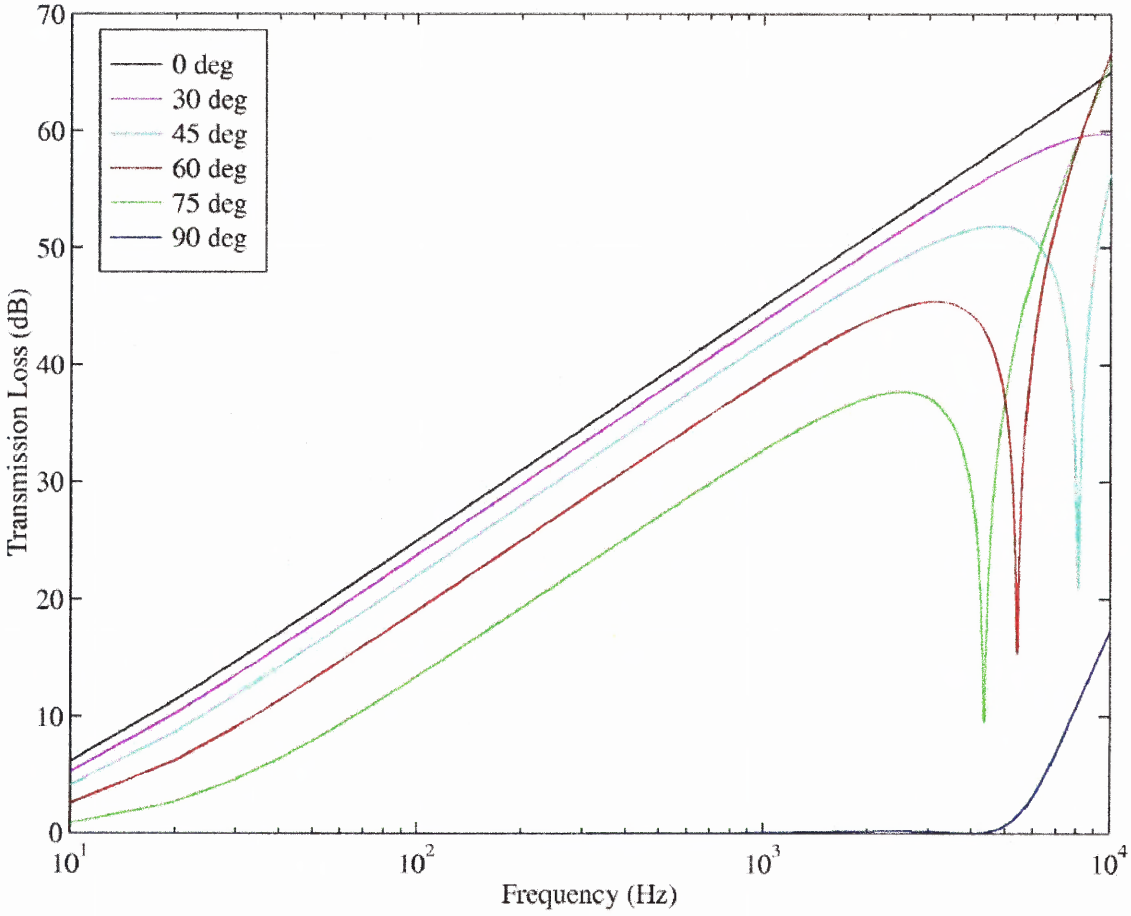

Figure 2.3 Variation of Transmission Loss with frequency for a single angle of incidence, ϕ= 0 to 90°

The STL of the panel is then calculated for each angle of incidence at each frequency of interest, up to a $\phi_{lim} = 90°$. The effect of the angle of incidence as a function of frequency is shown in Figure 2.3 above. The limit angle was chosen as such, since the transmission coefficient is considered to be weighted by the function that describes the directional distribution of incidence angle, and which was depicted to better represent a reverberation test chamber, where incident energy is actually not uniform over all incidence angles. The Gaussian weighting function is $\lambda(\phi) = e^{-\gamma\phi^2}$, where γ is a constant that varies between 1 and 2, and incorporates the effects of parameters such as the room shape and source position on directional distribution of energy (see Figure 2.2 for angles description) [14].

Based on this set of equations an analytical scheme was coded to evaluate the STL for any considered thermoplastic material using a γ=1.5 in the weighting function that is applied to the calculation of the transmission coefficient, and a ϕ_{lim} = 78° to improve correlation with measured data as shown later in chapter 6. The approach of the code was to evaluate Equation 2.2 for a given angle of incidence across frequency. The angle of incidence was incremented and the calculation of $\tau(f,\phi)$ was repeated across frequency. In this manner the following matrix of values for $\tau(f,\phi) = \tau(\phi,f)$ was created,

$$\begin{bmatrix} \tau(\phi_1, f_1) & \tau(\phi_1, f_2) & \tau(\phi_1, f_3) & \cdots & \tau(\phi_1, f_n) \\ \tau(\phi_2, f_1) & & & & \\ \tau(\phi_3, f_1) & & & & \vdots \\ \vdots & & & & \\ \tau(\phi_m, f_1) & & \cdots & & \tau(\phi_m, f_n) \end{bmatrix}$$

and the integration equation was then evaluated as,

$$\bar{\tau} = \frac{\sum \lambda(\phi)\tau(f,\phi)\sin(\phi)\cos(\phi)\Delta\phi}{\sum \sin(\phi)\cos(\phi)\Delta\phi}$$

which then led to the calculation of STL_d from Equation 2.1.

The general interest in the automotive industry is polymer noise materials that can displace the heavier metal counterparts, and that offer lower manufacturing cost advantage through the integration of sub-components [64], [65], etc. This is done, however, at the detriment of decreased acoustical performance primarily due to the wide differences in material properties that directly affect STL. Thus, it is customary to compare data obtained from polymer-based noise materials with data calculated using metal.

In order to validate the model, the calculated sound transmission loss of a constant thickness (3mm) plastic panel with constant specific gravity (1.38), was compared in shape to the published steel STL curve depicted in Figure 2.4, and to measurements from two different laboratories, including that was suggested in the SAE J1400 standard [9], and that was obtained from the theoretical model (see Figure 2.6). A good match between theory and experiment is readily observable throughout the frequency range, (the SAE J1400 calculations do not account for the critical frequency). The difference in the inter-laboratory testing data could be attributed to differences in laboratory structures, and in particular, to the test panel mounting and the design of aperture in the separation wall [39], [24]. In addition, in order to determine how the plastic panels' STL behave relative to metal, the STL of steel panel of the same thickness as several plastic panels, with various mechanical properties in consideration, was calculated as the baseline. The frequency range of interest for the materials is typically between 0 Hz and 1500 Hz,

however, the frequency range calculated was 0 Hz to 10000 Hz, so that the coincidence or critical frequency of the steel plate, described earlier (the large dip in the STL curve), would be shown. This provided a reference as to the frequency range, low or high, in which the selected plastic materials were responding relative to the steel panel. The material properties for comparison are given in Table 1.1 on page 28, and the STL composite graph for all materials is shown in Figure 2.5. The data confirms the decrease in the critical frequency with the increase in stiffness and mass.

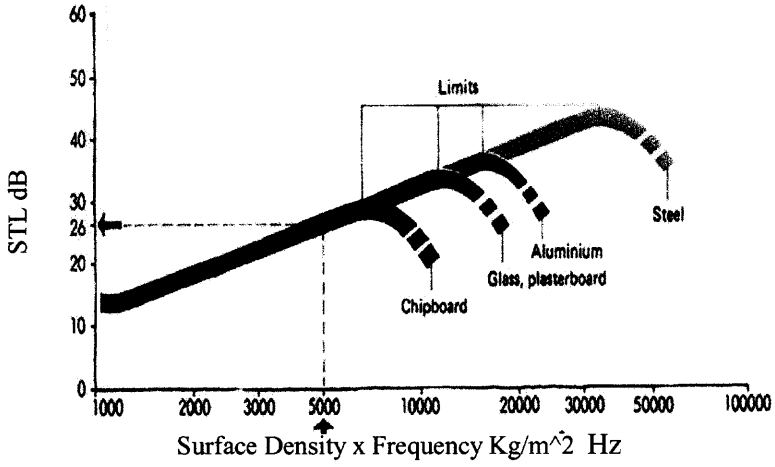

Figure 2.4 Sound transmission loss of single wall panels as a function of surface density (after ref. 72).

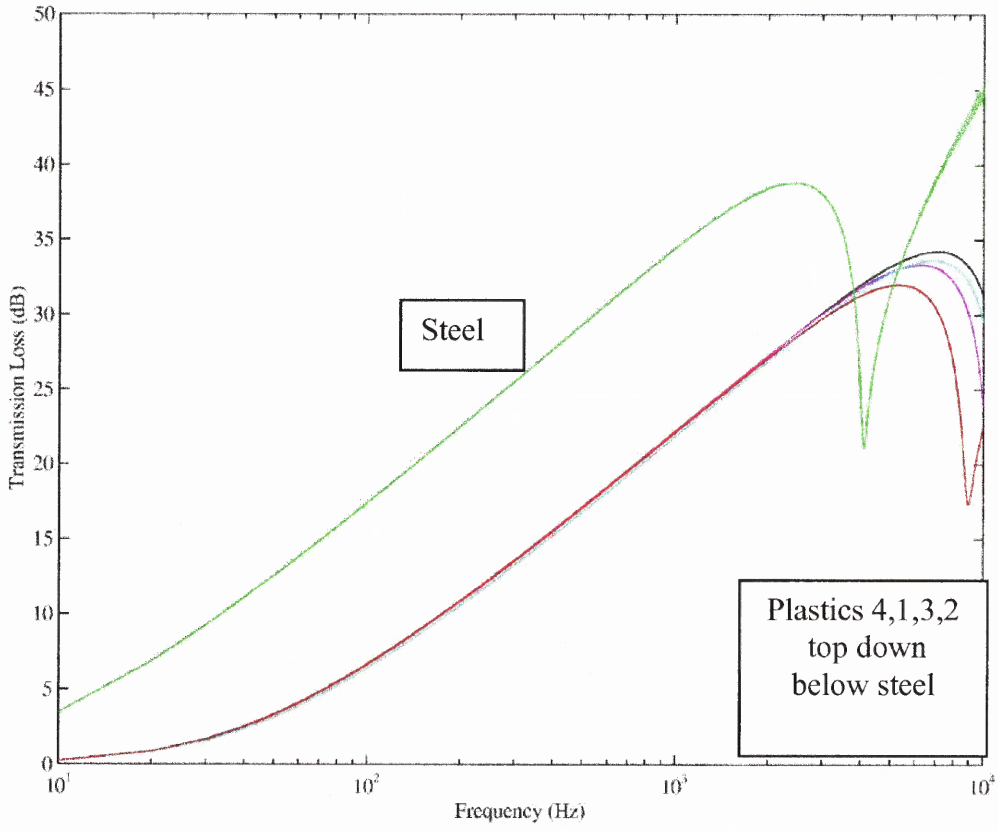

Figure 2.5 Composite Graph of four sets of physical parameters of plastic compounds analyzed for STL. Plastic materials and properties are listed in Table 1.1 on page 28.

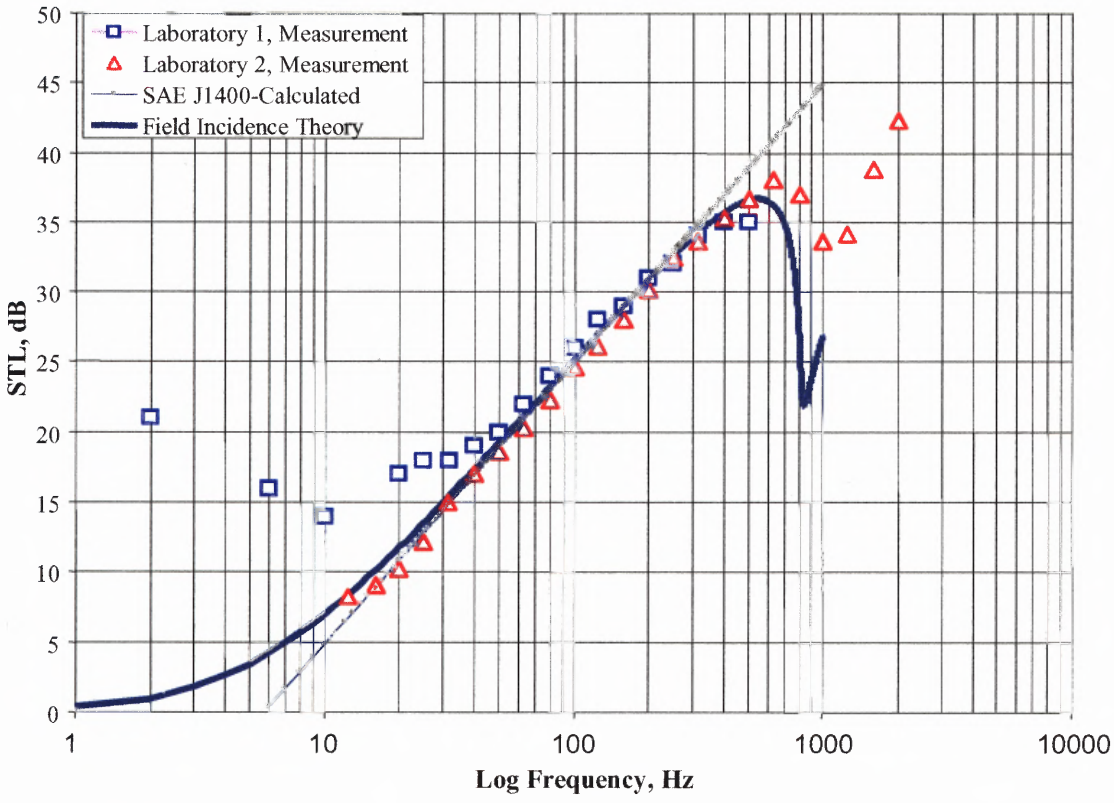

Figure 2.6 Variation of Transmission Loss measurements from inter-laboratory data are significant in the lower frequency range < mass law frequency. The field incidence theoretical prediction curve correlates well with lab2 data up to the critical frequency. Laboratory1: Noise Unlimited; Laboratory2: Kolano & Saha.

Table 1.1 Material Sample Properties used for STL Calculations.

Material	Density, ρ (ton/mm^3)	Young's Modulus, E (MPa)	Poisson's Ratio, ν	Loss Factor, η
STEEL	7.7e-09	19.5e04	0.30	0.01
PLASTIC 1 HPN9362	1.42e-09	4.414e03	0.35	0.01
PLASTIC 2 Capron®8267	1.48e-09	7.655e03	0.35	0.01
PLASTIC 3 Capron®8260	1.49e-09	5.517e03	0.35	0.01
PLASTIC 4 Minlon11C40	1.48e-09	5.240e03	0.35	0.01

2.3 Model Adaptation For Fused Layered Plates

It is of particular interest in this study to understand the effects of layered panels on the reduction of STL. It was previously highlighted that the mass-law theory is bounded in the lower frequency range by the resonance region. It is felt that a layered construction panel of a polymeric material fabricated by standard co-injection molding processes can provide the transmission reduction and stiffness criteria that will lead to reduce resonance effects. The analysis is limited to relatively thin (2mm to 5mm) panels that have identical homogenous materials in their face and bottom sheets, and homogenous core layers. Since sound waves would seek the path of least resistance, it would be suggested later to avoid core layers that exhibit voids or pores in order to realize a measurable STL advantage. The validity of the analysis for the layered case is confirmed by deducing the single layer case. In so far as the mathematical manipulation is concerned, the analysis for the elastic and viscoelastic cases will only differ with respect to the form of the Lamé constants λ and μ [57], [58], which are complex and frequency dependent in the latter case.

Motions in the core are described by the superposition of motions resulting from dilatational or irrotational and distortional plane traveling waves through the layers [66]. Since the physical treatment of this case is applied in nature, the problem in consideration, will be illustrated more clearly by following and restating the derivation steps suggested by Moore in reference [38], and making modifications and substitutions where appropriate. Motions in the face layers (which are considered to be of the same thickness h) are characterized by bending and extensional displacements. Shear deformations in the core layer are assumed negligible, and the core layer is assumed to be

rigid along the perpendicular plane. The normal bending displacements of the top and bottom layers are assumed identical (anti-symmetric mode of vibration). The neutral plane of bending is considered to occur in the middle of the core, and the extensional displacements to lie in the plane of the layers. An additional mode of vibration (symmetric mode), when the displacements of the top and bottom layers are out of phase, is assumed to exist and to promote the occurrence of coincidence effects. The expression for STL is obtained in terms of mechanical impedances of the layered panel construction for the symmetric and anti-symmetric modes of vibration. The formulation for the infinite case is adopted and modified to approximate the finite case in the calculation of the transmission coefficient, as presented in the previous section.

The geometry depicting the case of determining STL for a flexible layered panel of infinite extent is shown in Figure 2.7. The excitation is an impinging plane wave incident on the panel at an angle ϕ, with the normal to the plane of panels (the z axis) and the angle θ. The azimuth angle θ is defined as the angle that a vertical plane containing the z axis makes with the vertical plane defined by the x and z axes. The incident plane wave has a frequency ω in radians, and wavenumbers k_a, k_b, k_c, in the x, y, z directions, respectively. The wave numbers k_a, k_b, k_c and ω are related to the acoustic wavespeed c_o, as follows:

$$k_a^2 + k_b^2 + k_c^2 = \left(\frac{\omega}{c_o}\right)^2 \qquad \text{and}$$

$$k_a = k_o \sin\phi\cos\theta$$

$$k_b = k_o \sin\phi\sin\theta$$

$$k_c = k_o \cos\phi$$

$k_o = \omega / c_o$ is the wave number in the surrounding medium (air), c_0 is the speed of sound and ρ_0 is the density.

The layered panel responds to the incident wave by reflection and radiation simultaneously. The formulation follows the reflection case first, which simulates a rigid boundary condition with no top and bottom layer motion, then the radiation case is treated with assumed normal displacements such that

$$P_{reflected} = P_o e^{i(k_a x + k_b y + k_c (z-h) - \omega t)}$$

and

$$P_{incident} = P_o e^{i(k_a x + k_b y - k_c (z-h) - \omega t)}$$

represent a constant amplitude acoustic plane wave reflected upward in the +z direction, and incident in the –z direction respectively.

The sum of the incident plus reflected plane waves at the top layer (z = h) is equal to

$$2 p_o e^{i(k_a x + k_b y - \omega t)}$$

Applying the normal displacements, $\varpi_t = d_t e^{i(k_a x + k_b y - \omega t)}$ for the top layer and $\varpi_b = d_b e^{i(k_a x + k_b y - \omega t)}$ for the bottom layer will result in radiation (transmission) from the top and bottom layers according to the following:

$$P_{transmitted,top} = p_{r,t} e^{i(k_a x + k_b y + k_c (z-h) - \omega t)}$$

$$p_{transmitted,bottom} = p_{r,b} e^{i(k_a x + k_b y - k_c (z+T+h) - \omega t)}$$

where T is the thickness of the core, and the amplitudes $P_{r,t}$ and $P_{r,b}$ are complex constants determined from the acoustic boundary condition applied to the motions of the top and bottom layers. For small-amplitude motions, the momentum balance at the layers' surface boundaries, requires that the normal fluid's particle velocity $u = \dot{\varpi}$ be related to P through [15]:

$$\frac{\partial p}{\rho_0 \partial z} = -\frac{\partial u}{\partial t} = -\dot{u} = -\ddot{\varpi} = -\frac{\partial^2 \varpi}{\partial t^2}$$

thus,

$$\left.\frac{\partial p}{\partial z}\right|_{z=h} = -\rho_0 \frac{\partial^2 \varpi_t}{\partial t^2}$$

and (2.3)

$$\left.\frac{\partial p}{\partial z}\right|_{z=-(T+h)} = -\rho_0 \frac{\partial^2 \varpi_b}{\partial t^2}$$

respectively. Substituting the expressions for ϖ_t, ϖ_b and $P_{\text{transmitted, top}}$ and $P_{\text{transmitted, bottom}}$ into Equation 2.3 yields

$$p_{r,t} = -\frac{i\rho_o c_o \omega d_t}{\cos\phi}, \text{ and } p_{r,b} = \frac{i\rho_o c_o \omega d_b}{\cos\phi}$$

where $\rho_o c_o$ is the specific acoustic impedance of air and ρ_o is the density of air.

The sum of the incident and reflected waves can then be superimposed on the radiated waves and evaluated at the corresponding surfaces of the panel to fully describe the acoustic pressure field acting on the panel at steady state.

The angle dependent transmission coefficient, $\tau(\phi)$, is defined as the ratio of the transmitted acoustic intensity, I_{trans}, to the incident acoustic intensity, I_{inc}, as

$$\tau(\phi) = \frac{I_{trans}}{I_{inc}}$$

where (for harmonic plane waves) [73]:

$$I_{trans} = \frac{|p_{r,b}|^2}{2\rho_o c_o}, \quad and \quad I_{inc} = \frac{|p_0|^2}{2\rho_o c_o}$$

and the transmission coefficient in function of the incidence angle is given by [74] as:

$$\frac{1}{\tau(\phi)} = \left|\frac{p_0}{p_{r,b}}\right|^2 \tag{2.4}$$

In random incidence sound field (diffuse sound field), the sound intensity incident on a unit area of the panel from any angle, will be equal to the product of the incident intensity of the plane wave and the cosine angle of incidence. The total transmitted intensity is then $I_{trans}(\phi,\theta) = \int_{\psi} \tau(\phi,\theta) I_{inc} \cos\theta d\psi$ computed over a hemisphere of solid angle ψ, where $d\psi = \sin\phi d\phi d\theta$ and whose center is on the area of the panel. Using Equation 2.4, the expression of the transmitted intensity becomes $I_{trans}(\phi,\theta) = \iint I_{trans} \cos\theta \sin\phi d\phi d\theta$

In order to approximate experimental reverberant testing environment, the transmission coefficient is assumed to be independent of the azimuth angle. Thus, the common practice dictates using the upper limit on the cone angle, which can range from 78° to 85°, and the average transmitted acoustic intensity is computed as

$$\bar{I}_{trans} = \frac{\iint I_{trans}(\phi,\theta)\cos\theta\sin\phi d\phi d\theta}{\iint \cos\phi \sin\phi d\phi d\theta}$$

which leads to the average transmission coefficient $\bar{\tau}$ computed as

$$\bar{\tau} = \frac{\int_o^{\phi\ \lim} \tau(\phi)\cos\phi\sin\phi d\phi}{\int_o^{\phi\ \lim} \cos\phi\sin\phi d\phi} \tag{2.5}$$

As stated before, the sound transmission loss STL is defined with respect to the average transmission coefficient as follows

$$STL = 10\log_{10}(1/\bar{\tau})\text{dB} \tag{2.6}$$

The above procedure describes how to determine the STL in terms of the amplitudes of the incident and transmitted sound plane waves. The amplitude of the transmitted plane wave is determined by calculating the amplitude of the normal displacement of the bottom layer at z=-T. The normal displacements' amplitudes of the top and bottom face layers are determined from the prescribed pressure excitations on the faces as described previously. The normal displacements of the face layers are separated into symmetric and anti-symmetric components as follows (see Figure 2.8),

$$\varpi_{symmetric} = (\varpi_t - \varpi_b)/2$$

and

$$\varpi_{antisymmetric} = (\varpi_t + \varpi_b)/2 \tag{2.7}$$

The symmetric and anti-symmetric forces per unit area acting on the top and bottom face sheets are defined in a similar manner (see Figure 2.8). The symmetric and anti-symmetric normal displacements and forces per unit area *(F_0)* are in phase on the top face layer and 180° out of phase on the bottom layer. The symmetric and anti-symmetric impedances are thus, defined in terms of the amplitudes of the normal displacements and the forces per unit area as follows

$$Z_{sym} = \frac{F_{0,sym}}{v_{sym}}$$

for the symmetric mode and

$$Z_{asym} = \frac{F_{0,asym}}{v_{asym}}$$

for the anti-symmetric mode; where

$$v_{sym} = -i\omega d_{sym} \quad \text{and} \quad v_{asym} = -i\omega d_{asym} \tag{2.8}$$

and v_{sym} and v_{asym} are the amplitudes of normal velocities at the face layers for the symmetric and anti-symmetric modes.

Since the layered panel is considered to be symmetric in the z direction with respect to the neutral plane, the above separation into symmetric and anti-symmetric is valid for the case where the core layer is homogenous and the face layers are of the same material. Due to the separation into the symmetric and anti-symmetric motions, individual solutions to the problem may be obtained independently and linearly superimposed to obtain the complete solution.

The symmetric and anti-symmetric force per unit area amplitudes may be determined from the acoustic pressure (taking k_b as zero due to the azimuth angle independence assumption) is thus,

$$p_T e^{i(k_a x - \omega t)} = (2p_o + p_{r,t}) e^{i(k_a x - \omega t)} \tag{2.9}$$

and for the bottom face sheet as $p_B e^{i(k_a x - \omega t)} = p_{r,b} e^{i(k_a x - \omega t)}$, thus, the symmetric and anti-symmetric pressure amplitudes become

$$p_{sym} = \frac{p_T + p_B}{2} = p_o + \frac{p_{r,t} + p_{r,b}}{2}$$

(2.10)

$$p_{asym} = \frac{p_T - p_B}{2} = p_o + \frac{p_{r,t} - p_{r,b}}{2}$$

The pressures expressed in terms of the symmetric and anti-symmetric normal velocities of the face layers, are

$$p_{sym} = p_o + \frac{\rho_o c_o}{\cos\phi} v_{sym}$$

$$p_{asym} = p_o + \frac{\rho_o c_o}{\cos\phi} v_{asym} \tag{2.11}$$

Inserting the expressions for P_{sym} and P_{asym} into Equation 2.8, and taking into account that at the top face layer, a positive pressure is a negative force per unit area ($F_{o,sym}$ or $F_{o,asym}$), the following results occur:

$$\left(Z_{sym} + \frac{\rho_o c_o}{\cos\phi}\right) v_{sym} = -p_o,$$

$$\left(Z_{asym} + \frac{\rho_o c_o}{\cos\phi}\right) v_{asym} = -p_o$$

and the transmission coefficient in terms of impedances is

$$\tau(\phi) = \frac{|p_{r,b}|^2}{|p_o|^2} = \left| \frac{\frac{\rho_o c_o}{\cos\phi}\left(Z_{sym} - Z_{asym}\right)}{\left(z_{asym} + \frac{\rho_o c_o}{\cos\phi}\right)\left(z_{sym} + \frac{\rho_o c_o}{\cos\phi}\right)} \right|^2 \tag{2.12}$$

The expression for $\tau(\phi)$ includes radiation loading and the impedance of the acoustic half space defined by z < - (h+T). The *in vacuo* symmetric and anti-symmetric mode impedances Z_{sym} and Z_{asym} occur in series with the radiation loading impedance $\rho_o c_o / \cos\phi$. The total impedance for the panel is determined by the in-parallel addition

of the mode impedances including radiation. The impedance of the panel is defined with respect to the motion of the bottom face layer and incident pressure as

$$Z_p = \frac{\left(Z_{asym} + \frac{\rho_o c_o}{\cos\phi}\right)\left(Z_{sym} + \frac{\rho_o c_o}{\cos\phi}\right)}{\left(z_{asym} - z_{sym}\right)} = \frac{p_o}{-i\omega d_b}$$

The minus sign in the denominator results from the out of phase motion at the bottom layer.

From the latter expression, it can be deduced that a case may occur where there is no radiation from the bottom layer. Indeed, for a particular set of properties, incidence angle, and frequency, the response of the top layer to the incident wave is depicted by the symmetric and anti-symmetric components, which are in phase and have equal amplitudes. Thus, the transmission coefficient is zero (note that $k_a = \omega / c_o \sin\phi$), and no sound is transmitted. Since the impedances Z_{sym} and Z_{asym} are complex quantities, the normal displacements of the symmetric and anti-symmetric mode components at the bottom face sheet cancel out, and the absence of motion means that no radiation occurs. Also, if either Z_{sym} or $Z_{asym} = 0$, then the $\tau(\phi)$ assumes the following form

$$\tau(\phi) = \left| \frac{z_{sym}}{z_{sym} + \frac{\rho_o c_o}{\cos\phi}} \right|^2 = \left| 1 + \frac{Z_{sym}\cos\phi}{\rho_0 c_0} \right|^2 \qquad (2.13)$$

which is exactly the expression suggested by Beranek [15] for the case of normal incidence of a plane sound wave on an infinite single layer panel. This is the case when the faces of the panel vibrate in phase. This case is considered to approximate closely the practical case where the co-injected layers present fused interphased separation planes, and behave as a single plate. It has been a common practice that the sandwich

construction of double panels, for example, can be considered as a single panel whose bending stiffness is modified to combine the modulus and thickness of the facing panel and the interspace distance, in the evaluation of coincidence effects for some cases [8], [26], and by introducing an equivalent mass term in other cases [30]. If in addition, $|Z_{sym}| > \rho_o c_o / \cos\phi$ then $\tau(\phi) \cong 1$, which is a condition of high transmission. The condition where $Z_{asym} = 0$ above, means that in the absence of internal damping, a resonance condition exists for which normal displacements of frequency ω and wavenumber k_a propagate in the whole panel, unattenuated, and with phase velocity, ω/k_a. The model for the layered panel involves the input of two sets of material properties. The schematic diagram (see Figure 2.9) defines the multi-layer configuration, as produced using the co-injection molding process.

Based on the discussion above, the single layer analytical case is adjusted and adopted for the layered case, as it is well suited for the targeted practical applications where the frequency range of interest rarely exceeds coincidence. Therefore, when the thickness of the layers is defined, the skin thickness will be counted for twice since it occurs on both the top and bottom of the panel. The core layer is defined as a separate material or a version of the skin material. Inputting a percentage value of skin's density and thickness for the core material, then performing the calculation, realizes the latter.

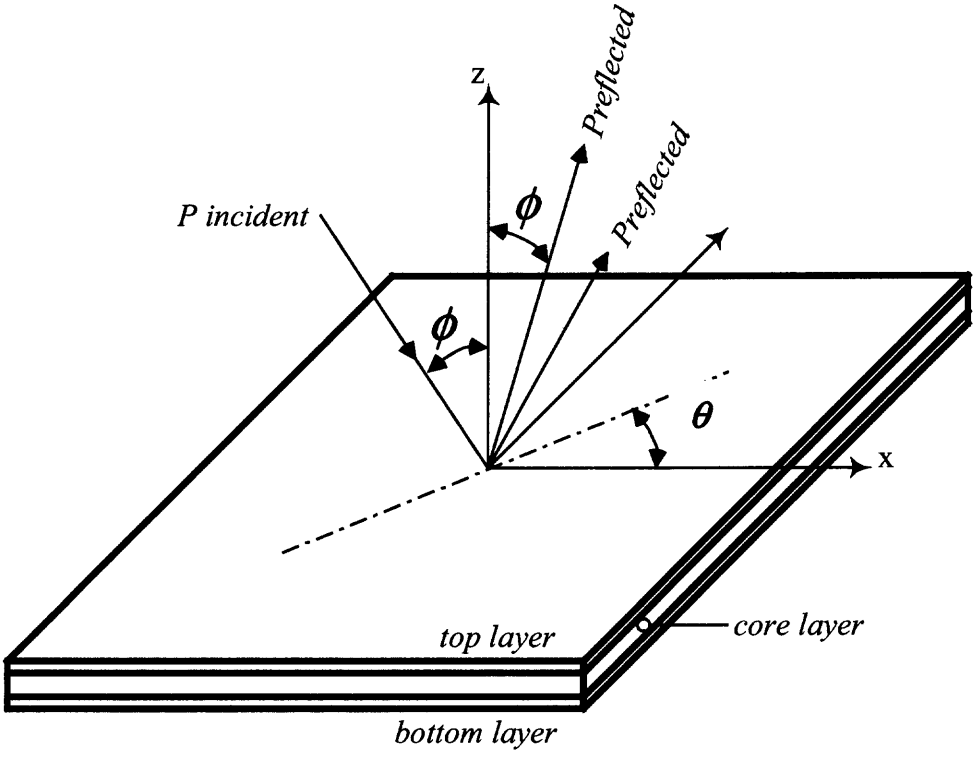

Figure 2.7 Geometry representation of layered panel STL problem. Incident oblique plane wave is impinging on top panel and reflected plane wave is traveling in +z (after ref. 38).

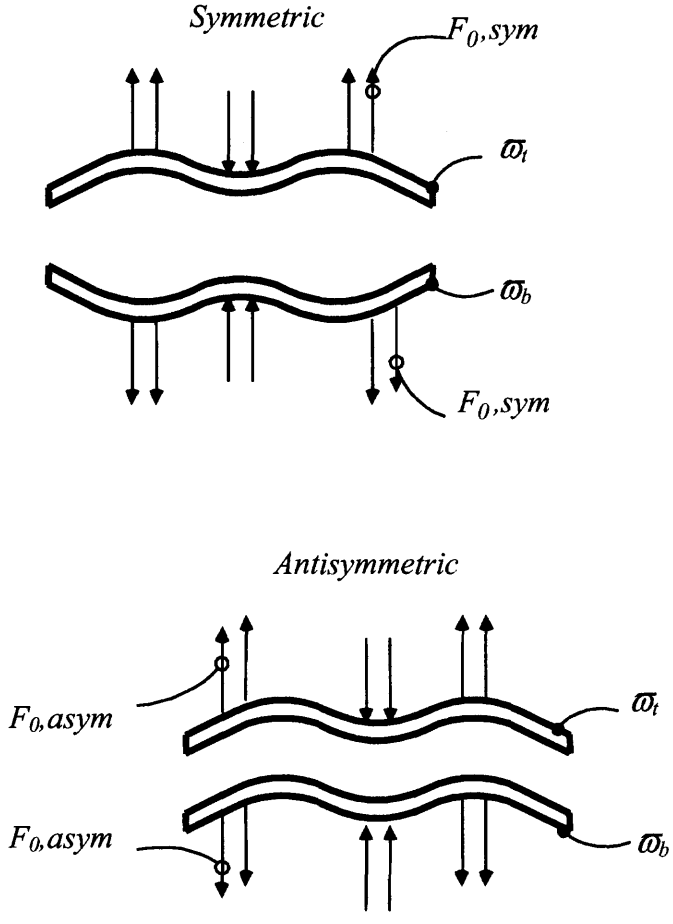

Figure 2.8 Schematic of symmetric and anti-symmetric motion of top and bottom layers (after ref. 38).

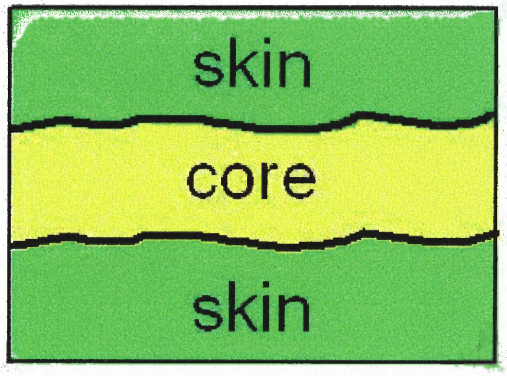

Figure 2.9 Schematic of layered panel cross section depicting a co-injected configuration with minute delamination at the interface planes.

2.4 Analytically Driven STL Determination

As mentioned previously, STL is a measure of the ability of a structure to serve as a mechanism for acoustic isolation. Since the focus here is materials for noise control in the vehicle environment, the calculation suggested in the SAE J1400 [9] standard (which is commonly adopted as the baseline in the automotive industry) was chosen as the matching baseline for analytical studies. It is worthy to mention, that this standard was derived from the original ASTM E90-90 [10] standard, and carries close similarities to the other mentioned industry standards, thus, evident that it can be applied to polymer-based material tuning in other industry applications.

A general modeling approach that compares the various wave incidence formulae (random, normal, and filed incidence) against the mass-law formula of the STL standard SAE J1400 is verified (see Figure 2.10), and confirms better matching to the field incidence theory, which was the basis for the model formulation section. In addition, the correlation function incorporated in the calculations of the transmission coefficient increases the model's potential usability to tune the structural characteristics that influence the STL performance of a polymer-based material.

Increasing the density of the material while maintaining the thickness constant, or vice versa, increases the surface mass and tends to shift the critical frequency down. This will reduce the effective range of application of the material. Previous studies have demonstrated that doubling the surface density of a panel will improve its STL performance by 6 dB [59], and that by doubling the surface density once more, the performance is improved by 12 dB. The negative effects to this improvement are the increase in weight and the undesirable decrease in critical frequency. In order to

establish a baseline for analytically tuning a polymer-based noise material in automotive applications, where aluminum is the usual incumbent baseline material, theoretical STL curves are compared to curves obtained with aluminum. The doubling of the wall thickness effect is shown in Figure 2.11 for the Aluminum panel alone. The curves clearly show the increase in performance due to the thickness effects.

In order to understand the specific gravity and density effects on STL performance, two variations in plastic panel properties (based on material filler content) are shown in Figure 2.12 (P1 with 15% glass fiber filler and 25% mineral filler, and P2 with 33% glass fiber filler, respectively) and compared to those of the Aluminum panel, while maintaining a constant panel thickness throughout (see Table 2.2, below for material properties).

Table 2.2 Mechanical properties of two standard products

	Specific Gravity	Modulus of Elasticity xe6 (psi)	Tensile Strength (psi)
Panel 1 Capron® 8233	1.38	1.3	29,000
Panel 2 Capron® 8267	1.48	1.1	20,000
Panel 3 XA2935	2.16	1.5	18,800

It is clear from the plots that absent a significant change in the specific gravity, and thus the mass density at constant panel thickness, the stiffness effects dominate as depicted by the performance represented by the aluminum curve. The issue was to determine in theory the effects of a significantly higher specific gravity (of such materials) on their sound transmission capacity, which is a positive advantage as shown in Figure 2.13.

For the multilayer case, the same materials listed in Table 2.2 were evaluated. Variations in the skin and core materials were considered using the standard material in the skin and the noise reduction material properties in the core in one case, and the standard material in both skin and core, in the other case. Initially, each layer thickness was considered to be equal to 3mm, however the skin layer's thickness was later doubled.

Analytical results from the second case showed an incremental improvement with the noise reduction material in the core. The positive effects of the mulltilayer construction on STL were also observed (see Figures 2.14a and 2.14b). However, upon selecting a core density equal to a small percentage of the skin's density (equivalent to co-injected foamed core construction with large voids), there was no noticeable advantage. In fact the corresponding STL curves were completely overlapped. This effect correlated well with experimental measurements highlighted later in Chapter 6. Variations in STL performance with respect to changes in materials and thickness attributes were in concert with the previous findings from the single layer case. Thus, to avoid redundancy, it was sufficient to extrapolate the STL improvements from the single layer case results. It was also concluded, that the layered case offered advantages in STL as long as voids or pores from processing could be avoided or minimized within the cores. This fact was later validated by experimental measurements (see Chapter 6).

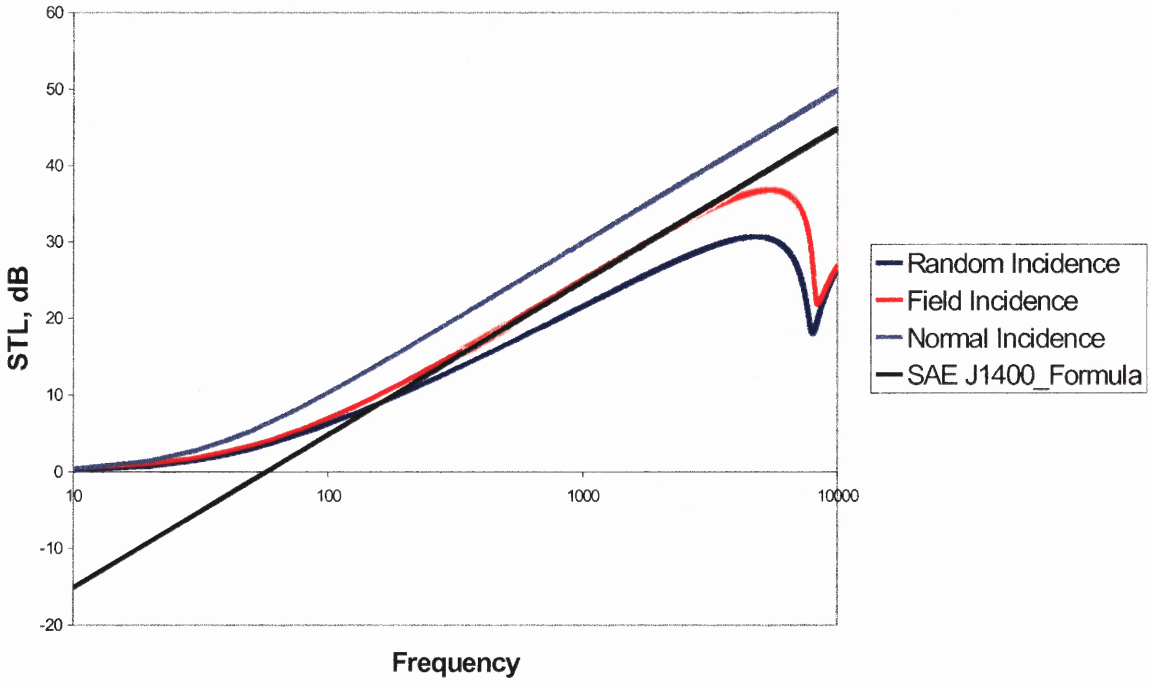

Figure 2.10 STL curves using various wave incidence concepts as compared to the SAE J1400 standard curve.

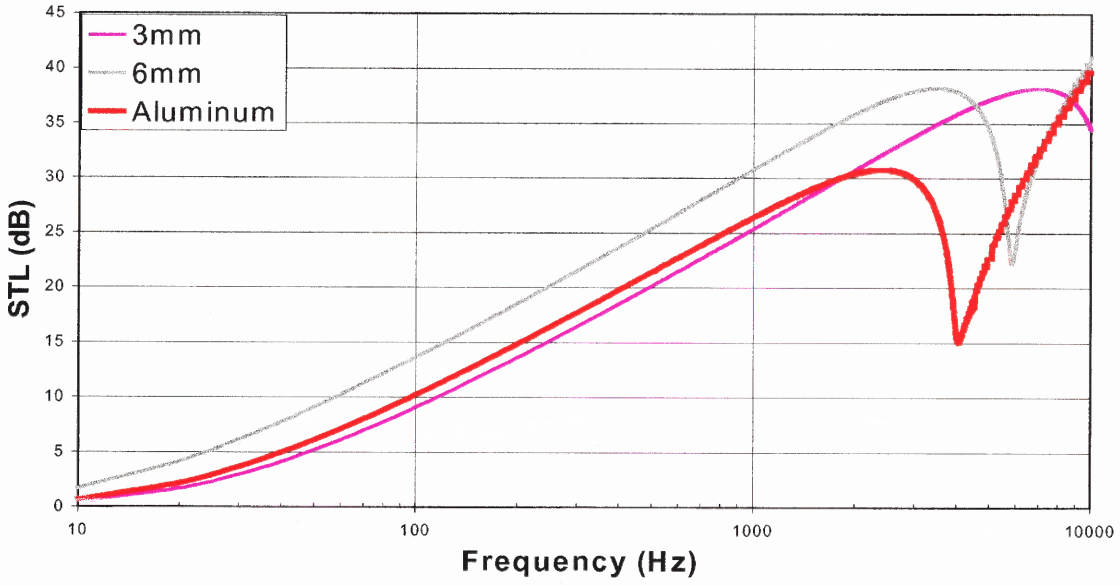

Figure 2.11 Composite graph of diffuse field STL (calculated) for noise material vs. metal. Thickness effect from 3mm to 6mm.

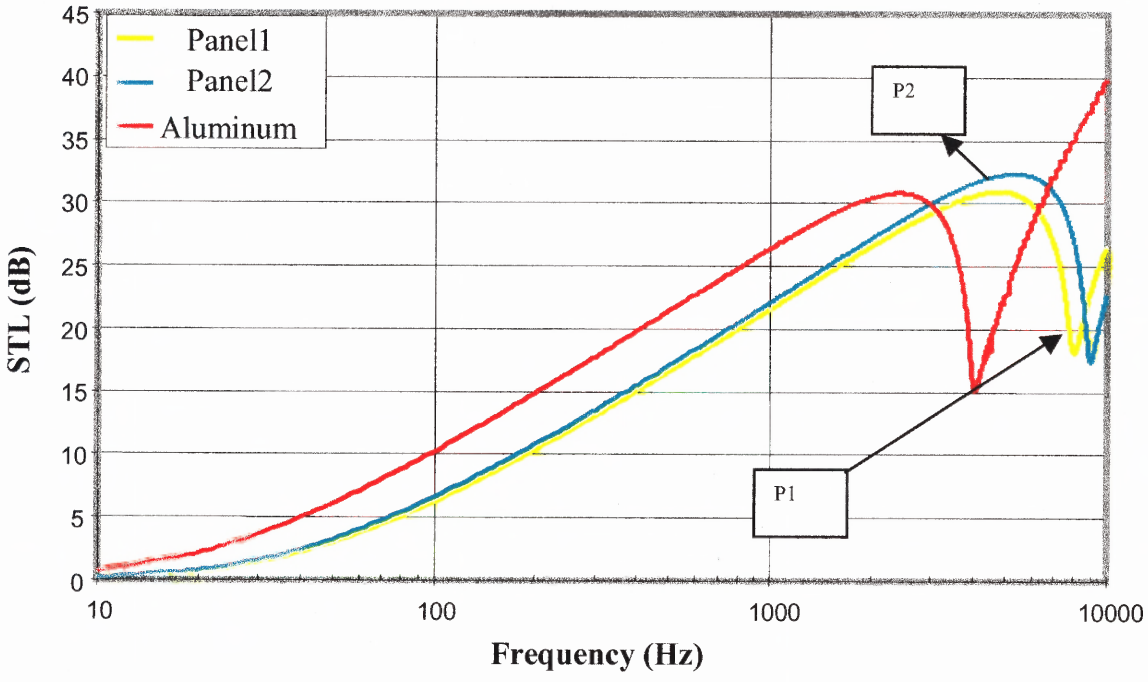

Figure 2.12 Diffuse STL (calculated) of standard 33% GF Nylon 6 and 15/25% GF/Mineral filled Nylon 6 vs. Metal. 3mm thick panels.

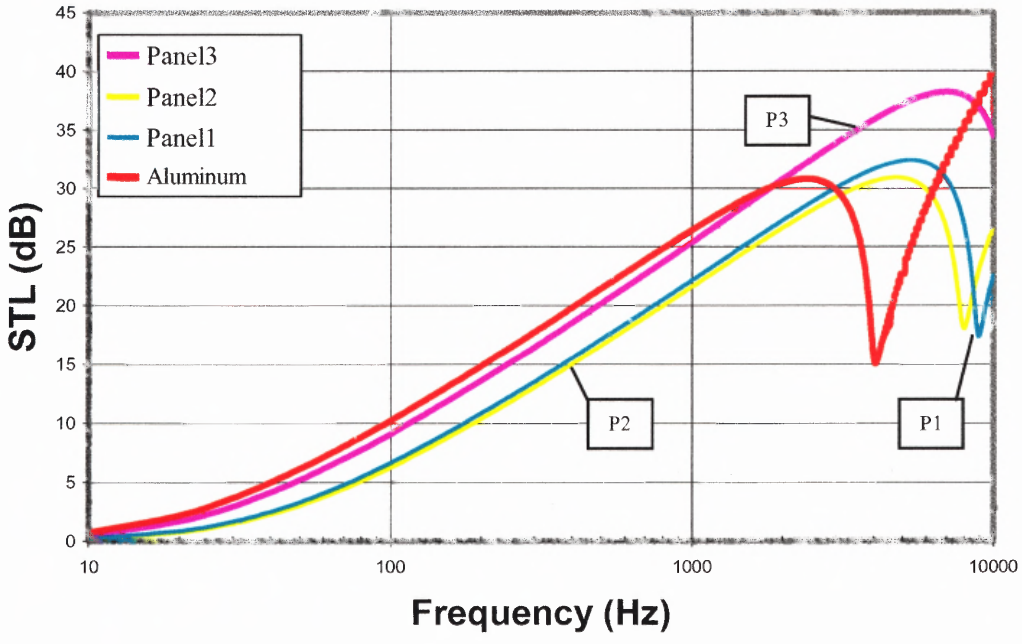

Figure 2.13 Diffuse STL (calculated) of 33% GF Nylon 6 and 15/25% GF/Mineral Nylon 6, and Noise reduction material vs. Metal baseline 3mm thick panels.

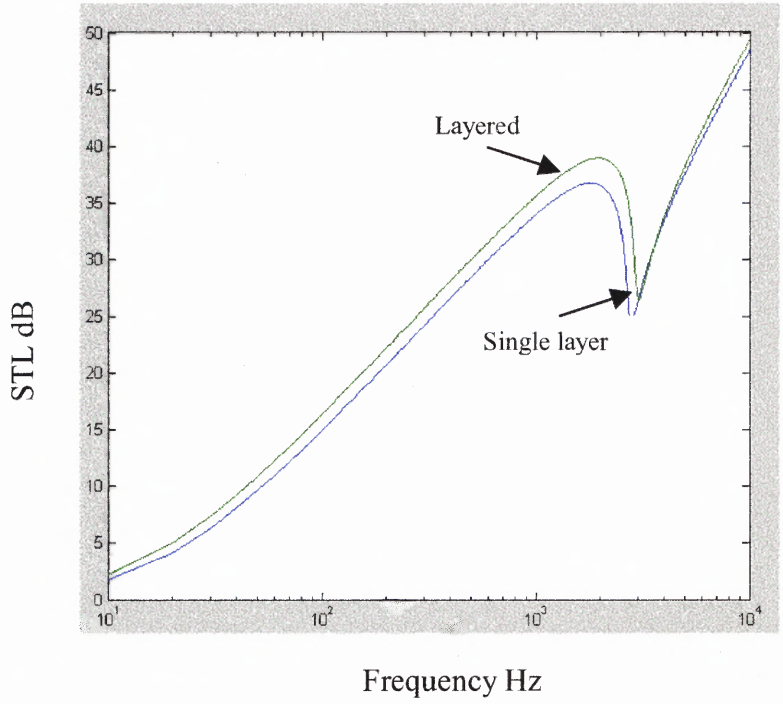

Figure 2.14a Diffuse STL in layered construction vs. single layer, same 3mm thickness. Material is all Capron 8233 (Table 2.2).

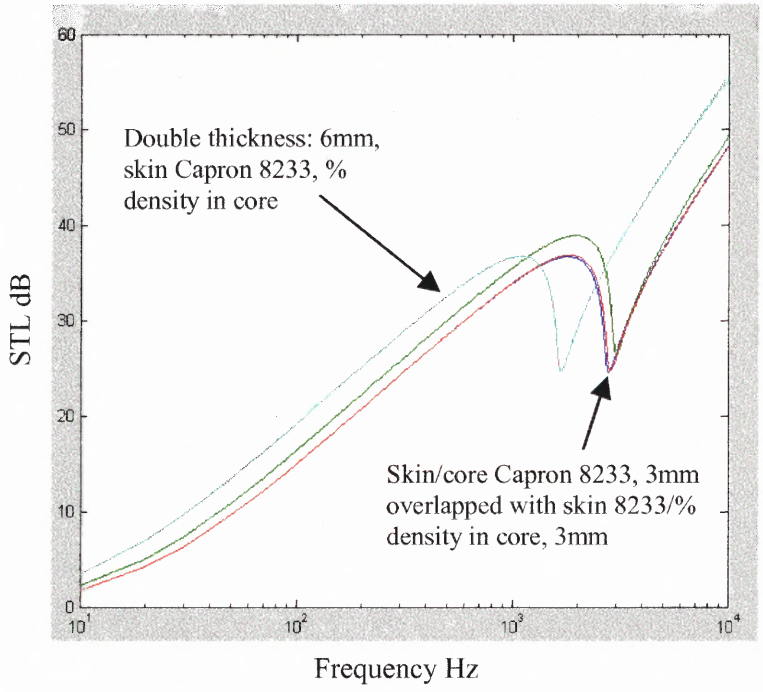

Figure 2.14b Diffuse STL in layered constructions. Repeatable behavior is observed with respect to thickness and material property variations as in single layers.

2.5 Summary

An analytical model to predict the sound transmission loss of a polymer-based panel has been explored and applied to the single layer configuration. The formulation was presented for the classical infinite dimension case and was modified to approximate the finite size geometry in a diffuse sound field medium. A correlation weighting function was applied in the calculation of the transmission coefficient for better approximation with measured data.

The sound transmission coefficient model for the layered case was formulated in terms of the impedance expressions for the specific configuration representing co-injected panels with fused inter-phase at the layers' interface planes. The impinging sound wave was assumed to cause bending and extension deformations in the top and bottom layers. For practical purposes, however, the core layer was assumed to be homogeneous with no shear deformation. The case for the co-injected panel was deduced to be a special case where the layers exhibit in-phase motion and behave as one plate. Parameter manipulations and attribute evaluations for high STL, obtained from the single layer case, were repeatable in trends for the special layered case. A percent adjustment in the core density with respect to the skin densities, along with mass and stiffness modifications, established the original model's usability for both configurations.

Analytically driven physical property determination for high STL revealed that critical macroscopic parameters could be linked to the resin matrix. By manipulating the primary factors affecting STL in the low and mid frequency range, and the secondary factors that can impact the high frequency range, an optimum set of properties could be backward integrated into the resin's formulation stage.

CHAPTER 3

MATERIAL TUNING FOR NVH CONTROL

3.1 Abstract

The control of noise and vibration in a wide range of applications inevitably requires the use of passive acoustical materials. As mentioned previously, there are three predominant methods to control noise, vibration and harshness (NVH). These include the panel/barrier, absorption, isolation and damping approach. Passive noise control materials are used in the latter applications/systems. For instance, barrier material systems are used in enclosures and walls; absorption materials are used as acoustical foams, fibrous blankets and acoustical tiles, and vibration isolators are used in equipment mounts and plastic or (rubber-based) bushings and grommets applications, and damping materials used as in plastic sheets and adhesive films.

In barrier and absorption systems the main mechanism of sound transmission is defined as airborne noise (noise propagating in the air). Isolation and damping deal with the aspects of structural vibrations, which can appear as airborne noise if either isolation or damping is lacking. In general, effective noise control can be achieved using a single or a combination of *both* barriers and absorbers for airborne noise, and *both* isolation and damping for structure-borne noise. It is worthy to note that a sound wave is an aspect of mechanical energy that follows the path of least resistance as it propagates away from the noise source. Thus, noise control is a process that interrupts the transmission path and transforms or eliminates that type of energy wherever possible.

3.2 Property Characterization For High STL Material

A sound panel usually acts as an acoustical reflector, interrupting the path of a sound wave, and may be a rigid structure, such as a concrete wall, or a limp sheet material such as a flexible noise curtain (see Figure 3.1). Noise reduction by a barrier is a function of primary and secondary physical parameters as stated before. The product of the specific gravity and thickness of a panel is the most important parameter; within a frequency range described as the "mass-law," and is typically referred to as the surface mass density. Thus, the weight per unit area is a good indicator of the sound attenuation capacity of a barrier. The modulus of elasticity, loss factor, and angle of incidence constitute the secondary parameters that affect the sound attenuation characteristics of a certain panel over the whole frequency range. Commonly, a lead sheet is considered the best choice for panel/barrier applications and is used as a calibrating tool when doing comparative STL measurement studies among different materials. Polymeric materials can be used as flexible panel/barriers to reduce noise in automotive engine and vehicle cabin compartments, and a wide range of other applications that encompass the appliance, off-road equipment, office space, marine and construction markets. They can also be fabricated into shielding enclosures for noisy machinery. One criteria for optimizing the performance of a barrier material lies in reducing the number and size of holes, gaps and other penetrations in the assembly to an absolute minimum, taking into account service accessibility and ventilation. In this case, the focus is on polymeric type panel/barriers, and more specifically, those that are made with Nylon 6 based materials.

One way to improve the STL performance of a polymer-based material without necessarily increasing the "mass," is to have a layered barrier construction achievable by

co-injection molding techniques. One distinct feature of such a construction is that the layers will exhibit fused interphase planes with small delamination characteristics. Due to their relatively small thickness (in real applications, the total thickness of such panels is usually less than 5mm), the construction can be considered to behave as a single panel with a modified bending stiffness [8]. Thus, a resin material can be tuned to offer the capacity of applying a flexible noise treatment in a single construction design.

The various factors to be taken into account in tuning the acoustical characteristics of a polymer-based material, are linked not only to the reduction in material's mass, but also to its structural stiffness and surface mass density. The density parameter directly affects the STL of the material (see Figures 3.2 and 3.3). Depending on the application, stiffness plays an important role in the materials' capacity to control sound. This is especially true in the low frequency range, where rigidity against structural-borne low frequency vibrations is paramount. Increasing the critical frequency can also expand the frequency range of usability. This can be accomplished by varying the material's stiffness attributes starting with damping, then modulus and specific gravity respectively. The higher the damping, the less potential for the coincidence dip (see Figure 3.4). It is, thus possible to raise the critical frequency by increasing the stiffness and damping, however, below the critical frequency, the density affects the STL in a positive way. Thus, adjusting material properties for better balance between damping and density, improves the STL performance (see Figure 3.5), and the overall stiffness can be controlled by design.

The previously described theoretical model was formulated in terms of "macroscopically" measurable physical properties of the panel and material. The

advantage of such an approach is that it enables the investigation of the influence of the directly measurable physical properties, so that an optimum variation in a particular set of physical parameters can be identified. These can result in a polymer-based material having a targeted optimal performance. It should also be noted that there is a direct link between the microscopic structure of a material and its macroscopic properties. User-friendly analytical models should provide the preliminary step in linking the microscopic properties of a material to its macroscopic properties [25]. The analysis example described in the latter, provides a clear direction on what to target with respect to damping and stiffness. Accordingly, various material compositions can be conceived to provide a bracket of properties for narrower evaluations.

3.3 Summary and Conclusion

It is concluded that in practice, an optimum noise control material can comprise at least one of Nylon 6, Nylon 6/6 and Nylon 6/66 (also referred to as Polyamides). The high specific gravity filler can comprise a mineral and/or metal filler, and more preferably at least one of barium sulfate and tungsten. The reinforcement fiber, if present, can comprise at least one of glass fibers, carbon fibers and steel fibers. Preferably, the polyamide is present in an amount of about 20 to about 45% weight, and the high specific gravity filler ranges from about 40 to about 70% weight. The reinforcement fiber may be present in amounts up to about 30% weight. One polyamide resin is found especially well suited for resin containing glass fibers and mineral filler. The mineral filler has a specific gravity in the range of 4–20, such as barium sulfate or tungsten. In the resin,

barium sulfate is present in an amount substantially equal to about 53% by weight, and the amount of the glass fiber reinforcement is substantially equal to about 15% by weight.

Optionally, in the lower frequency regions, noise can be reduced by shifting the local natural frequencies away from the input driving frequency domain, and adding lumped mass. The location and number of the distributed masses or blisters can be optimized based on the locus and amplitude of noise appointed for filtering out (see Figure 3.6). Such an arrangement of blisters increases the mass effect, and their locations are selected to increase noise transmission losses. Where feasible, and depending on the type of application considered, double layer panel construction, comprising an inner and outer layer of high STL polyamide resin, separated by air core cavity, may be employed. Preferably the air gap has a thickness ranging from 1 to about 25mm, and the polyamide resin layers contain glass fiber reinforcement and mineral filler. The mineral filler is barium sulfate, and is present from 40% to about 70% by weight of the polyamide resin composition (see Figure 3.7). The amount of the glass fiber reinforcement present ranges from about 0% to about 30% by weight of the composition. An alternate approach to noise reduction is to adopt layered constructions utilizing a high STL skin material, and a percentage of the skin thickness in the core.

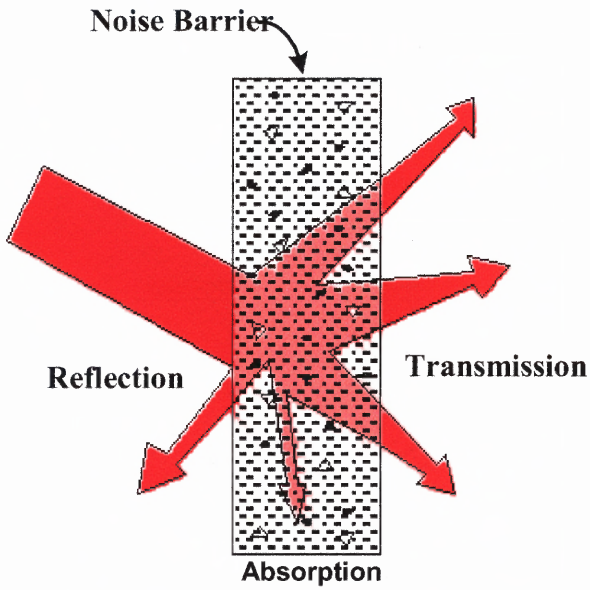

Figure 3.1 Typical barrier panel sound insulating characteristics.

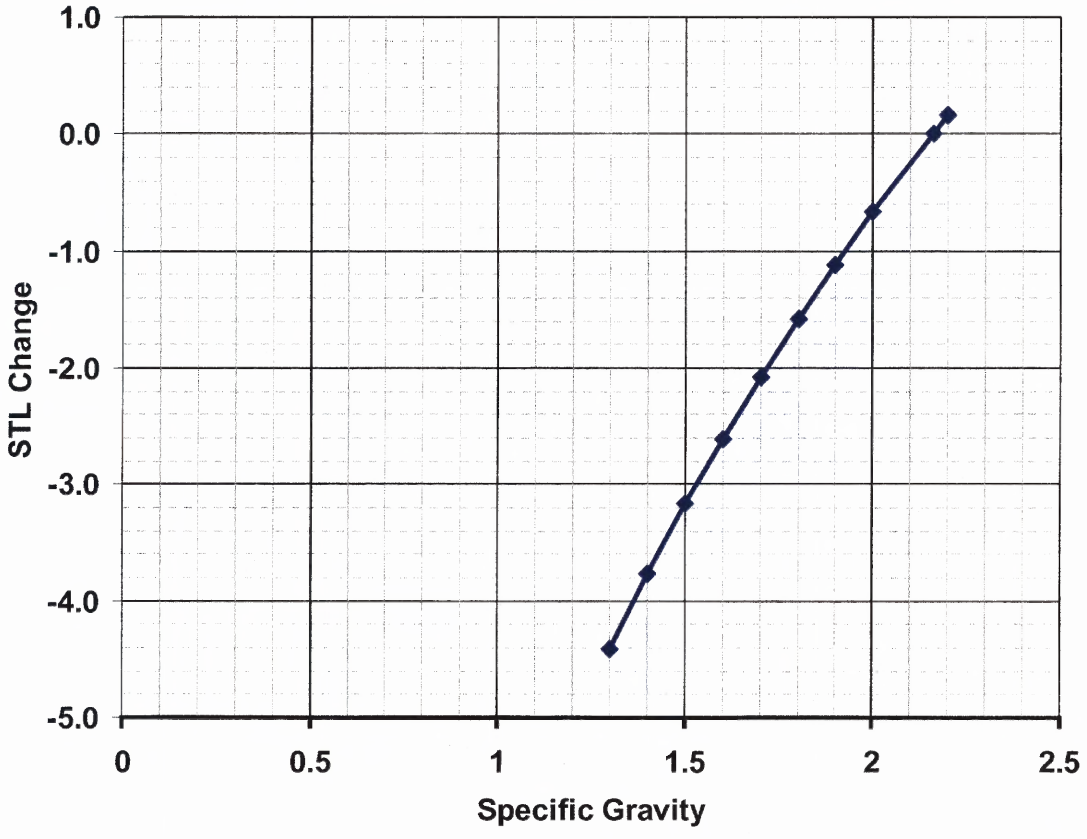

Figure 3.2 STL varies in function of specific gravity. In the mass-law region, increasing the specific gravity at constant wall thickness results in a positive STL change.

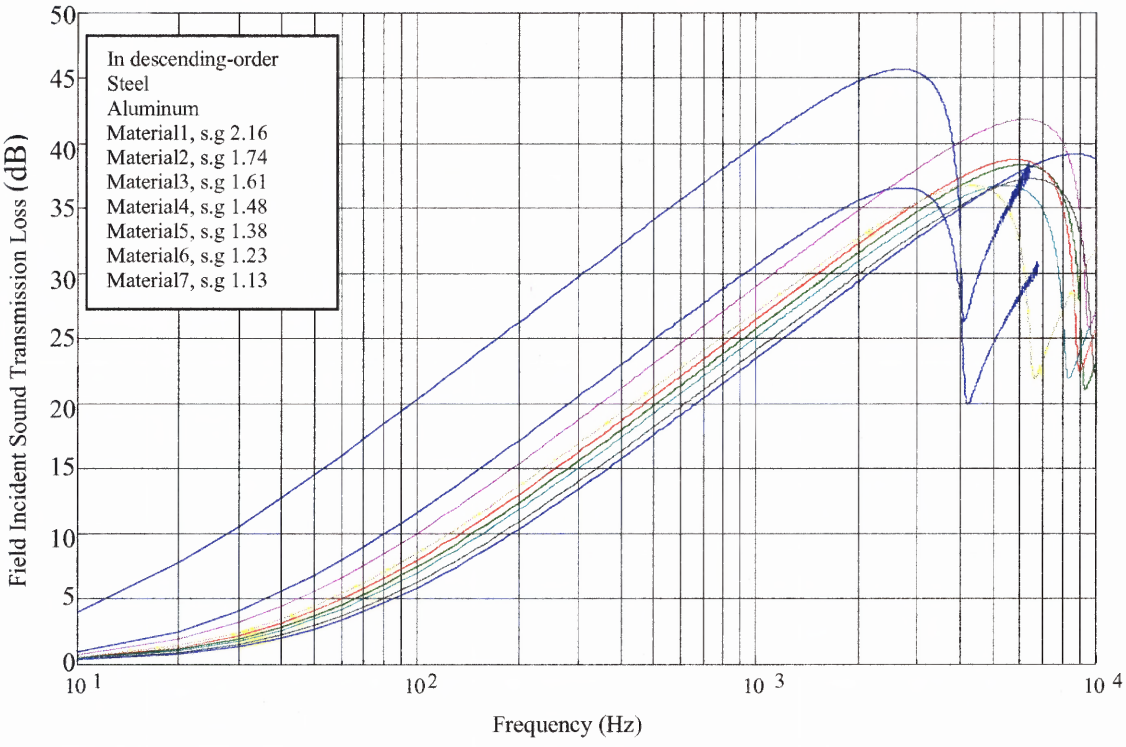

Figure 3.3 STL decreases in descending order with specific gravity. In this case S.G varies from 2.16 to 1.13.

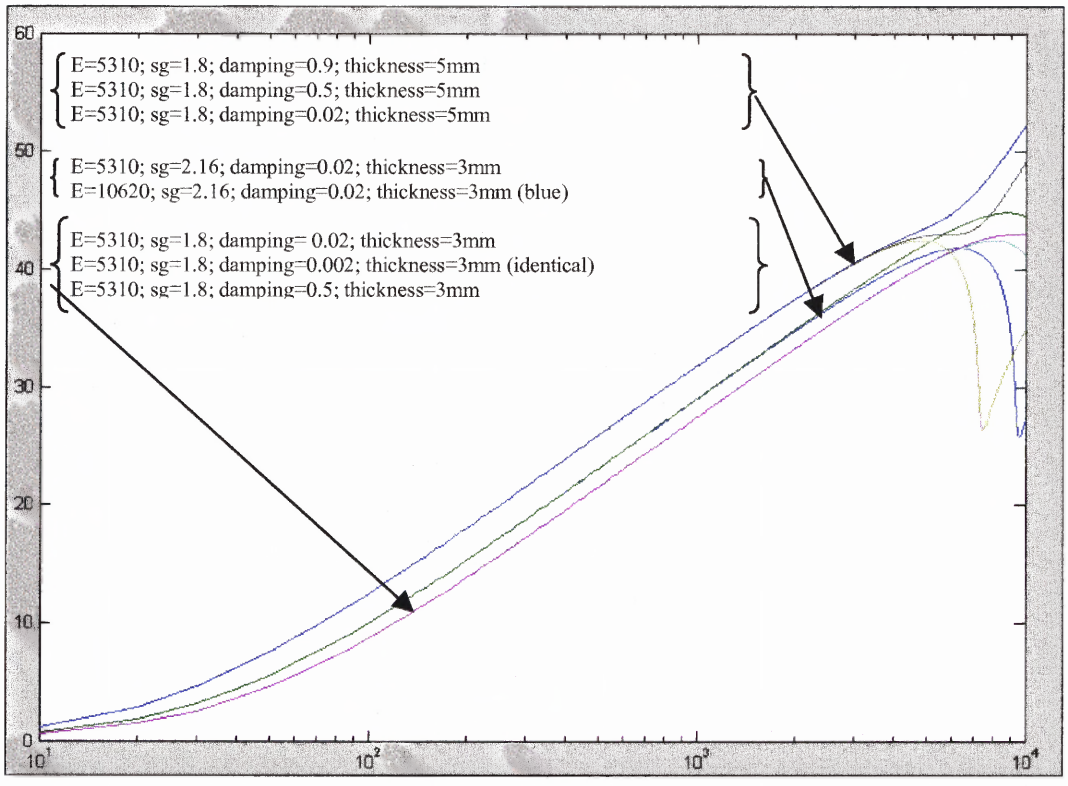

Figure 3.4 Higher damping reduces coincidence effects. At constant mass density and stiffness, and for η =.5, coincidence is reduced to a minimum.

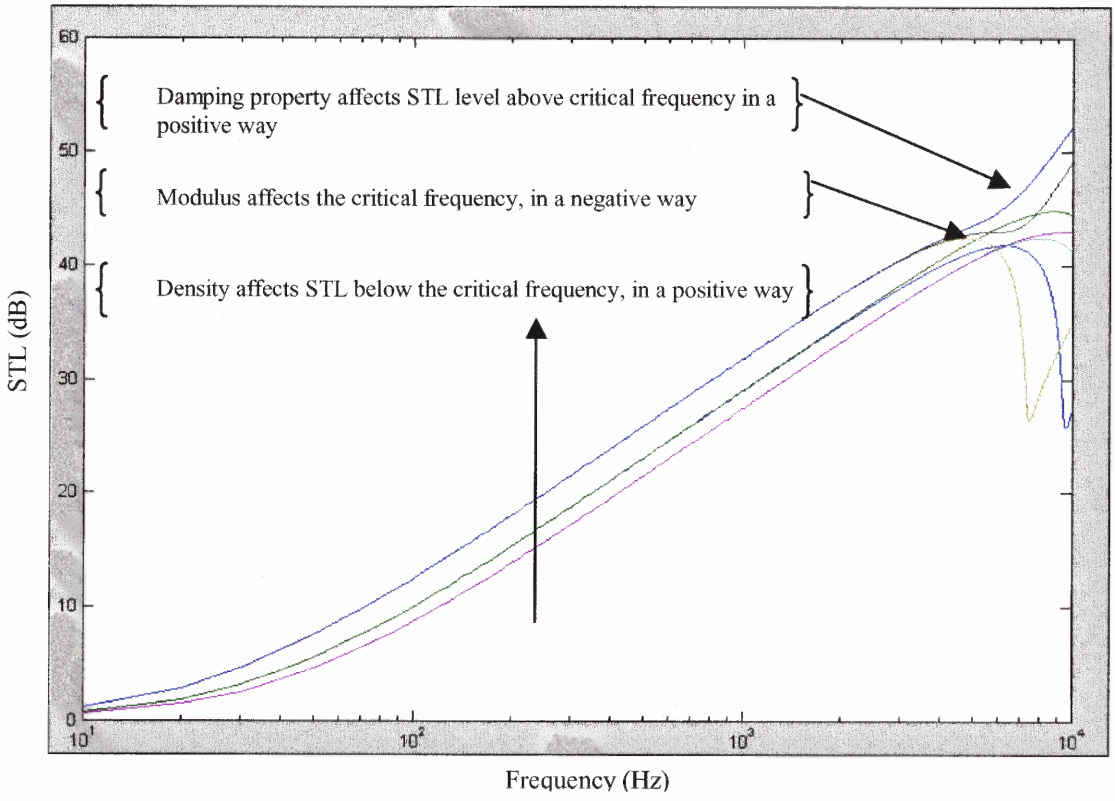

Figure 3.5 Balancing damping and density will have a direct + effect on STL. Indirect control of stiffness can be achieved through design.

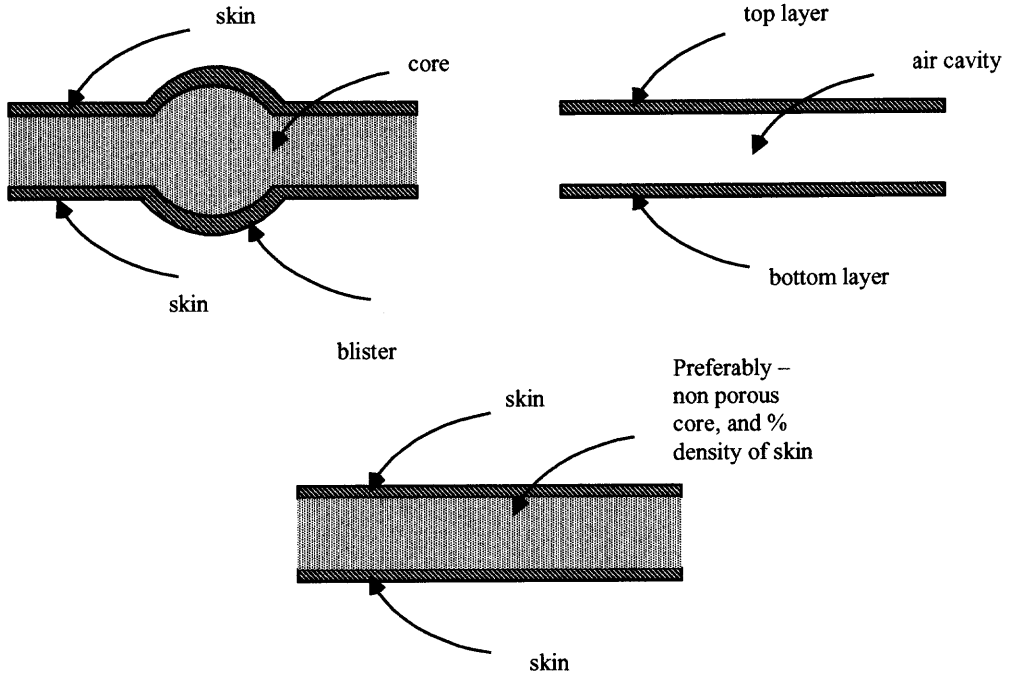

Figure 3.6 Conceptual cross-sectional design configurations with high STL material.

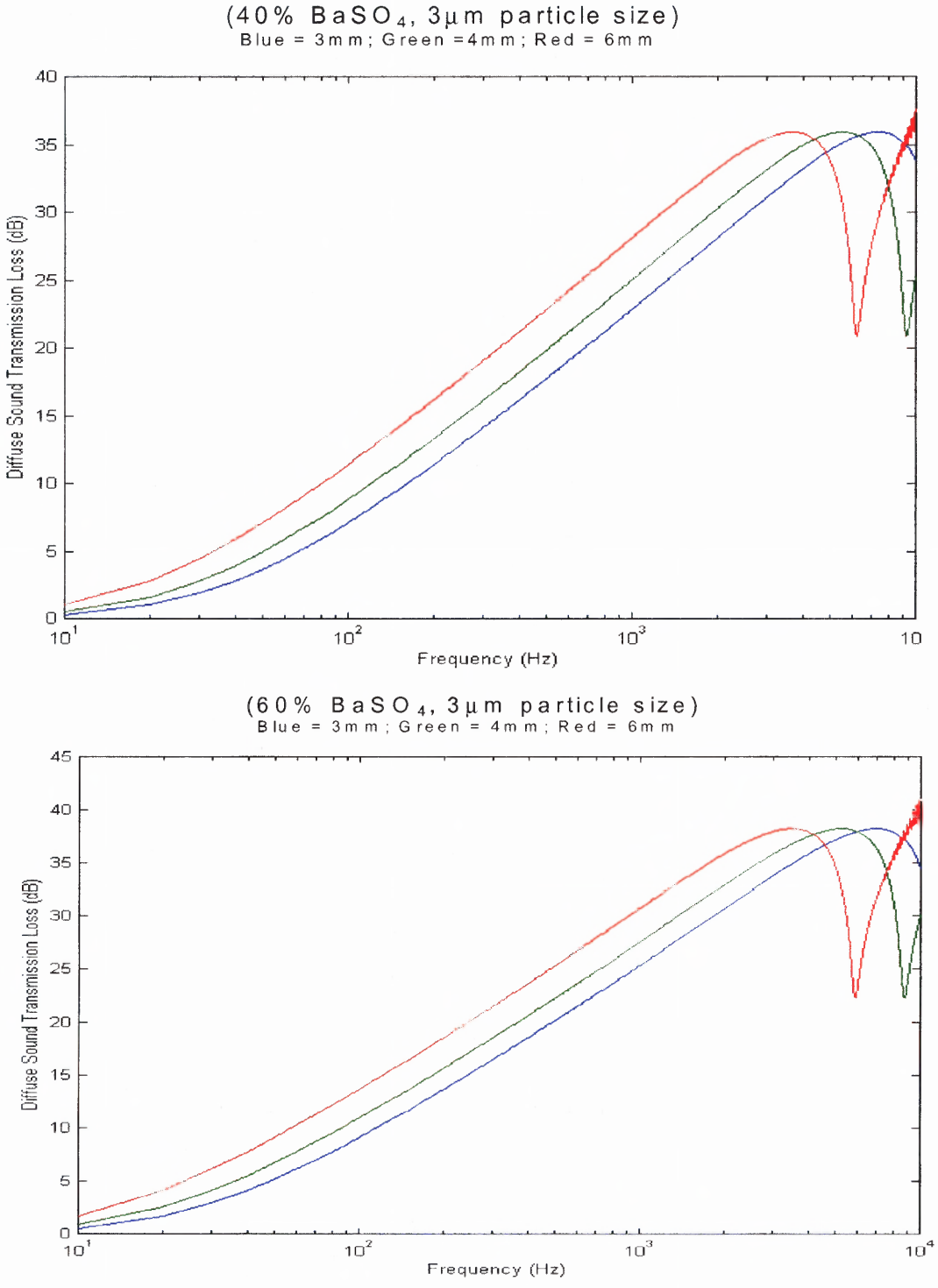

Figure 3.7 Percent threshold value of mineral filler at 3µm particle size.

CHAPTER 4

NUMERICAL ACOUSTIC CHARACTERIZATION

4.1 Preface on methodology

One way to integrate acoustic analysis earlier in the design cycle, when it's less costly to make design changes, is with boundary element analysis techniques using the boundary element method. The boundary element method (BEM) numerically predicts acoustic characteristics for both internal and external problems in three dimensions. Although it doesn't replace finite element analysis (FEA), the BEM is superior to it for acoustic design optimization because the analyst needs to model only the boundary of the acoustic domain to solve exterior radiation or interior response problems.

Acoustic boundary element software calculates the sound radiated from the vibrating structure or generated within an enclosure. Boundary element methods can compute pressure, intensity, acoustic velocity, radiated power, sound transmission, insertion losses, and acoustic sensitivities. In addition, they calculate element or element-group contributions and acoustic mode participation factors to determine their relative effect on the acoustic response of areas of interest on a model.

The first step in an acoustic analysis, typically, is to obtain velocities from a structural dynamic FEA (usually modal analysis). The accuracy of the results is critical to the accuracy of the BEM's noise predictions. When the structural dynamic FEA is complete, an acoustic boundary element model is created. This model coincides with the structural FEA model, where the velocity results act as boundary conditions and affect the acoustic response. (The mesh densities of the structural and acoustic models do not

have to be equal at their interface; interpolation schemes can be used to map the velocity boundary conditions from the structural finite element model to the acoustic boundary element model.)

The next step is to define the acoustic properties of the acoustic medium and specify the boundary conditions, which are applied as surface velocities, pressures, acoustic impedances, and simultaneous velocities and acoustic impedances. One can also specify monopole and plane-wave sources. Analyses can be performed in free-space (anechoic) or half-space (hemi-anechoic) environments.

Finally, one can use either direct or indirect boundary element methods. Both methods are commonly used to perform acoustic analysis in the frequency domain, but they can also be used to perform transient analysis. They are also appropriate for analyzing couples or uncoupled structural and acoustic problems. Acoustic sensitivities can be predicted and linked with structural sensitivity results using either method.

Results can be obtained away from the acoustic boundary at data recovery points, which can be thought of as microphone locations, and on a data recovery mesh (also commonly known as field point mesh (FPM)), a surface created solely to present a contour plot of the results. Results may also be obtained on the acoustic boundary elements, but the computation is more straightforward when the direct method is used. Both the direct and indirect methods give consistent results on a FPM and are sometimes used interchangeably. Each, however, has advantages and limitations.

Models are relatively easy to generate with both methods because only the boundary of the acoustic domain must be defined. The indirect method allows transmission-loss-type problems to be solved with coupled analysis. The acoustic

medium is solved simultaneously on both sides of the model with the indirect method. The direct method should not be used on designs with free edges or for open structures. Those with ribs and openings can be modeled with a single layer of elements using the indirect method. Only the indirect method can solve a plate problem with free edges. With it, constraints can be applied to account for boundary conditions on free edges and multiple element intersections.

Because the indirect method creates symmetric, fully populated matrices (as opposed to the direct method, which generates asymmetric ones), models of equivalent size require less memory with the indirect method. However, the direct method allows the use of multi-zone analysis, which reduces memory requirements and run times. (In multi-zone analyses, different acoustic properties can be assigned to each zone.) The indirect method's formulation limits it to a single zone, and therefore, one acoustic property. Interior openings can be modeled with the direct method using multi-zone analysis.

The indirect method is more suited to problems with complex geometries and structural/acoustic coupling. Because it considers the acoustic media on both sides of a model, the differences in the acoustic pressure and in the normal gradient of the pressure between the two sides of the model are used as primary variables.

The indirect methods solve problems of noise transmission through flexible structures and, as mentioned earlier, accommodate openings and thin ribs. It assembles a symmetric system of equations, which reduces memory requirements and consequently allows larger problems to be solved than would be possible with a single-zone model using the direct method.

For example, one using the indirect method can predict the noise generated in a car interior by airborne engine noise coupled through a dash panel. Noise generated by the engine can excite the dash panel, which in turn excites the air in the completely enclosed passenger compartment. The modal basis of the dash panel is first calculated by an FEA code and then processed by a BEM code.

In uncoupled analysis, the acoustic medium does not affect a structure's vibration. Thus, the structural frequency response analysis is performed first, and the computed vibration is used to define the velocity boundary conditions for the acoustic analysis. An uncoupled analysis is usually a two-step process: the structural vibration is computed using a general-purpose FEA code, and the corresponding radiated noise is calculated using a BEM program.

In a coupled analysis, both the structural vibration and the acoustic response are computed within the same BEM. The structural normal modes are computed by the FEA code, and the modal basis is used to model the coupled part of the structure in the coupled BEM. The combined structural/acoustic response is calculated by the boundary element method.

In a coupled analysis the excitation can come from acoustic noise sources, acoustic boundary conditions, and mechanical loads exerted on the structure. As in the case with an uncoupled analysis, the structural and the acoustic models can have unequal mesh densities. However, in the coupled analysis, this is addressed when the coupling matrices are assembled. When the indirect method is used for coupled acoustic analysis, both sides of the structural acoustic boundary can be coupled to the structure, allowing calculation of the pressure loss across a structural boundary.

4.2 Theory Description of Model for Exterior Problems

As mentioned previously, the indirect formulation allows simultaneous handling of interior and exterior fluids, meaning that the fluid on both sides of a closed or open surface is taken into account. The acoustic pressure and the acoustic velocity are the primary variables defined in the direct method, however, the difference in the pressure and the difference in the normal gradient of the pressure are the primary variables utilized in the indirect method [44], [45], [46]. The formulation is developed by accounting for the acoustic medium on both sides of the model; therefore, the primary variables contain information from the interior and exterior acoustic space [42]. This is possible using single and double layer potential densities σ and μ, which are related to jumps of pressure and normal derivative of pressure through the boundary surface S [47]. The indirect formulation can be combined with a variational approach in deriving the primary system of equations. Then by taking into account the boundary conditions a numerical solution can be produced [42], [43]. The attractive feature of such an approach is that the boundary element system of equations is symmetric, and thus requires reduced computer time.

What follows allows a brief identification of the mathematical background behind the computational model. The intention here is to give a general overview and to describe the modeling technique as applied to actual geometries for acoustical material characterization. In developing the acoustic equations, reference is made to Figure 4.1 which describes a plate with small deflections, and to Figure 4.2 which depicts an open surface.

Starting with the linear wave equation, and taking the divergence of the Euler's equation

$$\nabla \cdot \left(dm \frac{d\mathrm{u}}{dt} \right) = \nabla \cdot \left(-\nabla p dV \right)$$

$$dm \cdot \frac{d}{dt} (\nabla \cdot \mathrm{u}) = -\nabla^2 p dV,$$

substituting the divergence of the velocity $\nabla \cdot \mathrm{u}$

$$dm \cdot \frac{d}{dt} \left(-\frac{1}{\rho c^2} \frac{\partial p}{\partial t} \right) = -\nabla p dV$$

and using the identity $dm = \rho dV$

$$-\frac{1}{c^2} \frac{\partial^2 p}{\partial t^2} = -\nabla^2 p$$

leads to the linear wave equation

$$\nabla^2 p - \frac{1}{c^2} \frac{\partial^2 p}{\partial t^2} = 0.$$

This equation describes the propagation of waves, and in this particular case, of acoustic waves traveling with the propagation speed (speed of sound) c. Next, assuming a separable and time harmonic solution to the linear wave equation

$$p(\mathrm{r}, t) = \Phi(\mathrm{r}) \cdot e^{j\omega t},$$

the second time derivative of the pressure can be written as

$$\frac{\partial^2 p}{\partial t^2} = -\omega^2 p(\mathrm{r}, t).$$

Substituting this in the linear wave equation and introducing the wave number, or spatial frequency, $k = \omega / c$ gives the Helmholtz equation

$$\left(\nabla^2 + k^2 \right) p = 0.$$

Solving the homogeneous Helmholtz equation in terms of the fluid pressure and the inhomogeneous Helmholtz equation in terms of the Green's function for the Laplacian of the pressure and Green's function respectively, where δ is the three-dimensional Dirac function, gives

$$\nabla^2 p = -k^2 p$$
$$\nabla^2 G = \delta - k^2 G.$$

Here, and in the following formulae, the dependency of p and g on r is dropped for simplicity.

Constructing a function

$$F = p\nabla G - G\nabla p$$

and applying Gauß's integral theorem

$$\int_v \nabla \cdot F dV = -\int_S F \cdot \mathrm{n} dS.$$

However, in order to apply the Gauß's integral theorem, take the divergence of the function F

$$\begin{aligned} \nabla \cdot F &= p \cdot \nabla^2 G - G \cdot \nabla^2 p \\ &= p \cdot (\delta - k^2 G) + G k^2 p \\ &= p \cdot \delta, \end{aligned}$$

and substitute the solutions of the above Helmholtz functions into this equation. The volume integral in Gauß's theorem is (applying the definition of the delta function $\int_v a \cdot \delta dV = a \cdot \varepsilon$)

$$\int_v p \cdot \delta dV = p \cdot \varepsilon$$

with $\varepsilon = 1$ for a point in dV, but not on the plate surface, and $\varepsilon = 2$, for a point on the plate surface. This is physically reasonable because of the assumption of a source and a

mirror source, which form one source for a point on the boundary surface, and thus lead to the double pressure.

The function under the surface integral of Gauß's theorem is given by

$$\begin{aligned} F \cdot \mathrm{n} &= \mathrm{n} \cdot (p\nabla g - g\nabla p) \\ &= p\frac{\partial g}{\partial n} - g\frac{\partial p}{\partial n}. \end{aligned}$$

Bringing the volume and the surface integral together to form Gauß's theorem results in

$$p \cdot \varepsilon = -\int_S \left(p\frac{\partial G}{\partial n} - G\frac{\partial p}{\partial n} \right) dS, \tag{4.1}$$

which is the Helmholtz integral equation. Since this is an integral over the active surface area, this is much easier to evaluate than the inhomogeneous Helmholtz equation, which is an integral over the volume of the fluid. For a closed surface, the general form of Equation 4.1 becomes

$$p(x) = \int_S \left(p(y)\frac{\partial G(x,y)}{\partial n_y} - G(x,y)\frac{\partial p(y)}{\partial n_y} \right) dS(y).$$

For a thin body, where the thickness is less than the wavelength $S = S^+ \cup S^-$, the integral on S becomes

$$\begin{aligned} p(x) = &\int_{S^+} \left(p(y^+)\frac{\partial G(x,y^+)}{\partial n_y} - G(x,y^+)\frac{\partial p(y^+)}{\partial n_y} \right) dS(y) + \\ &\int_{S^-} \left(p(y^-)\frac{\partial G(x,y^-)}{\partial n_y} - G(x,y^-)\frac{\partial p(y^-)}{\partial n_y} \right) dS(y) \end{aligned},$$

and for,

$$S^+ = S^- = \bar{S}$$
$$y^+ = y^- = \bar{y}$$
$$\vec{n}_{y^+} = -\vec{n}_{y^-}$$
$$\frac{G(x,y^+)}{\partial n_{y^+}} = -\frac{G(x,y^-)}{\partial n_{y^-}}$$

the integral equation becomes

$$p(x) = \int_S \left(\mu(\bar{y}) \frac{\partial G(x,\bar{y})}{\partial n_y} - G(x,\bar{y})\sigma(\bar{y}) \right) dS(\bar{y})$$

$$\mu(\bar{y}) = p(y^+) - p(y^-) \tag{4.2}$$

$$\sigma(\bar{y}) = \frac{\partial p(x,y^+)}{\partial n_y} - \frac{\partial p(x,y^-)}{\partial n_y}$$

The normal derivative of Equation 4.2 for x located on the surface S must be used for expressing the velocity boundary conditions on S [40], because

$$v_n = \frac{\partial p}{\partial n} / (-i\rho\omega)$$

if only velocity boundary conditions are considered on S, σ vanishes on S, so that the only unknowns are the nodal pressure jumps μ. Thus, Equation 4.2 can be written in a discretized form

$$[D(k)](J) = -i\rho\omega[C](V),$$

where J is a vector of the unknown nodal pressure jumps, D is a frequency dependent matrix, which is complex but symmetric, while C is a geometrical coupling matrix, and ρ the density of the fluid [40]. If after the solution of Equation 4.2 the vector J is known, it can be used to determine the sound pressure level at any point x in the vicinity of the

vibrating system. An exhaustive treatment of the theory has been the topic of several researchers over the years, and for more reading on the subject, the author refers to some key publications by Volahopoulos and Coyette [42], [43], [48] and [50], [55]. It is the intention of the author to leverage the knowledge and expand application of the theory in a novel approach for the analysis and characterization of acoustical materials, refer to Reference [71] for more on the case of enclosures (closed systems).

4.3 Suggested Numerical Approach for STL

An integrated finite element and boundary element method approach offers good potential for evaluating the acoustical characteristics of a material from simple shape problems such as flat panel, to more complex geometries such as air intake manifold. A novel approach to characterize acoustic materials in air intake manifolds is presented in the Appendix A section of this study. Homsi et al. (2003) [71] described a new practical method to perform a hybrid simulation thereby avoiding noise contamination in the solution. The utility of this approach can be expanded to other systems with multiple airflow orifices where the airborne sound element is the controlling factor. Better characterization accuracy can be achieved with such approach [67].

For the simple shape case, there have been a handful of modeling examples [53], [54], [61] based on Biot's theory [51], [52], which was formulated specifically for elastic porous materials. The work is aimed to suggest a quick and reliable numerical procedure for the transmission loss prediction of a simple structural component such as panels.

The FEM code in Sysnoise is used to extract the uncoupled structural modes of the structure, and then a coupled FEM-BEM calculation is performed. In particular, the

panel structural behavior is assessed by the FEM modal analysis, and the calculated normal velocities are imposed as boundary conditions for a BEM analysis of the transmitted noise field. Numerical modeling of sound transmission is based on a baffled boundary element (BEM) formulation in Sysnoise, which can handle structural geometries lying outside the plane of the baffle, as well as co-planar with it [56] (see Figure 4.3). The structural geometry can include double-walled structures, ribs, and junctions between panels. The acoustic boundary element model is based on the indirect approach with a variational solution scheme. The modal behavior of the finite structure with defined edge support conditions is taken into account. The acoustic elements can be given a known plane wave excitation source. The source reference location is usually above the baffle, and may have an amplitude of 1Pa (for trend comparisons), independent of the frequency. The plane waves can be oriented to impinge on the baffle at a skew angle. By definition, there is no incident field below the baffle if the reference location is above it. By solving for the forced response case, the transmission loss of the panel can easily be evaluated. Sound Transmission Loss (or Sound Reduction Index, SRI) has been defined as the logarithm to the base ten of the ratio of incident sound power to transmitted sound power.

The transmitted power is computed directly as power through the field point mesh (see Figure 4.5). The incident power is found from the pressure due to the incident plane wave, assuming free-field propagation and projecting the area of the panel normal to the plane wave direction. It is worthy to note that a diffuse incident field can be modeled as a combination of uncorrelated plane waves: a pre-processing step sets up multiple independent load-cases, with power spectral density spectra (PSDs), and cross-spectra,

which add up to equal the spectrum of the diffuse field at all points in the half-space on the "source" side of the baffle. Alternatively, if a pressure distribution is known across the "loaded" side of the baffled structure, but the pressures are (partially) random, this can be set up as a random surface pressure loading, with spatial correlation functions [56]. The procedure can be repeated for various material property comparisons. The case for the selected glass/mineral filled material versus the standard 33% glass filled material, confirm the advantage of the noise material (see Figure 4.4 where impinging wave was evaluated at one angle of incidence). This rather simple procedure is a quick and effective way to evaluate the effect of material property variations on STL.

4.4 Conclusion

In conclusion, the STL of a structural-acoustic 3-D finite panel can be modeled with the indirect baffled BEM formulation, which includes coupling to a conventional structural FEM model. The indirect baffled BEM approach or acoustic transparency approach offer all possible combinations of acoustic surface characteristics and boundary conditions. Those elements and boundary conditions can exist in or out of the plane of baffle. This will enable quick validations of elements with finite and simple geometries, and can be extended to the more complex shapes.

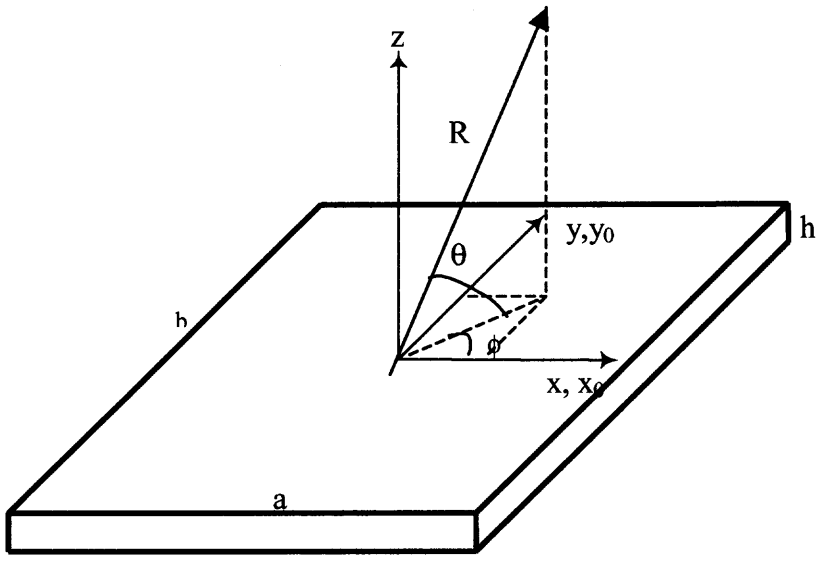

Figure 4.1 Normal deflections on plate are in global z. Coordinates with zero index are in the plane of the plate.

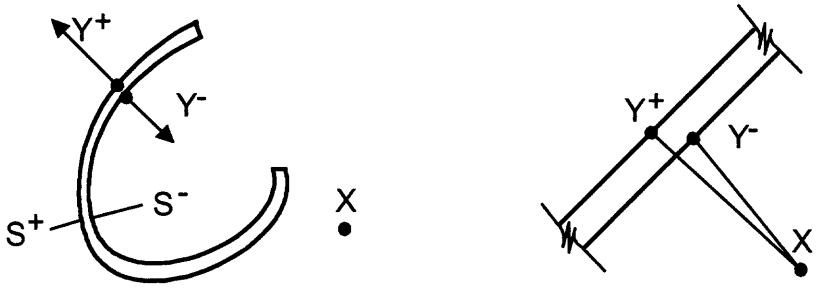

Figure 4.2 Schematic representation of surface and coordinates of jump of pressure for the indirect BEM [49].

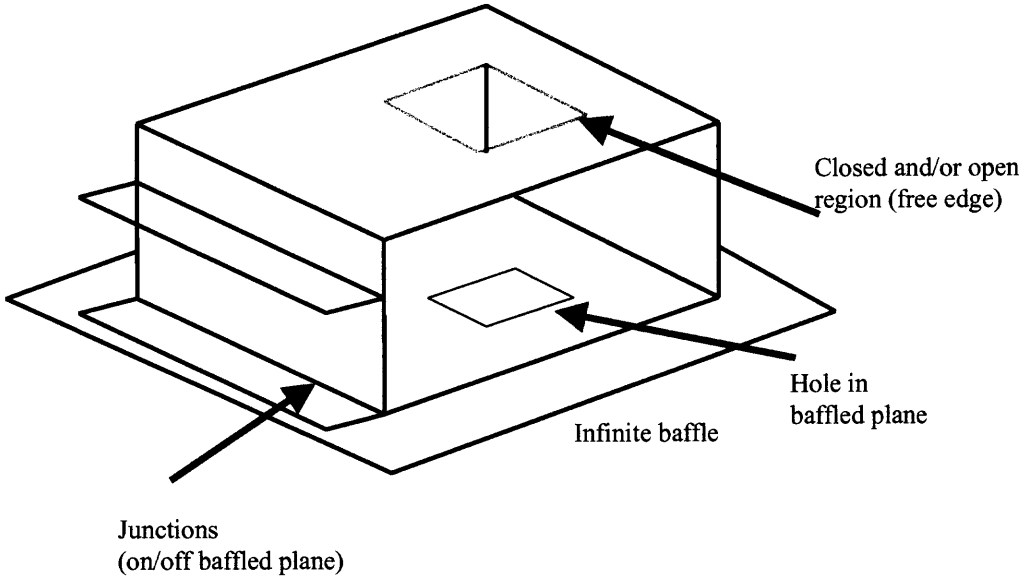

Figure 4.3 Schematic of possible model elements for STL evaluations [56]. Boundary conditions: known velocity, known impedance, known pressure (single/double sided) and transfer impedance.

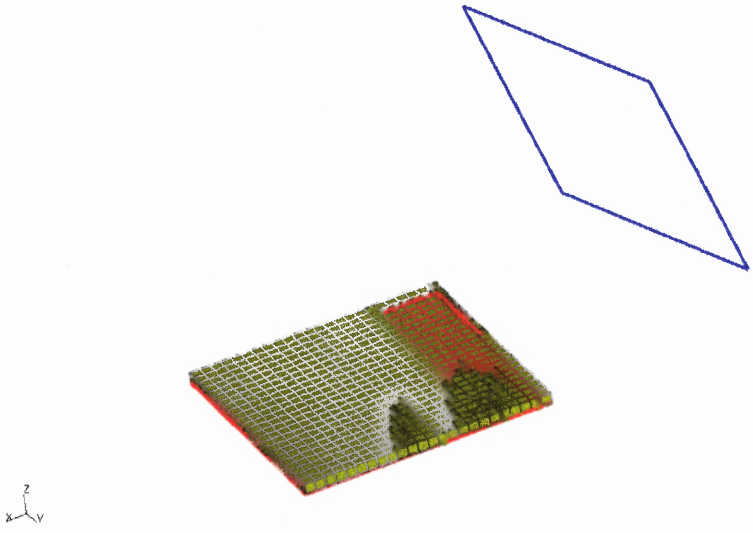

609.6 x 609.6 x 3 mm

Noise Reduction Mat E=10,621 MPa, n=0.35, r=2.16E-09 Ton/mm^3
Standard Mat E=5,130 MPa, n=0.35, r=1.38E-09 Ton/mm^3

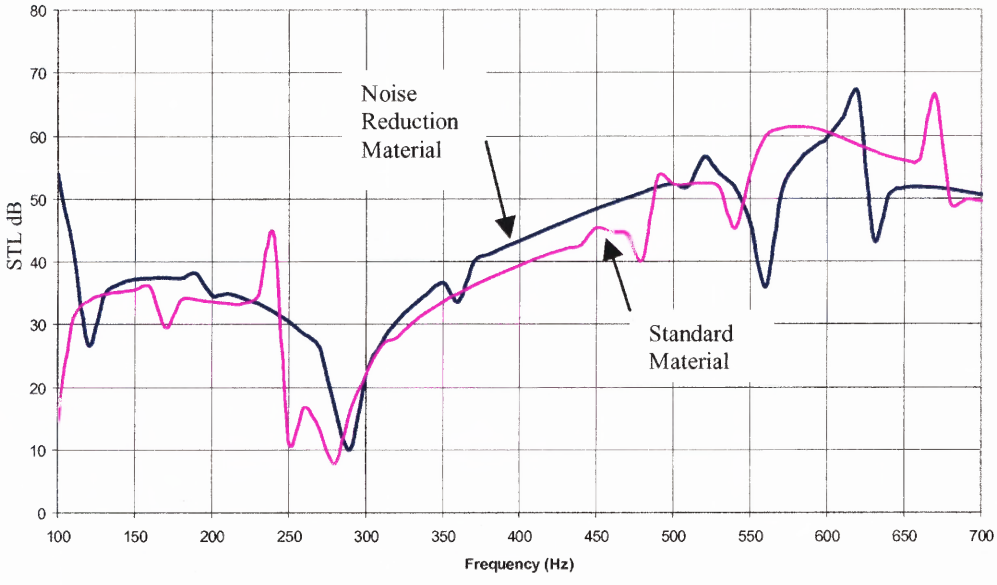

Figure 4.4 Acoustic transparency computational calculation of STL.

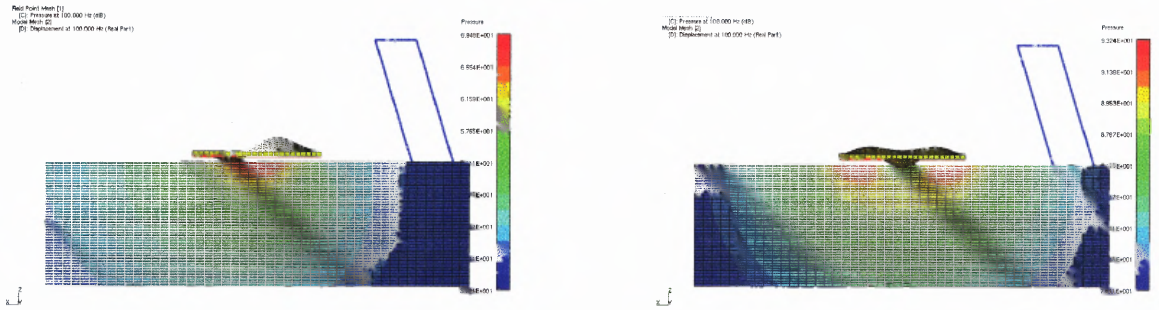

Field Pressure at 100Hz

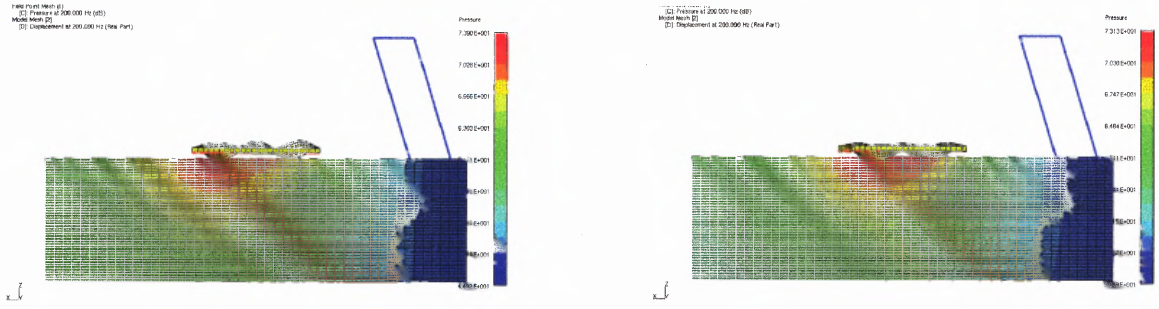

Field Pressure at 200Hz

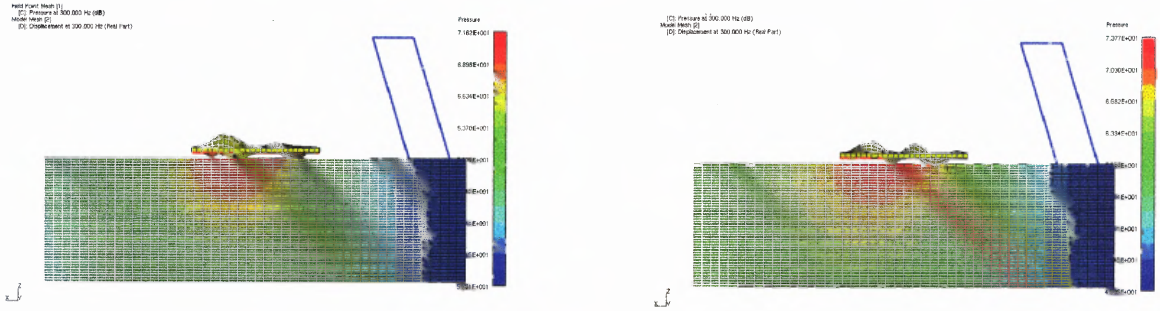

Field Pressure at 300Hz

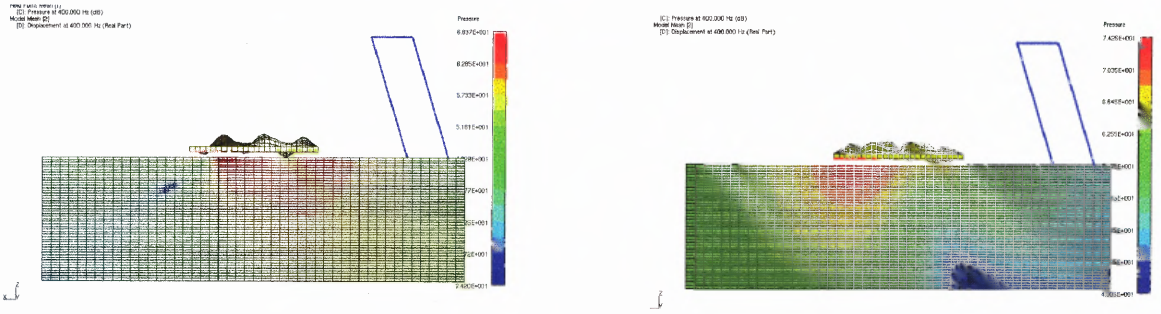

Field Pressure at 400Hz

NVH Material

Standard Material

Figure 4.5 Field recovery mesh depicting transmitted power of panels from NVH material vs. standard 33%GF material.

CHAPTER 5

MATERIALS, METHODS AND PROCEDURES

5.1 Introduction and Description

A polymer-based compound or material can be tuned to offer improved STL performance. It is believed that targeted applications for such a material can include engine covers, enclosures, and barriers. Optimal material configuration and overall material characteristics can be achieved and validated using specific measurement techniques and test set-ups. What follows is a brief restatement based on reference [24] describing test procedures that can be used to assess and compare the acoustic performance of such a compound. Results from these test procedures will be used to quantify improvements and optimize the overall configuration.

The acoustical performance of a panel/barrier can be characterized by measuring its power transmission coefficient (or its decibel equivalent, the transmission loss). The power transmission coefficient is defined as $\tau = Wt / Wi$ where Wt is the sound power transmitted by a barrier, and Wi is the incident power. The sound transmission loss is then $STL = 10\log\frac{1}{\tau}$. The STL is normally measured by inserting the barrier in an aperture between two reverberation rooms or between a reverberation room and an anechoic space. In the latter case the transmitted sound power can be measured directly by scanning an intensity probe over the transmission side of the barrier [25].

5.2 Transmission Loss Measurements of Plastic Panels

The first procedure performed is the assessment of noise reduction. The sound reduction index SRI, also commonly referred to as the sound transmission loss, is the most usual product-related acoustical quantity determined in laboratory or field conditions after noise emission measurements of machinery. The test procedure is conducted in a specialized two chambers set-up. The configuration of this set-up is illustrated in Figure 5.1 and Figure 5.2. The driver or source will be positioned in the source chamber. The source microphone is positioned such that it is measuring the free field response. The receiver microphone is positioned in the receiver chamber as illustrated. Position 1 is used to measure noise reduction, which is simply a measure of the source sound level minus the receiver sound level.

The test set-up and measurements follow the SAE J1400 test procedure standard [9]. The large 200 m^3 reverberant chamber is coupled to the reception anechoic chamber by means of a window, upon which the test sample is installed, usually with a metal frame. The clamping configuration is such that the frame is clamped at eight locations some small distance from the edge, and at two positions on each side (for a rectangular or square panel). The panels' typical dimensions were (508mmx508mm) based on a 0.72m diagonal opening between the two rooms. A broadband noise signal is generated in the source room. By measuring the sound pressure levels in the reverberant chamber and in the reception chamber, the STL of the panel can be determined in 1/3 octave band frequencies that range from 31.5 Hz to 16K Hz.

In practice, high STL insulators are frequently installed on the surfaces of the cab of the vehicle to reduce the outside vehicle noise sources, such as exhaust, engine, wind and tire/road noises, from entering the passenger compartment.

The principle of STL measurement method has remained the same over the years. The first theoretical formulation to determine STL of a partition between two rooms was presented in the 1920's by Davis and Buckingham [32] and [33]. The first ASTM standard was based on London's proposal in 1951 [34] and [35]. The present test standards are e.g., ISO 140-3 [4], DIN 52210 Part 3 [26], ASTM E-90-90 [10], and SAE J1400 [9], which are, in a physical sense, equivalent [24]. The sound reduction index, SRI, is defined by

$$SRI = 10\log\frac{1}{\tau} = 10\log\frac{Wi}{Wt} \text{ dB}$$

where τ is the transmission coefficient, and Wi and Wt are the incident and transmitted sound powers, respectively. The source room is supposed to emulate a diffuse sound field. Thus, the incident sound power can be determined by the average sound pressure p_1 in Pa as follows

$$Wi = \frac{p_1^{\,2}}{4\rho_0 c_0} S$$

where S is the area of the test specimen in m^2, ρ_0 is the density of air in kg/m^3 and c_0 is the speed of sound in air in m/s. The transmitted sound power is determined, accordingly, in the steady-state situation, when the sound power radiated by the specimen equals the absorbed sound power in the receiving room as follows

$$Wt = \frac{p_2^{\,2}}{4\rho_0 c_0} A$$

and

$$A \approx 0.16\frac{V}{T}$$

where p_2 is the average sound pressure in the receiving room, and A is the room absorption area of the receiving room in m^2. A is approximated by the Sabine equation where V and T are the volume and reverberation time of the receiving room, respectively. Thus, the *SRI* is determined by

$$SRI = STL = SPL1 - SPL2 + 10\log\frac{S}{A} \text{ dB} \qquad (5.1)$$

where SPL1 and SPL2 are the average sound pressure levels in the source and receiving room, respectively, that is, the SRI is determined indirectly from the average sound levels of the adjacent test rooms. The sound reduction index is usually determined in third-octave frequency bands. Equation 5.1 is based on the assumption that presupposes that all sound energy is transmitted via the test specimen. In practice, a certain part of the total sound energy measured in the receiving room is always radiated by other room surfaces, which is due to flanking transmission discussed in the next chapter.

5.3 Radiation Efficiency Measurements Quantified by Sound Pressure Level

The radiation efficiency of a panel depends on the longest physical dimension of the sample. Usually, the radiation efficiency drops off significantly when the ratio of panel length to wavelength is equal to one. In reference to Figure 5.1, the acoustic radiation component can be evaluated by moving the source to position 2. The distance between the source and sample will simulate the distance between a typical engine and engine cover. Two source signals can be emitted; first a broadband random or swept sine signal can be utilized, a second signal can be a time capture of actual engine compartment

vehicle signatures. These signals would need to be recorded during normal operating conditions and the resulting sound pressure levels would be measured in the receiver chamber. Results from each sample could be overlaid and compared. The relative amount of radiated acoustic energy could be directly attained from these results.

In laboratory settings, radiated sound power by vehicle components can be directly calculated from sound intensity (SI) measurements. The SI measurements are acquired on specific measurement grids providing a locating means for the intensity probes (see Figure 5.3 and Figure 5.4) for illustration. The amplitude part of sound pressure is a scalar quantity, which lacks information about the direction and the magnitude of energy flow. On the other hand, sound intensity in W/m^2 is a vector quantity, which describes the sound power per unit area. It is defined as the product of sound pressure p in Pa and the vector quantity particle velocity $\vec{v}$ in m/s. The two-microphone technique (p-p) is the most usual method to determine the one dimensional time-averaged particle velocity in the x direction, $\vec{v}_x$, and is determined by the time-averaged pressure gradient between two microphones using Euler's equation [24]

$$\vec{v}_x = -\frac{1}{\rho_0 \Delta r}\int (p_B - p_A)dt$$

where Δr in m, is the distance between the microphones A and B, t in s, is time, and p_A and p_B are the pressures sensed by the microphones A and B, respectively. The phase information contained in the pressure signals is fully utilized in the two-microphone intensity technique. To calculate the intensity, the pressure is determined by the average of the two microphone signals by $(p_A+p_B)/2$. The distance between the microphones is usually set at $\Delta r = 6$ to 50 mm, depending on the frequency range of interest [37].

The main assumption of the two-microphone method is that the inherent phase difference between the microphones is negligible. However, in practice, there is always some inherent phase mismatch between the microphones and the channels of the analyzer, so that a small residual intensity, L_R, is produced. The pressure-residual intensity index, σ_{pR}, is determined as the difference between the pressure level and intensity level when both microphones are exposed to the same sound pressure (phase and amplitude). Thus, the SI measurement procedure requires an intricate calibration process. The microphones are first calibrated using a sound pressure level calibrator. From this calibration, absolute amplitude adjustments are made. Secondly, the microphone pair is situated in a sound intensity calibrator. This apparatus is used to create a function, which compensates for any phase adjustments. Each sound intensity measurement is then corrected utilizing phase and amplitude corrections.

The main application of the intensity method was the direct determination of sound power, because the determination of the sound power presupposes the movement of the probe normally to a hypothetic surface that encloses the sound source (surface integral) [24], [7]. The vector nature of intensity is lost because the orientation of the probe is not fixed. It is usual that a small gap exists between the test specimen and the planar intensity measurement surface, and a proportion of the transmitted power may be transported via this gap leading to underestimation of radiated sound intensity. The underestimation can be significant, especially in the neighborhood of the critical frequency, where the radiation of sound at large angles greater than 75° is stronger than that radiation perpendicular to the specimen. The best situation is to minimize the gaps

between the measurement surface and the test specimen by placing the measurement surface right in front or on top of the test opening.

It is worthy to note that laser Doppler techniques can be used to aid in extracting the vibratory signature of the test sample subjected to the same vibratory excitation source. Doppler-shifted light is detected when scattered from a moving surface. A live color video can readily simulate the operational deflection shape of the test specimen, over a user defined measurement grid that can confirm the link between the surface vibrations and the sound measurements (see Figure 5.5).

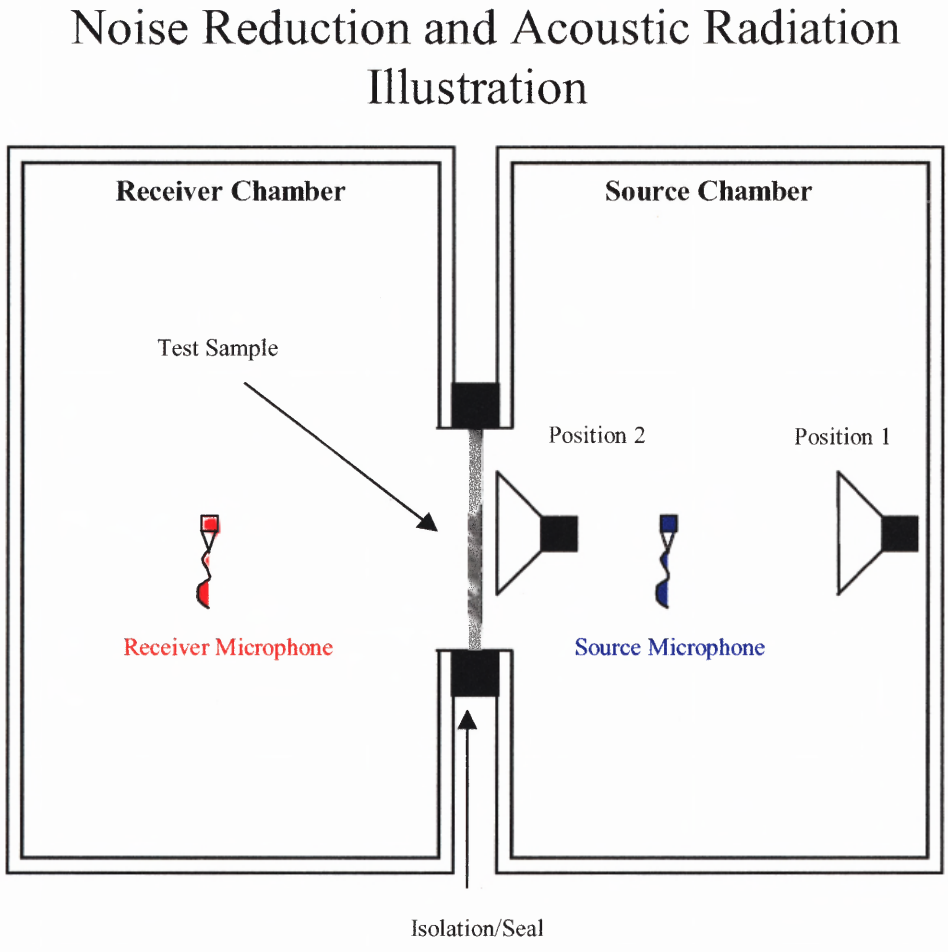

Figure 5.1 A schematic representation of specialized two-chamber test set-up that allows transmission and acoustic radiation measurement on small samples 30mmx30mm. With source in position 1, both microphones are used. With source in position 2, only the receiver microphone will be used.

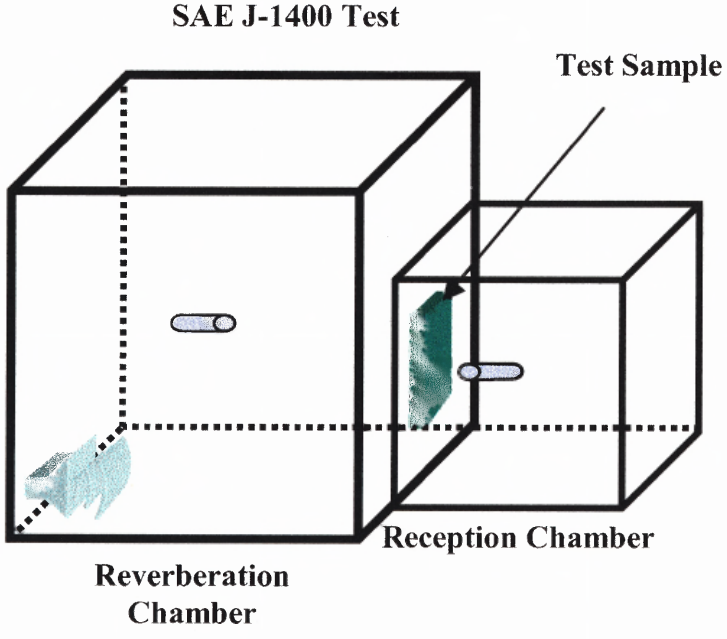

Figure 5.2 Schematic representation of SAE J1400 test set-up. Panels are fitted with sealed edges in a wall opening separating a source reverberation chamber and a receiving anechoic chamber [9].

Figure 5.3 Sound Intensity measurement grids are laid on top of tested sample. Measurements are acquired at grid junctions normal to the radiating surface using the phase-matched two-microphone technique.

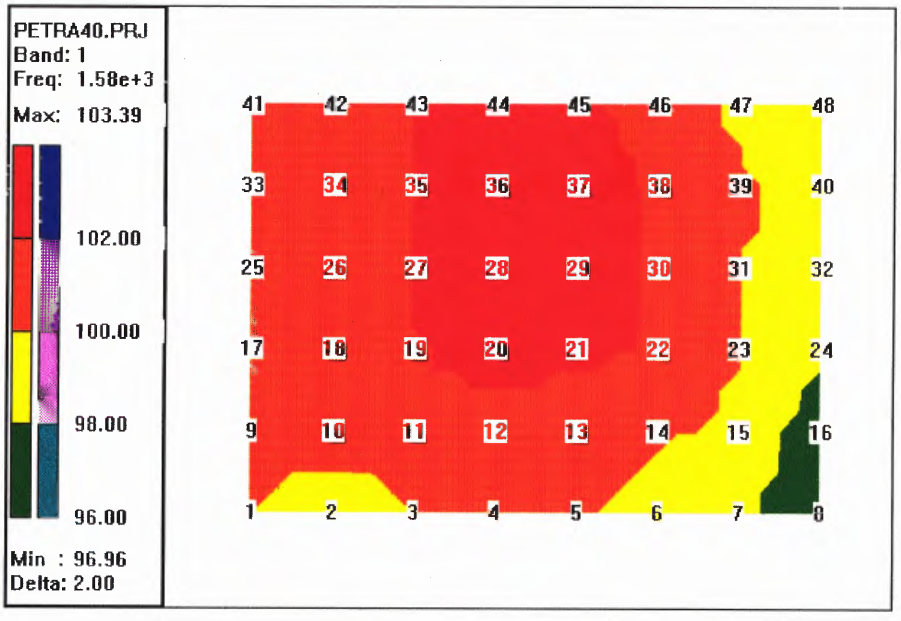

Figure 5.4 Sound intensity map from a measurement grid laid over the tested sample. Sound power is determined by integrating the sound intensity over the radiating area.

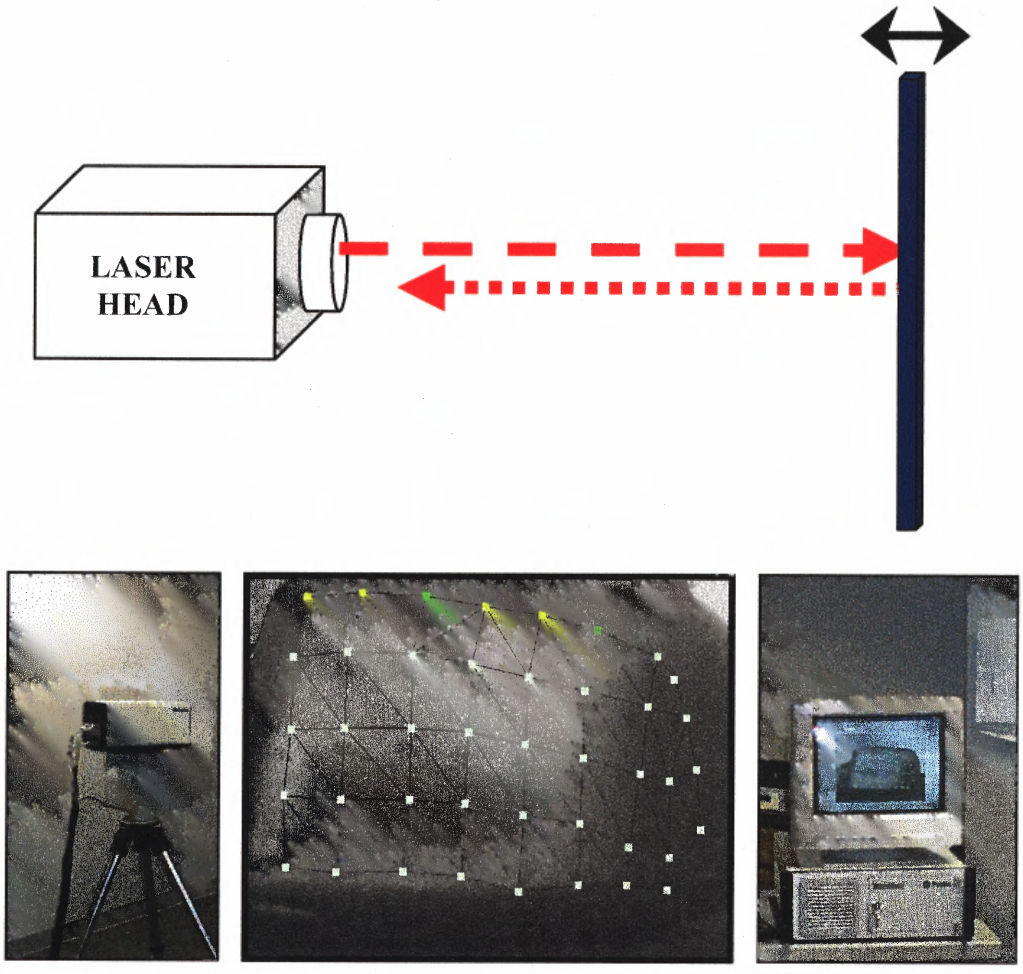

Figure 5.5 Doppler-shifted light is detected when scattered from a moving surface. Backscattered light from moving surface has frequency Doppler shifted by $f_D = 2v/\lambda$. Velocity is directly proportional to frequency shift.

CHAPTER 6

TRANSLATIONS AND RESULTS

6.1 Sound Transmission of Plastic Panels

6.1.1 Single, Double and Layered Effects

Reducing the sound levels in vehicle passenger compartments, for example, has long been sought by the motor vehicle industry. In order to improve customer's image, the focus is on employing high STL attenuating materials in the fabrication of polymeric components and sub components. It was stated previously that an insulating panel material could offer good STL because it has the capacity to reflect incident acoustical energy on one surface, or dissipate the sound energy passing through the material, so that little sound is transmitted off the secondary surface [29]. The intention here was to verify the effects on STL of selected material parameters in multiple panel configurations.

While absorbers are effective at dissipating sound, they typically are not good for STL because sound propagates readily through the pores. However, if two or three layers of elastic materials are combined so as to mismatch the acoustical impedance at their interface, the attenuation of sound passing through the system is much improved [29]. It has also been mentioned that a double panel system separated by an air cavity can provide STL improvements over single panels [14], [17], [21], depending on the panel wall thickness and the size of the interspace, and this is readily practiced in window glazing designs. [8], [26], [27], [28]. On the other hand, appreciable differences in the performance of small or large components in the vehicle industry with such configurations may not be feasible due to space limitations.

For single and double panel STL evaluations of selected material parameters fabricated by standard extrusion molding techniques, tests were conducted (on 3mm thick panels) according to the procedures specified in the SAE J1400 standard [9], and described in Chapter 5. A thin lead panel of 4.9 Kg/m^2 (1.0 lb/ft^2) surface weight was used to compute the correlation factor as referenced in SAE J1400. The lowest usable frequency band of measurement for this test (in a 508mm by 508mm or, 20 inch by 20 inch opening) is 125 Hz (based on the 0.72m or 2.36 ft diagonal of the opening between the source room and the receiving room). Measurements were made at six microphone locations in the source room and at one location 100mm (4 inches) away from the sample, and six times in the receiving room. The results in Figure 6.1 and Figure 6.2 are shown from 31.5 Hz to 16 KHz in third octave frequencies. The theoretically computed TL "mass law" per SAE J1400 of the lead sheet is also shown in the graphs for comparison purposes. The panel materials' physical properties are shown in Table 6.1. These included standard core properties in a single and double panels (with 6mm air gap) configurations, respectively, and single panels with high STL material properties. The intention was to show the effects of double panel configuration alone on STL irrespective of the advantages obtained from an attenuating material in single panel design.

The results shown in Figures 6.1 clearly show the increase in performance obtained with a high STL parameter material over standard materials. The performance of the double panel system confirms the theoretical assessment over the single wall in the mass-law range. The performance dip in the high frequency region is due to the mass-air-mass resonance, and the other performance dip in the low frequency region is likely due to the inter-panel depth resonance effect [8], [30]. These dips are usually controlled

by the addition of damping in the high frequency region, and by design and damping in the lower frequency range.

Table 6.1 Panel Materials Physical Properties

Sample No.	Sample Description	Measured data Surf. Wt. Kg/m^2 (lb/ft^2)
1	XA2935 Nylon based polymer: Single Wall 3mm	6.0 (1.2)
2	XA2935 Nylon based polymer: Single Wall 3mm	6.3 (1.3)
3	Capron® 33% GF Nylon Based core polymer: Single Wall 3mm	4.0 (0.8)
4	Capron® 33% GF Nylon Based core polymer: Double Wall (2 layers separated by 6mm air gap)	8.0 (1.6)

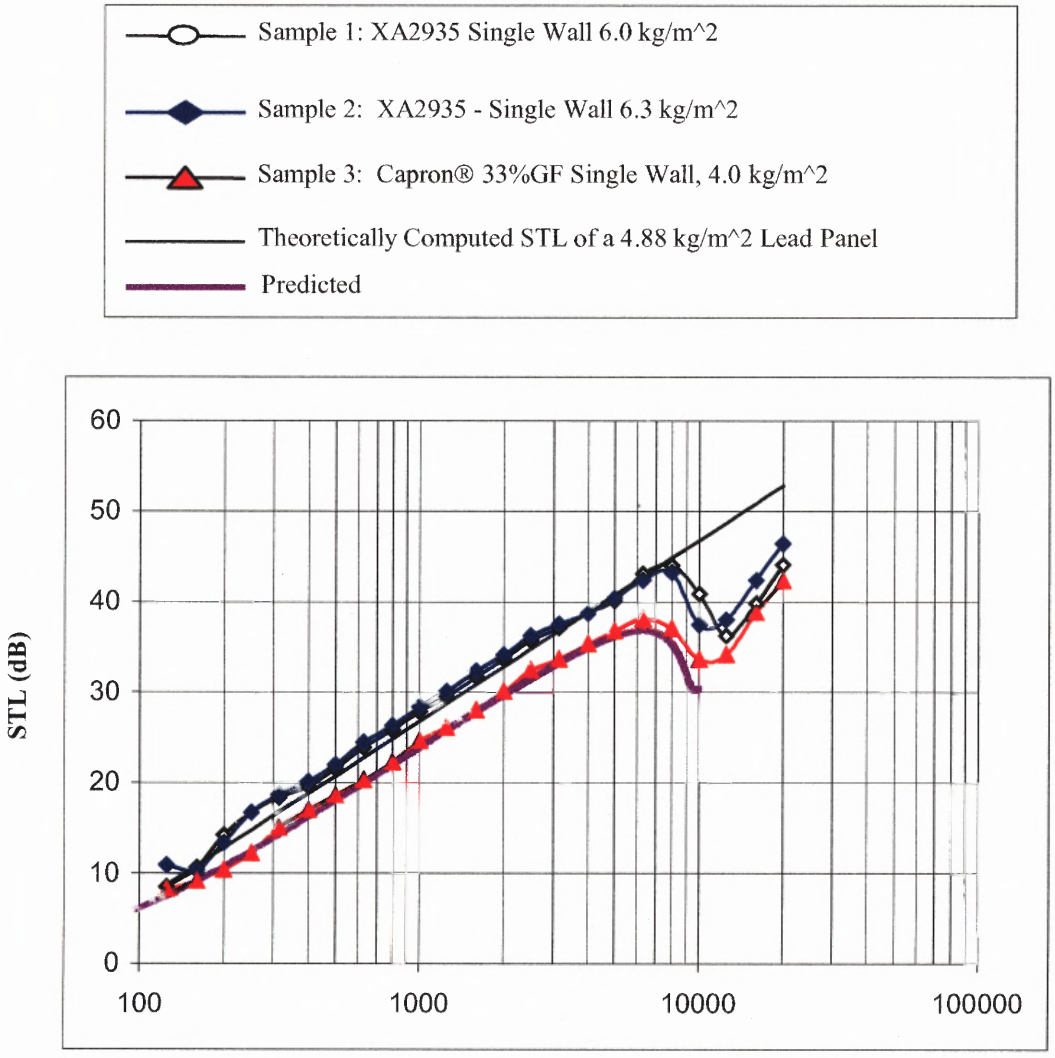

Figure 6.1 STL data obtained from samples of NVH materials overlaid with calculated lead sheet data from SAE J1400. The results shown in the figure show increase in STL performance obtained with mass density at constant wall thickness of 3mm vs. Standard 33% GF material.

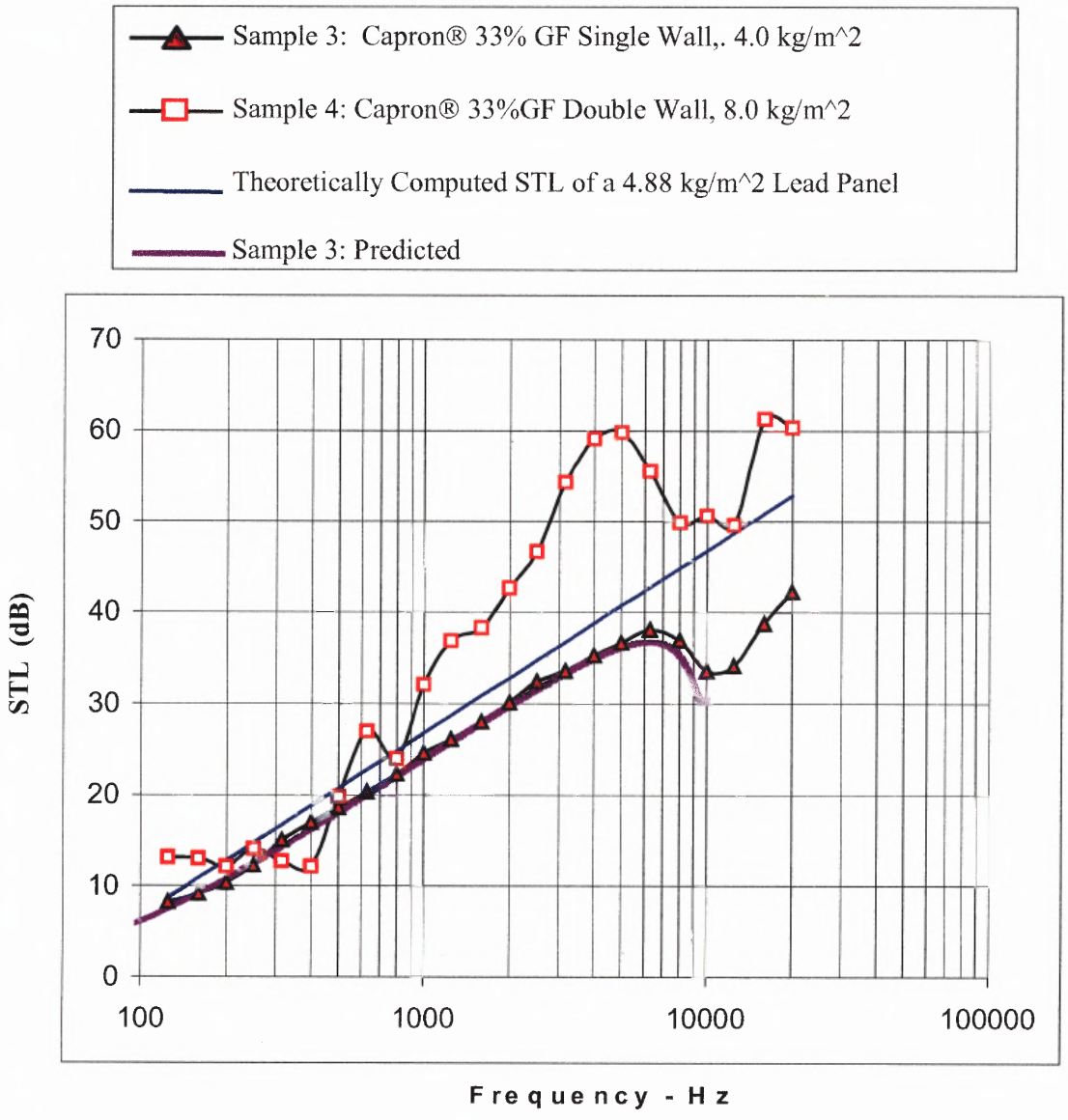

Figure 6.2 STL curve of single panel of 33% GF material vs. the double wall configuration with 6mm air space. Significant increase in STL in mass-law region. Double wall resonance in the low frequency region decreases STL. Panel thickness constant 3mm.

A second set of tests was conducted using the same set-up and procedure as described above, on sample panels (520mm x 520mm) fabricated by standard co-injection molding techniques using standard Nylon 6 polymer with 35% glass fiber. All samples had varying surface mass densities determined by their respective thickness. In addition, four of the samples had a core layer with scattered voids created by utilizing chemical blowing agents during the injection process. The intention was to evaluate the effects of non-homogenous core layers on STL performance. The samples' pertinent physical parameters are listed in Table 6.2.

Comparing the STL of the foamed core samples as well as the single layer samples with respect to their increasing surface mass density (see Figures 6.3) confirm the increase in STL and the corresponding decrease in critical frequency in compliance with the mass-law theory. However, results obtained by comparing the foamed core panel sheets to the single layer panels did not show an improvement in STL for the same thickness and surface mass density. It was also observed that a decrease in STL at coincidence had occurred. The void inclusions within the core did not provide a decoupling effect but likely a leak-through path for the propagating waves. It was concluded that the foamed core layer alone did not offer any STL advantage. The same comparative results were obtained as samples 1 and 7 were compared for different wall thickness, but similar surface mass density (see Figure 6.5), however, no appreciable STL improvement up until coincidence. Comparing the single to layered panel for the same surface density but for double the thickness (see Figure 6.4), it was concluded that no appreciable change in the STL was obtained by creating voids in the core layers.

Table 6.2 Physical Parameters of 35% GF Material in Single and Multi-layers

	Thickness mm	**Surface Density Kg/m^2**	**Type**
Sample1	4.0	4.0	Foamed Core
Sample2	8.0	10.5	Foamed Core
Sample3	6.0	8.0	Foamed Core
Sample4	5.0	5.2	Foamed Core
Sample5	6.0	7.5	Single Layer
Sample6	4.0	5.1	Single Layer
Sample7	3.0	3.9	Single Layer
Sample8	3.0	8.2	Calibrating Panel

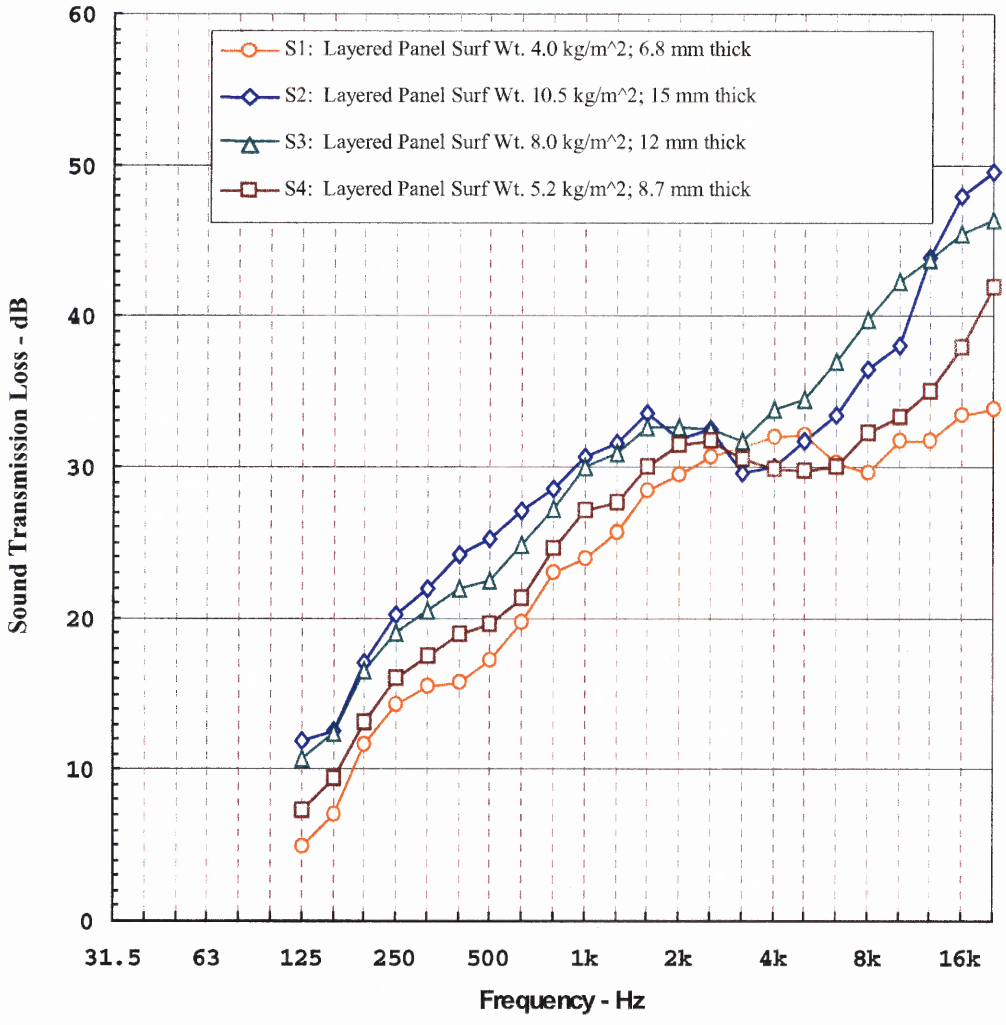

Figure 6.3 Increase in the surface density results in higher STL up until coincidence, but decreases coincidence and limiting the useful range of frequencies – layered panels.

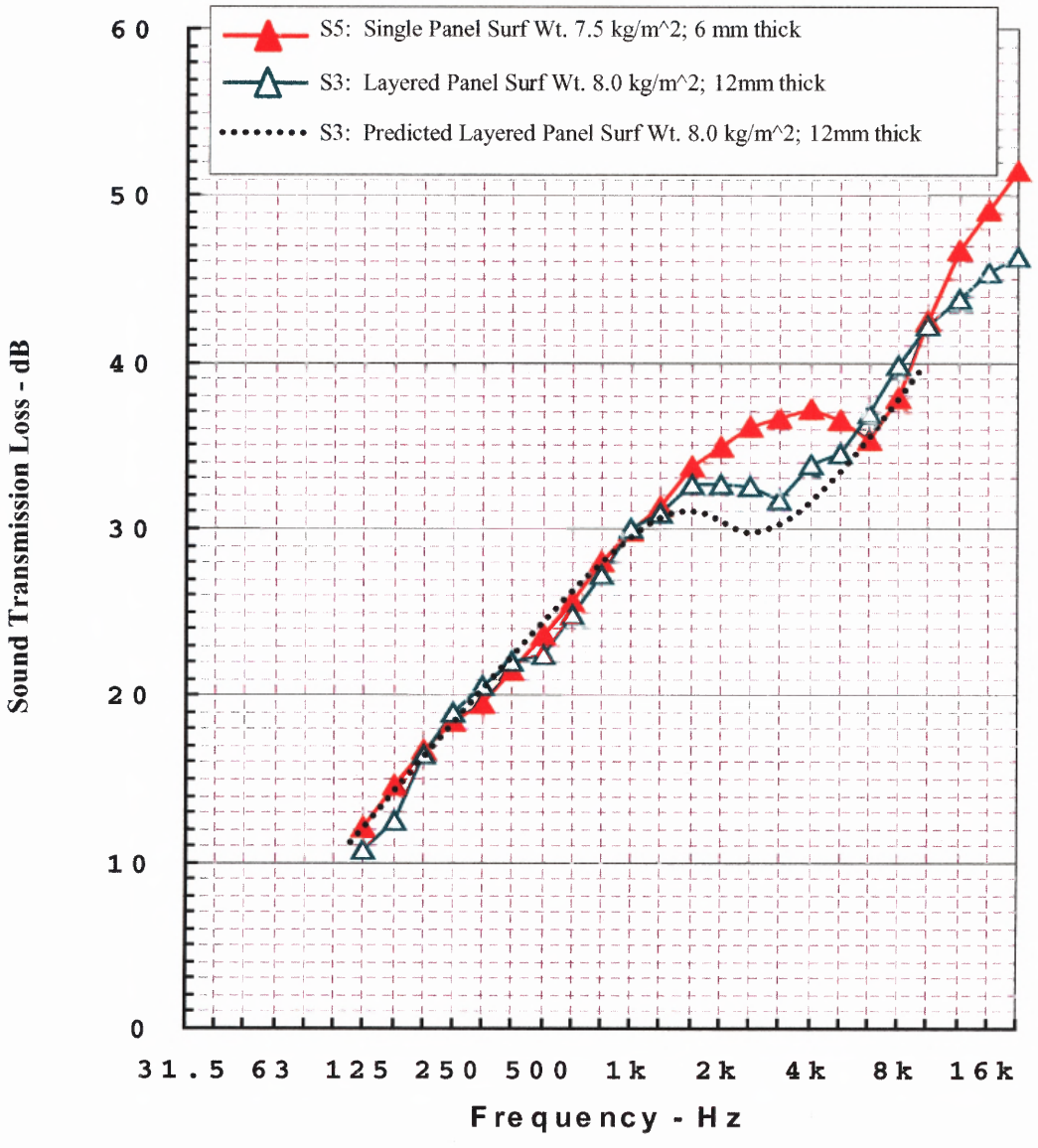

Figure 6.4 Increase in thickness 6mm to 12mm, same density. STL is the same for single and layered panel up to coincidence.

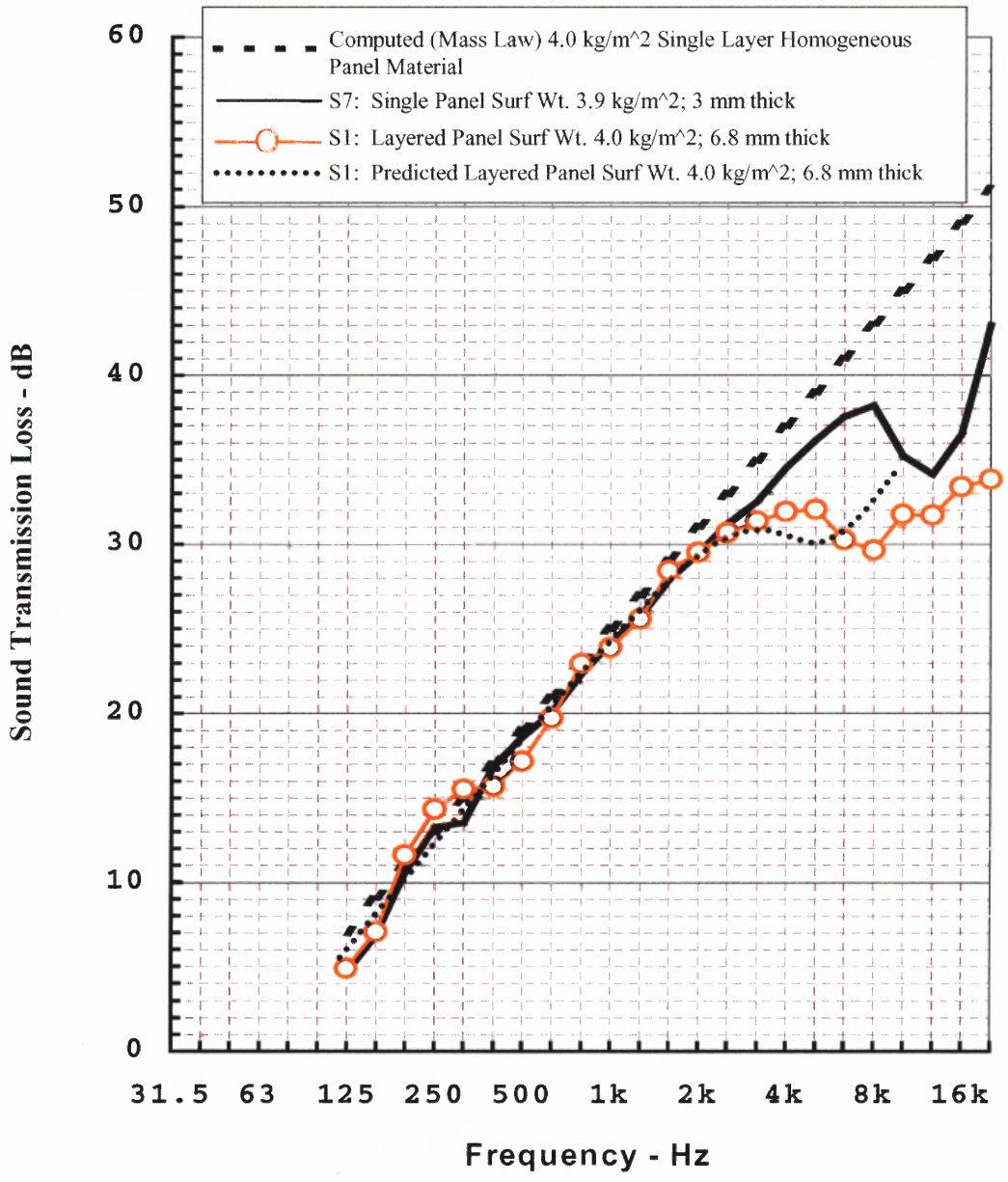

Figure 6.5 Increase in the thickness with constant surface density results in no STL change up until coincidence, but decreases coincidence and limiting the useful range of frequencies.

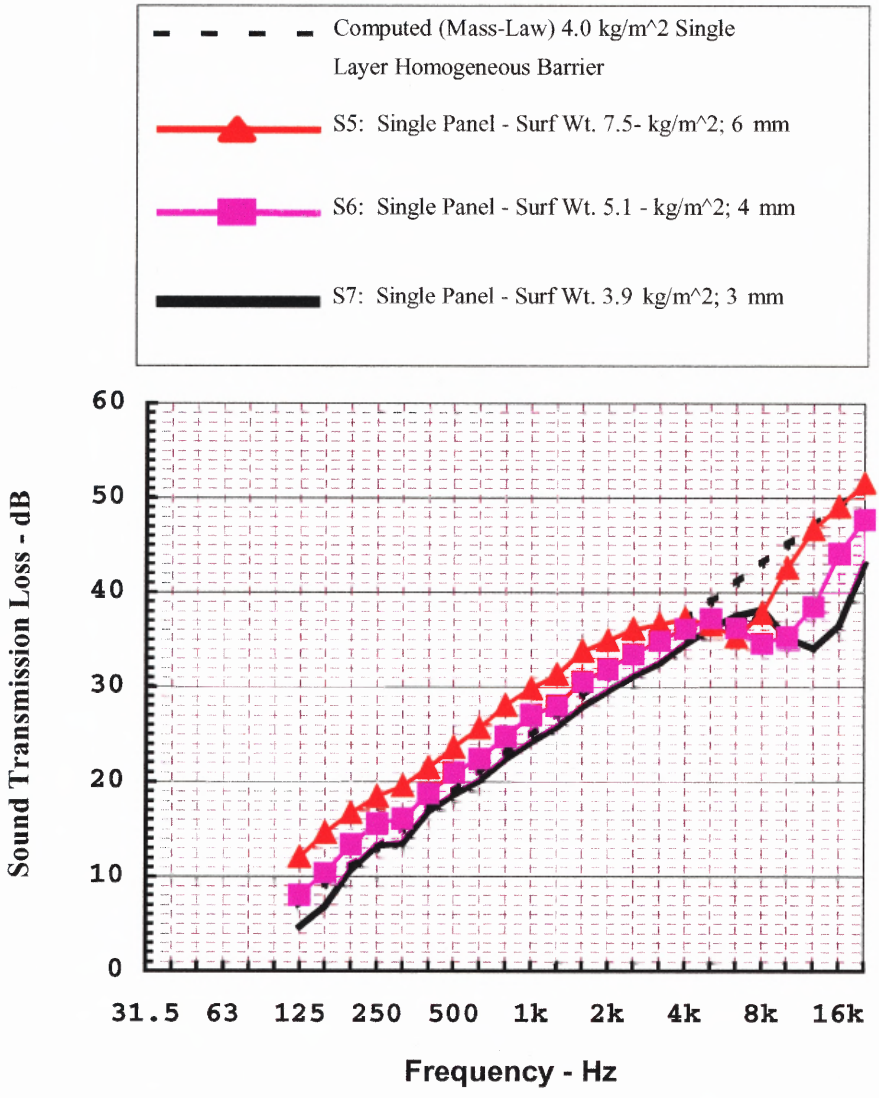

Figure 6.6 Increase in the surface density results in higher STL up until coincidence, but decreases coincidence and limiting the useful range of frequencies – single layer panels.

6.1.2 Summary of Results

Starting with an empirical method to predict the STL of polymer-based materials typically used in automotive applications based on basic expressions of STL performance in single and layered wall configurations, one can characterize and tune the primary and secondary physical parameters that affect the STL performance of the material. Once an optimum set of parameters is identified, it is linked to the basic material properties at the microscopic level.

The field incidence mass-law, applicable to uniform, thin, unbounded elastic panels, suggests that the STL for a single panel barrier increases by 6 dB if the surface mass of the barrier material is doubled. However, for a finite size barrier, the stiffness and resonance regions at low frequencies and the coincidence at high frequencies bound the mass-law performance [30]. The STL prediction method is also based on basic STL theory of double-wall systems, which accounts for the double-wall resonance and the standing wave resonance between the two walls.

In the lower frequency regions, the two panels are coupled together and behave as a single mass, which results in an STL performance analogous to the single barrier. The upper limit of the coupled mass is bounded by the mass-air-mass resonance, where the frequency of motion of the walls is out of phase, and the mass densities and the spacing in between the walls affect resonance. At this frequency, the STL performance is drastically reduced. Above this resonance, the STL of the double wall increase at a rate of 18dB, until the double wall decoupled region is attained. The portion of the STL curve that represents this increase is referred to as the transition region, and is bounded by a

point, which defines the double wall decoupled region. This region in turn is limited at high frequencies by the coincidence effect [30].

The material considered for high STL as shown exhibited better performance as predicted by theory, over standard materials. The double panel system with air space proved to offer superior STL readings, and the layered system with foamed cores proved ineffective at high frequency and did not produce any noticeable improvement in the lower frequency regions. In practice, an ideal double wall system may not be possible due to space limitations, and intermediate decouplers are typically used to control the double wall resonance effects. A single layer high STL material is a better option from a manufacturability and cost point of view, and layered constructions may provide an intermediate option if the core's homogeneity is kept close to that of the skin layers.

6.2 Acoustic Engine Cover

6.2.1 Acoustic Material Comparative Sound Level

A major characteristic of NVH reduction material development is the continuous balance of influencing factors with each modification or step of improvement. The risk of spending effort on ineffective measures is high, and therefore, validation efforts are definitely required. The validation study aimed at quantifying the relative performance of engine covers (closest representation of a panel noise barriers) molded from the new NVH material formulations. Engine noise is one of the dominating sources of vehicle interior noise [31].

Among other under the hood engine components, engine covers are used as cosmetic shields in their simplest form and function. Often such configurations are significant contributors to overall engine noise, since they tend to radiate specific structural borne noise of various mechanical actions within the engine. Some of these covers, however, are fully treated with absorbing material layers such as cellular foam or fiberglass mats that are bonded on the inner face of the cover, and act in conjunction with the cover material, to reduce sound energy going through or emanating form the system. Such configurations, though with limited positive effects, are characterized with an appreciable cost penalty. In practice, single layered polymer-based covers made with an acoustic materials can provide significant performance and cost advantages over current design. Traditional acoustic measurement methods, such as 1m SPL (Sound Pressure Level) measurement and acoustic intensity measurements are based on single point microphone data [31].

6.2.2 Results

Sample acoustic covers fabricated from the acoustic polymer material were fitted on a PV8 Corvette engine bed simulator. Two specific sets of measurements were taken at top microphone positions, 1m above the cover in five locations (see Figure 6.7), for a 900 and 2500 engine rpm sweeps, respectively. Figures 6.8, 6.9, 6.10 show data recovered directly above the engine cover and the overall sound power for the various configurations that were evaluated. The configurations were compared according to the following: cover with no noise layer treatment, and cover with light foam sealing gaps at the edges. The baseline cover had a layered construction and consisted of a 15% glass filled nylon 6 material with a glass fiber mat bonded on the inner side. The data showed no appreciable noise reduction (in the three decibel range). While the noise reduction above the engine was not significant, the readings were affected by noise leakage and open source path transmission. The detrimental effects of flanking transmission leakages (see Figure 6.11) on the acoustic performance of sound attenuating and insulating panels are shown in Figure 6.12 [29]. Based on the data obtained from these and on previous investigators' published results, it is evident that sound package design is an important other factor that influences the acoustical performance of an attenuation system. Components of a well-designed package should fit snugly in the vehicle and display minimal amount of openings, except for those that are needed for routing, wiring, and ducting systems, for example. Avoiding these will ensure better acoustical shielding performance.

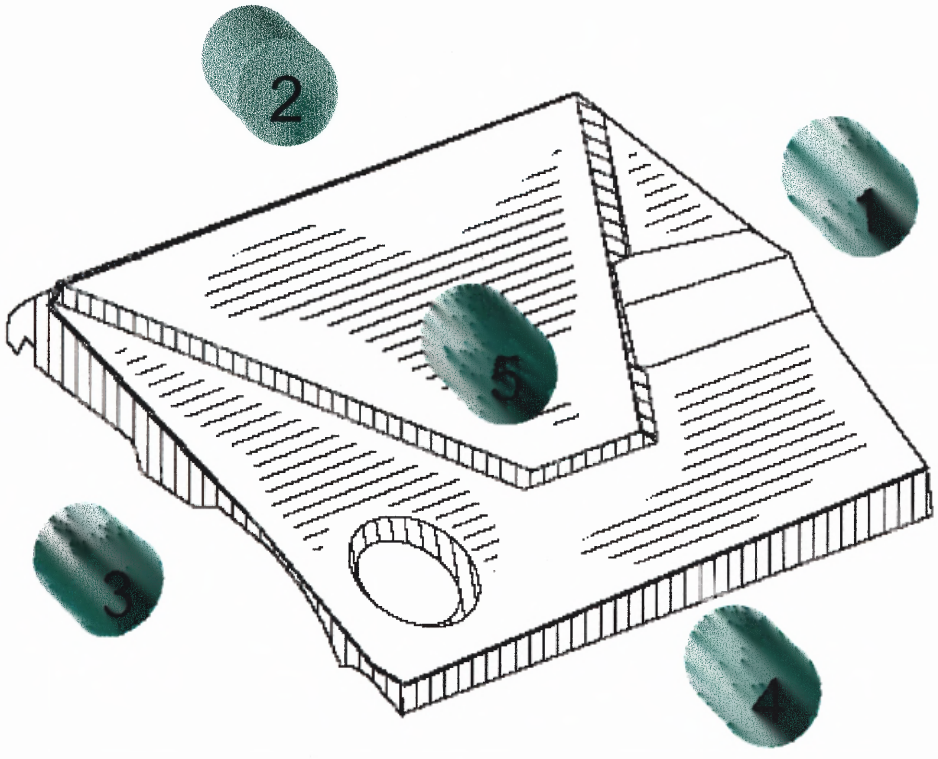

Figure 6.7 Engine cover molded from NVH material. Each microphone located 1m from the five surfaces: Top and 4 sides.

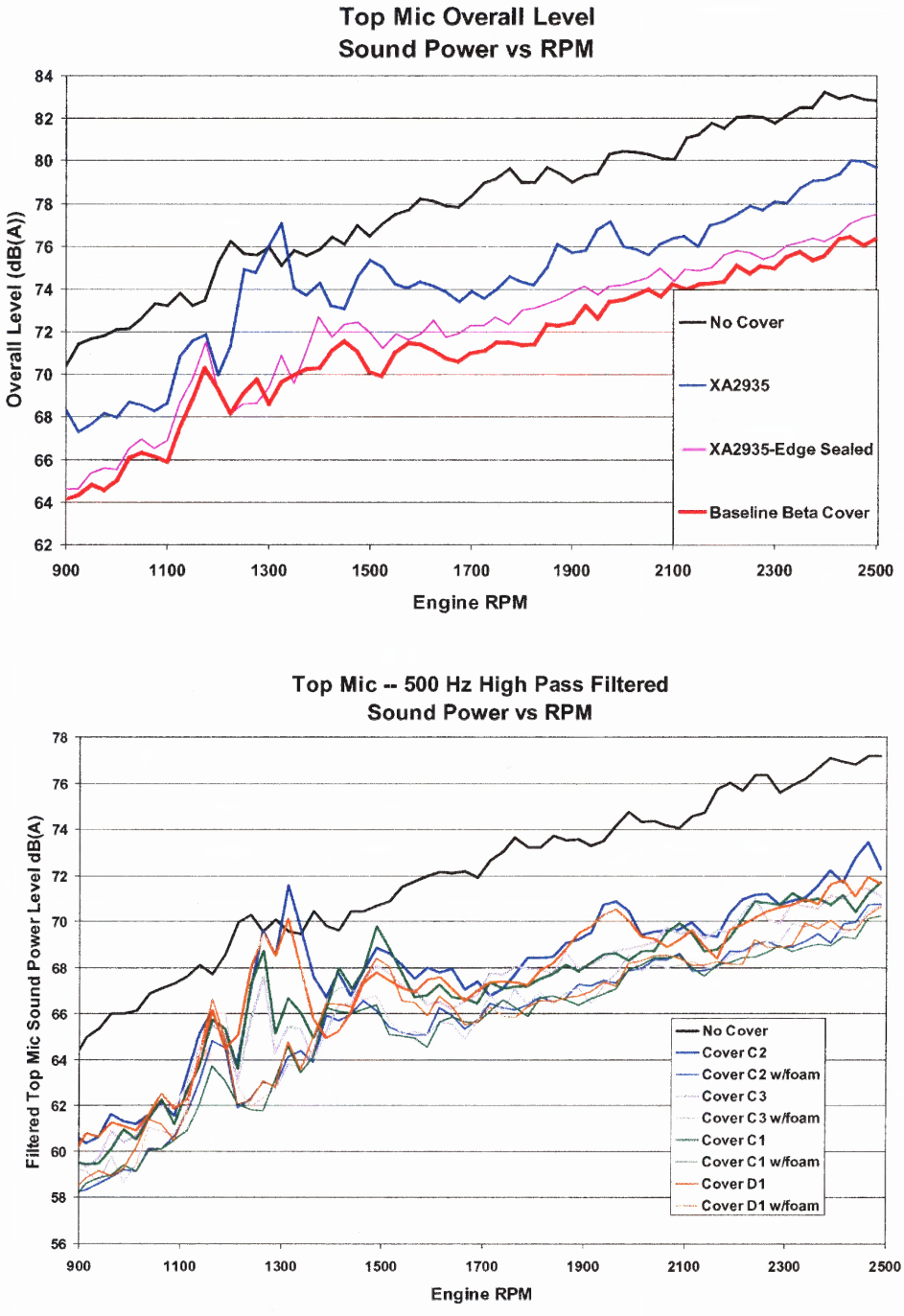

Figure 6.8 Overall sound level assessments. Four different configurations including sealed and non-sealed. NVH performance in open systems is highly sensitive to noise seal.

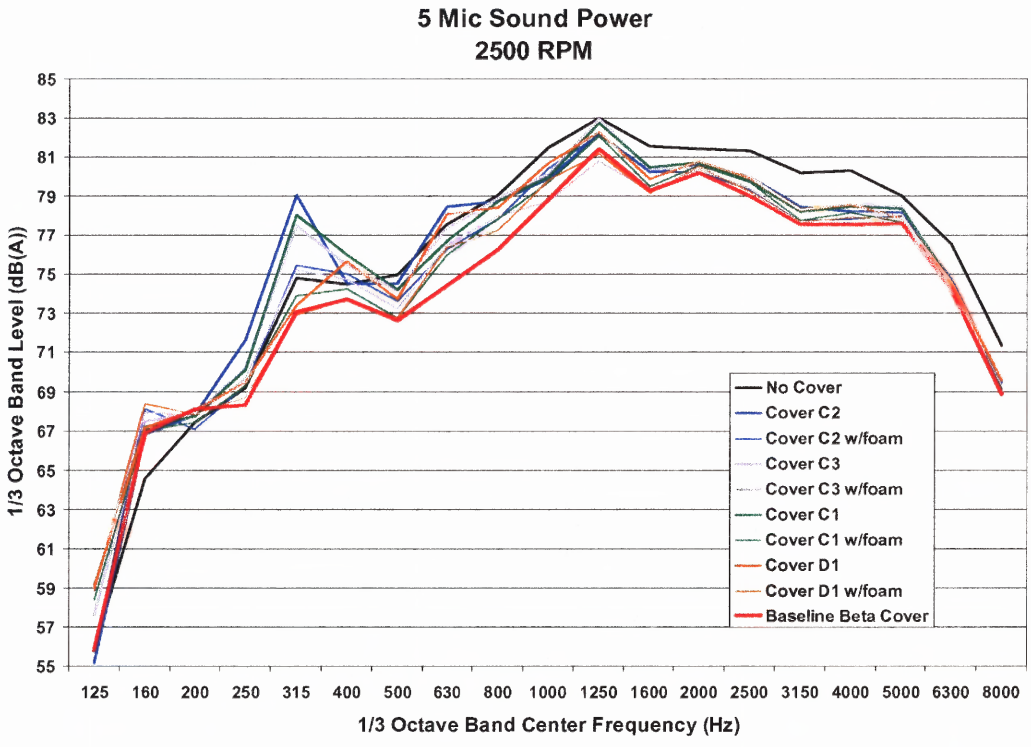

Figure 6.9 Sound power at 2500 engine rpm of four NVH material versions. No significant improvement due to flanking transmission.

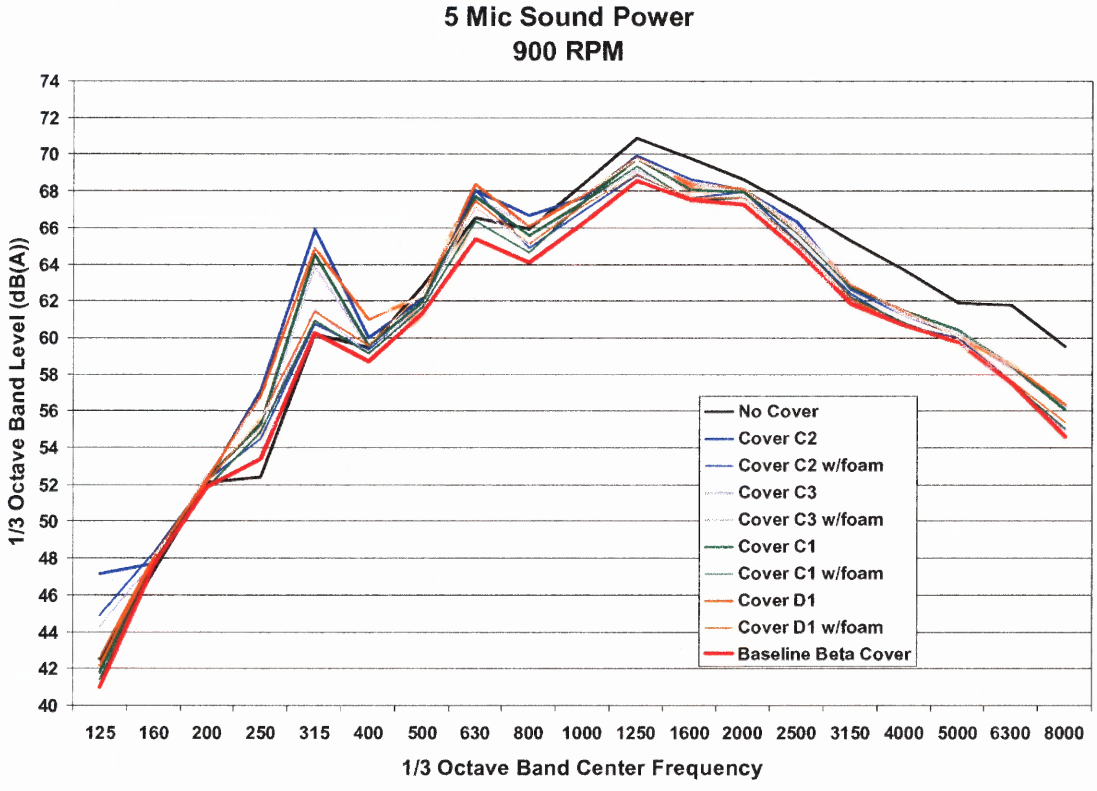

Figure 6.10 Sound power at 900 engine rpm of four NVH material versions. No significant improvement due to flanking transmission.

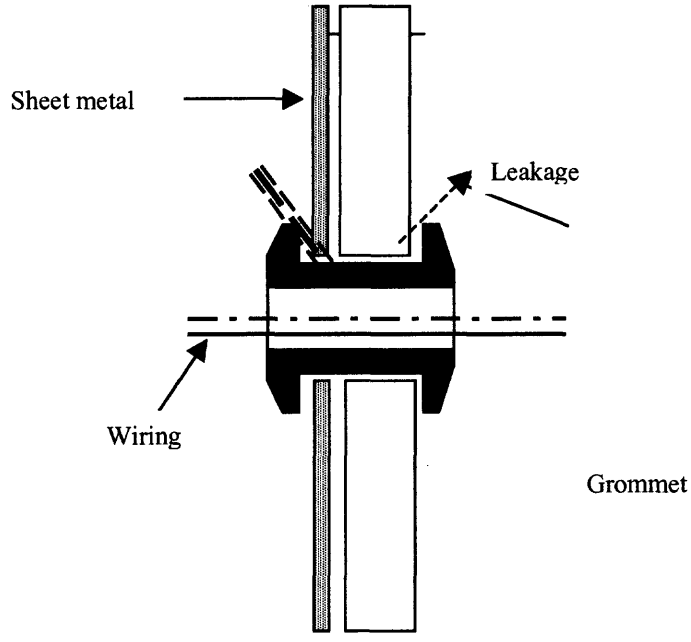

Figure 6.11 In vehicle system flanking transmission through duct and wiring opening and gaps reduce the STL capacity of the sound attenuating package (after ref. 29).

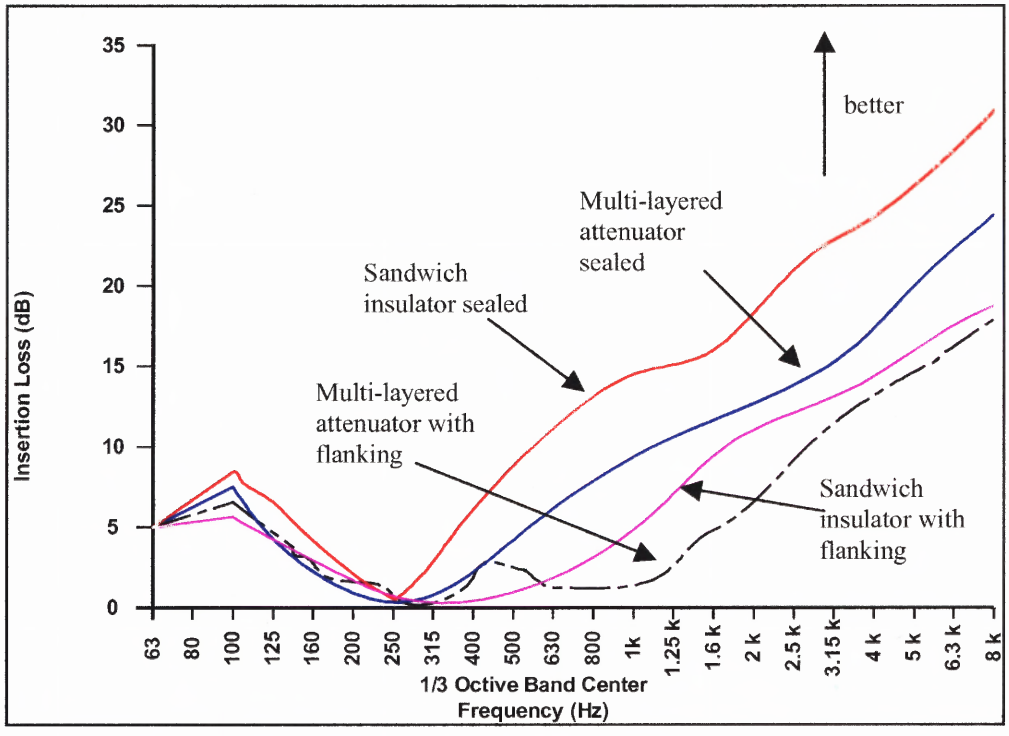

Figure 6.12 Effect of flanking conditions on insertion loss (after ref. 29).

6.3 Vehicle Air Intake Manifold Acoustics

6.3.1 Comparative Acoustic Evaluations of Various Resins

Noise Vibration and Harshness (NVH) has become an issue for vehicle manufacturers since the development of plastic underhood components, such as air intake manifolds. The noise problem has been augmented due to noise reduction legislation that has gained increasing momentum over the years [69].

The basic material used for such components directly impacts their acoustic behavior, especially when insulation of airborne noise and damping of structure borne noise is required. The inherent difference between plastic made components and their metal incumbent counterparts, stems from the fact that plastics compounds exhibit very different acoustic characteristics depending on the type of basic polymer and fillers [64]. A major characteristic of an NVH reduction material development is the continuous balance of influencing factors with each modification or step of improvement. The risk of spending effort on ineffective measures is high, and therefore validation efforts are critical.

This phase of the study aims at quantifying the relative performance of air intake manifolds molded from different materials including that of high STL characteristics. The construction of these manifolds represents the concepts elucidated in Chapter 3. Validation results of SPL testing, to investigate the effects of various composite intake manifold materials and constructions on vehicle noise are presented. The goal was to verify performance predictions, identified previously using analytical predictions, of an NVH material molded in a real component. The test vehicle was a 1995 Chevrolet Lumina with a 3100 V-6 engine. The baseline intake manifold was aluminum made. In

addition to the baseline manifold, five other configurations were tested. They were as follows:

- Standard Grade 33% GF Single Wall Manifold
- NVH Grade Single Wall Manifold
- Standard Grade 33% GF Double Wall Manifold
- NVH Grade Double Wall Manifold
- NVH Grade Isolated Wall Manifold

The objectives of the testing were to evaluate the effects of:

- Composite materials
- Welded double wall construction
- Isolated double wall construction

The bulk of the testing performed included SPL measurements at driver's ear and engine locations. The testing was conducted in a hemi-anechoic chamber. The vehicle's front wheels were set-up on rolls to allow them to spin under resistance simulating flat road conditions. The rear wheels were locked to level the vehicle. The vehicle exhaust was routed directly into the cell's ventilation system exhaust chamber via a flexible hose attached to the tailpipe.

In order to quantify small differences in noise radiated from the test samples, a special hood was made of 12.7mm thick high-density polyethylene (HDPE). The hood was constructed so that it fit closely over the engine compartment. It was sealed along the perimeter with foam and duct tape (see Figure 6.13). A hole was cut in the hood to expose the top surface of the intake manifold. This setup was effective at reducing noise contamination from other components within the engine space. Noise from these sources

that is radiated upward toward the hood is thus reflected downward. When the noise reaches the concrete floor of the cell, it is again reflected-up and toward the wall. When the noise reaches the wall it is absorbed.

Isolating noise from other engine components is important. Order and/or frequency analysis can adequately separate the measured noise into parts related to a particular engine order or frequency [70]. However, when the two phenomena occur at the same engine order, it is nearly impossible to further separate them into individual contributions with this type of testing. Intake noise always occurs at the same engine order as exhaust noise. In order to separate their contributions in this type of testing, it is essential to design the test setup so that the separation is accomplished experimentally. In other words, if exhaust noise is not desirable, it must be removed in location by manipulating the path that the exhaust noise takes to the microphone.

Figure 6.13 Hood construction to expose top surface of manifold.

Figure 6.14 Microphone position at driver's ear. Engine RPM was measured using an optical pickup that senses a strip of reflective tape stuck on the crankshaft pulley.

Noise measurements were made at three locations:

- Driver's right ear
- 1m directly above the manifold
- 1m from the manifold above and forward at a 45 degree angle

The microphones were hung loosely in position by their cords (see Figures 6.14 for driver's ear). A switch was installed to manually over-ride the radiator cooling fans. This was done to prevent the fans from switching on during the test. The data was acquired during sweeps from idle (750 RPM) to redline (5400 RPM). Stacking spectra estimated at intervals of 25 RPM created data for waterfall plots. The sweeps were done in first gear and lasted approximately 2 minutes. All measurements presented are the result of averaging 3 independent sweeps. This is done to reduce the variance in the measurements. All data is A-weighted to reflect subjective response [68].

6.3.2 Summary of Results

The data was processed in two ways. Order tracking was used to produce order spectra of constant engine order bandwidth, relating the measured sound to engine orders. Constant frequency waterfall analysis was used to produce spectra of constant frequency bandwidth at each RPM interval. The order-tracked data is essentially a subset of the constant frequency data. It allows much more detail about discrete tones related to engine phenomena. Overall levels and order slices are computed from the appropriate waterfall data. In this context, and to avoid repetitiveness, only the constant frequency data is presented.

Figures 6.15 to 6.21 contain the measurements made directly above the manifold. Figure 6.15 exhibits the overlaid overall level versus rpm for each manifold. The next six

figures contain waterfall data for the tested configurations. The waterfall figures are arranged so that single wall and double wall manifolds of the same material fall on the same page for easier comparison. Annotations are given on the plots explaining interesting features. Figure 6.22 summarizes overall data measured at the 45 degree location, and Figure 6.23 summarizes the data from the driver's ear.

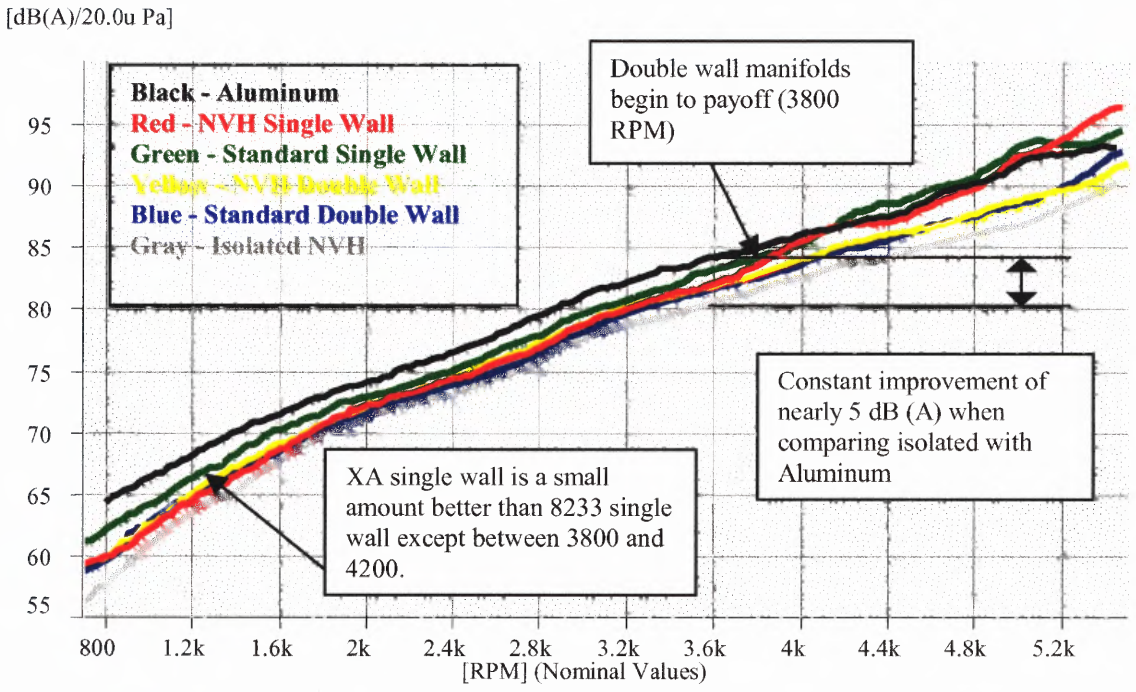

Figure 6.15 Overall level comparison – manifold

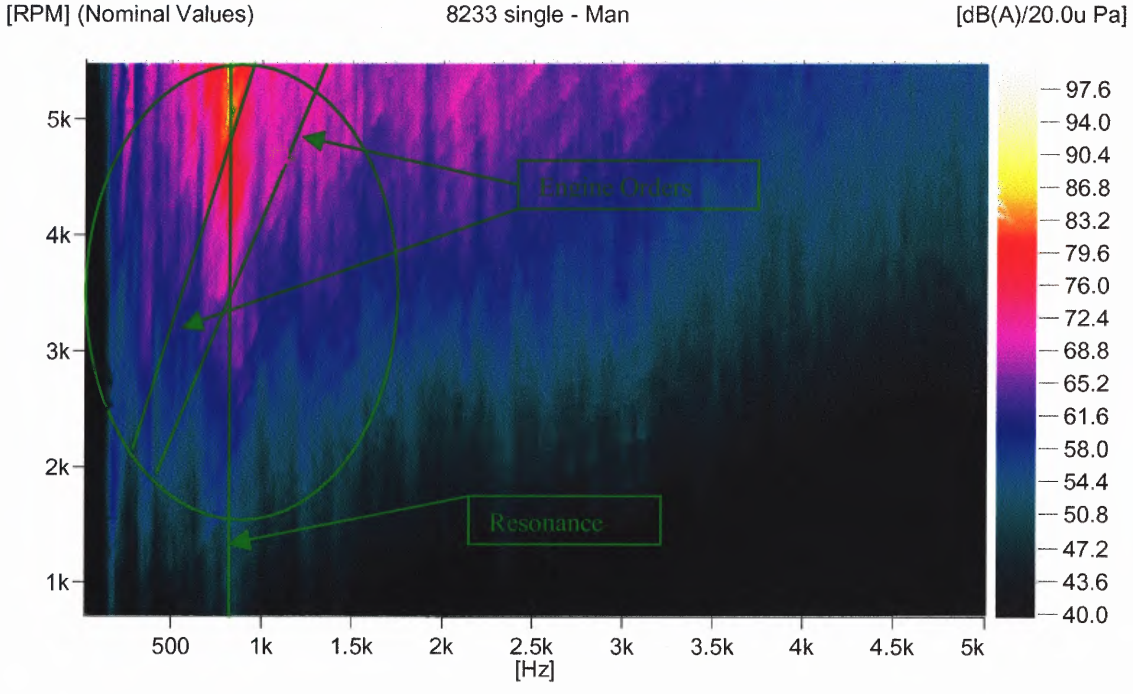

Figure 6.16 Standard material 33% GF single wall - manifold

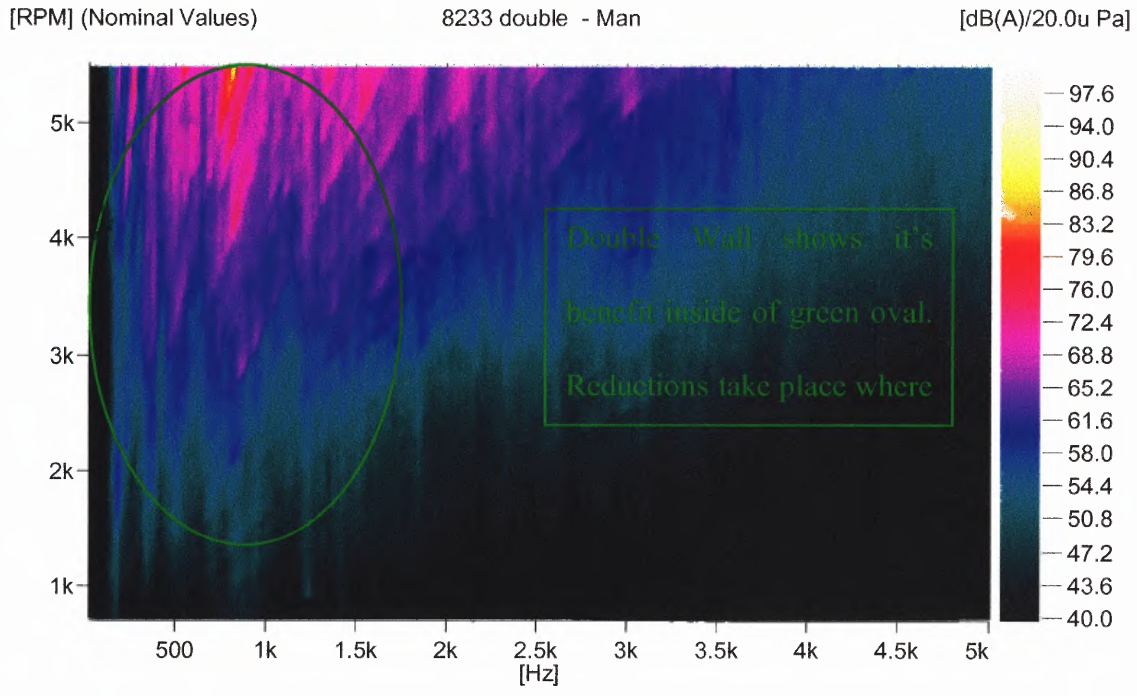

Figure 6.17 Standard material 33% GF double wall - manifold

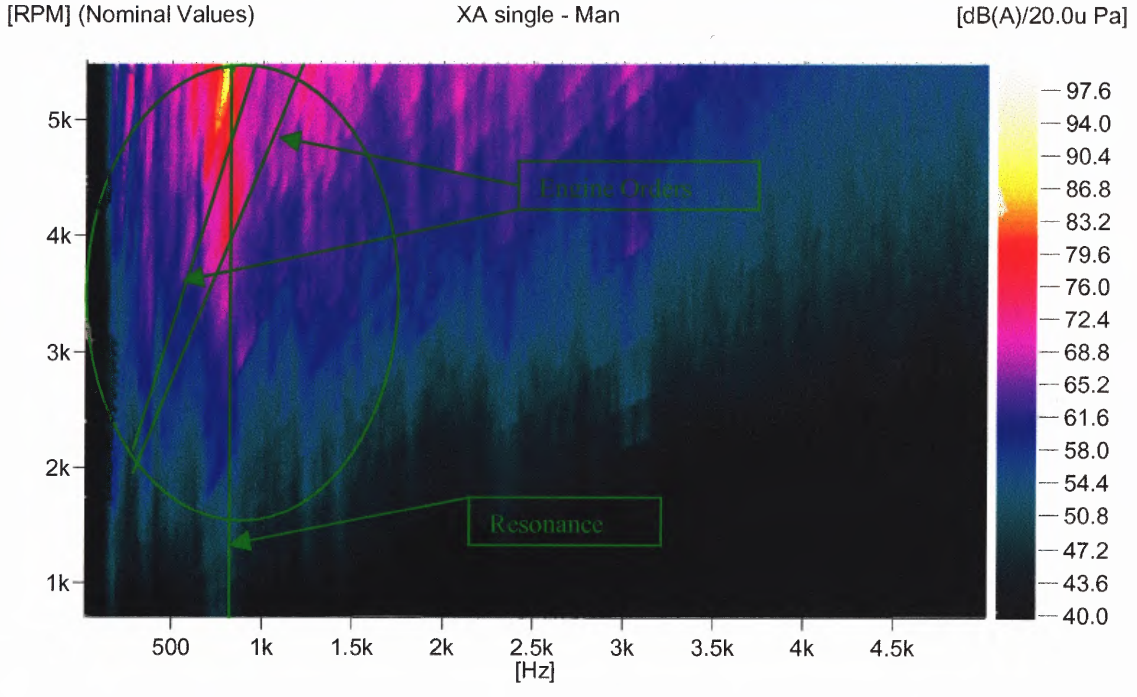

Figure 6.18 NVH material single wall - manifold

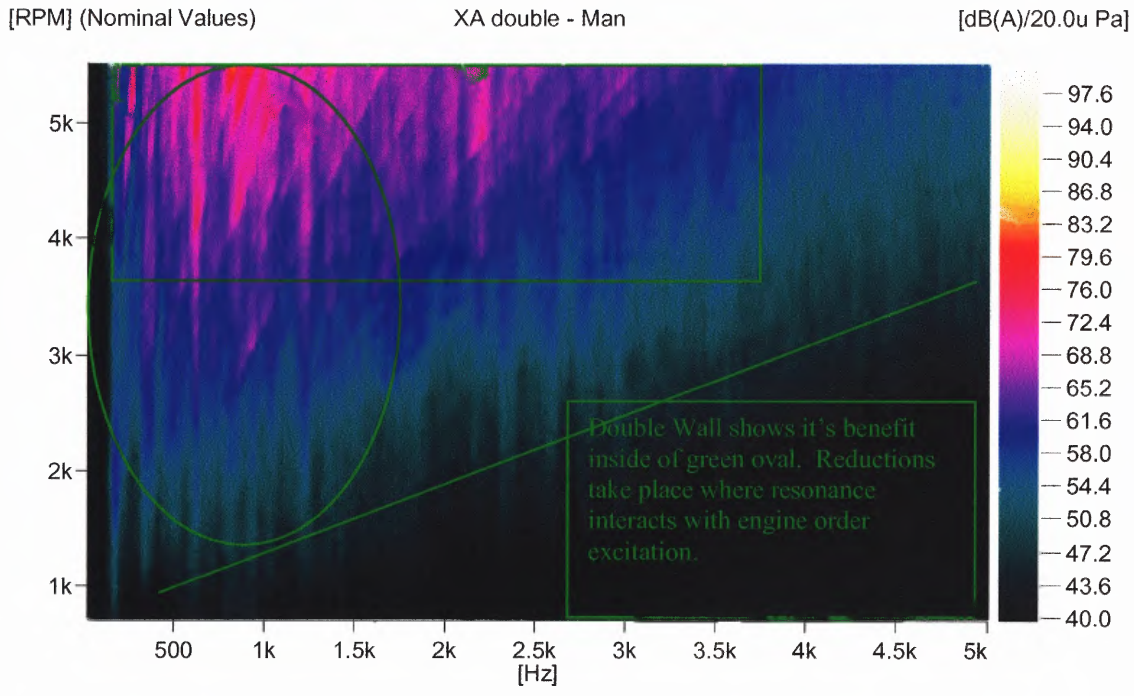

Figure 6.19 NVH material double wall - manifold

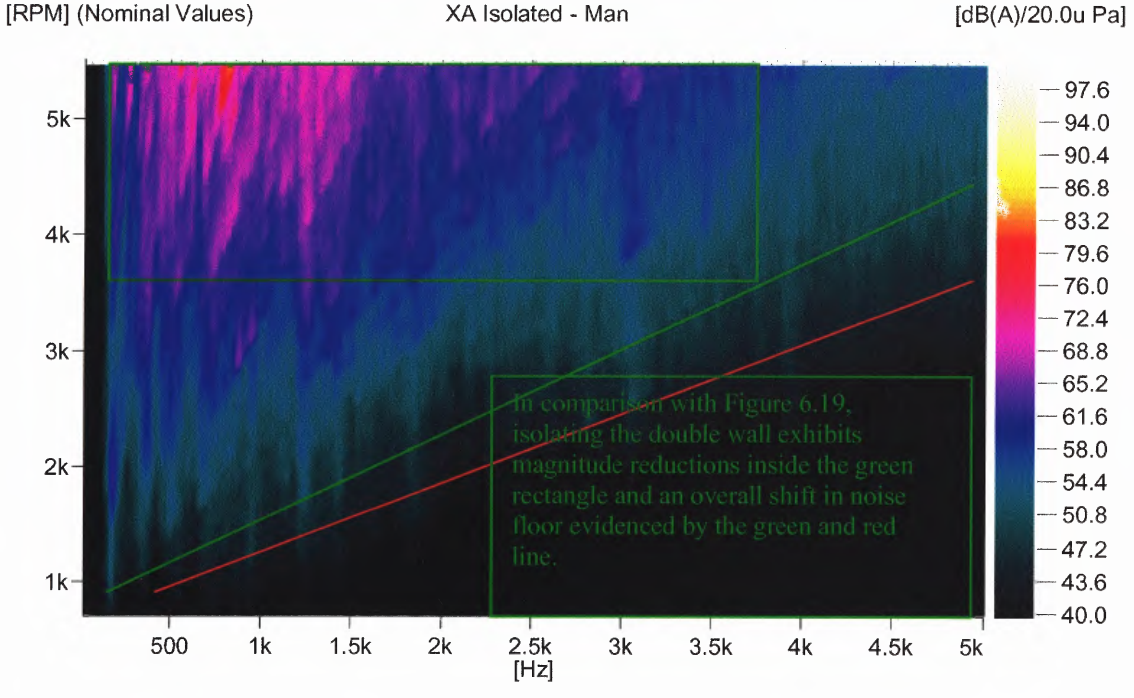

Figure 6.20 NVH isolated wall - manifold

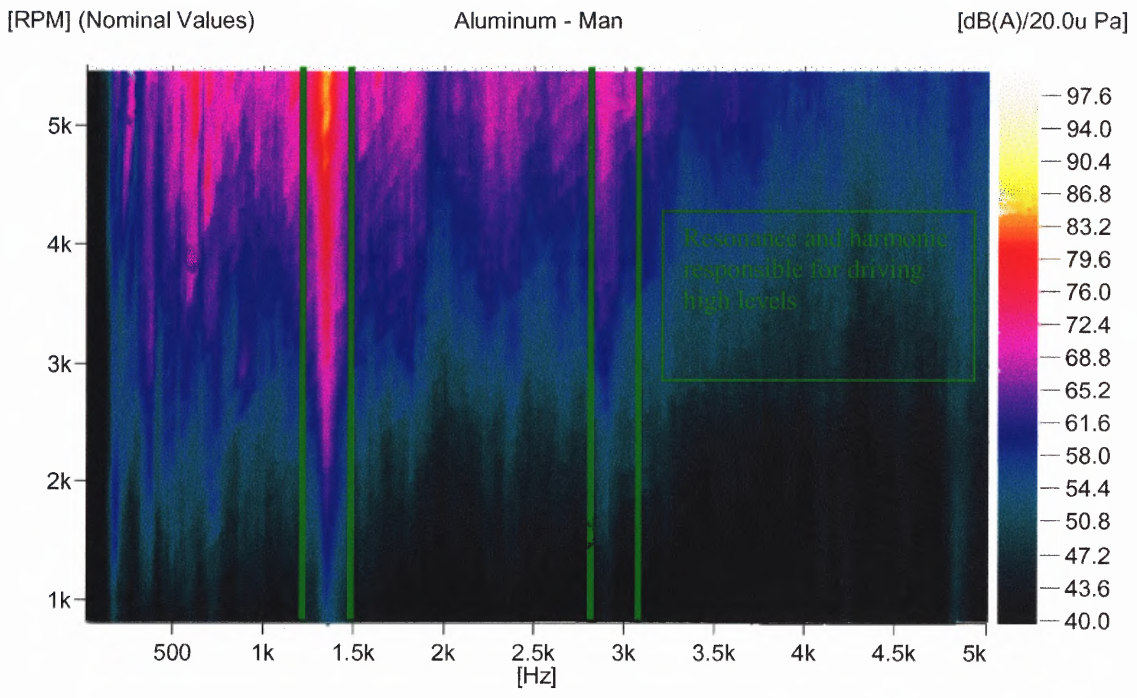

Figure 6.21 Aluminum – manifold

The significant points in the above measurements are as follows:

- The single wall manifold exhibits reductions when compared to the aluminum until about 3800 – 4000 RPM. The levels in the aluminum manifold are driven almost entirely by the strong resonance at 1300 Hz. The corresponding resonance in the single wall manifolds occurs at a lower frequency of about 700 Hz. The waterfall plots of Figures 6.16 and 6.18 show that the resonance in the single walls does not appear to be substantially excited below 3800 RPM. The reason for the reduction in the excitation of resonance, is due in part to the A weighting curve, which penalizes one level at 700 Hz by nearly an additional 2 dB when compared to another level at 1300 Hz.

- The single wall NVH outperforms the single wall standard, except from 3800 to 4200 Hz. This is where the dominant engine orders pass through a resonance of the single wall manifolds.
- All double wall manifolds show a drastic reduction in the dominant resonance compared to the single walls and the aluminum manifold. This is the reason that the double walls continue to show benefits at and above 3800 RPM.
- The isolated NVH double wall shows an overall reduction in levels. This is evident both at the forced frequencies, and in the noise floor.

For the sake of brevity, the data acquired at the microphone location 45 degrees over and in the front of the manifold will not be shown in its entirety. The data at 45 degrees shows the same information as that acquired directly over the manifold. However the reduction apparent at 45 degrees are not as drastic. This is due in most part to flanking from other sources. However, this demonstrates the effectiveness of the test setup in isolating noise from the manifold only.

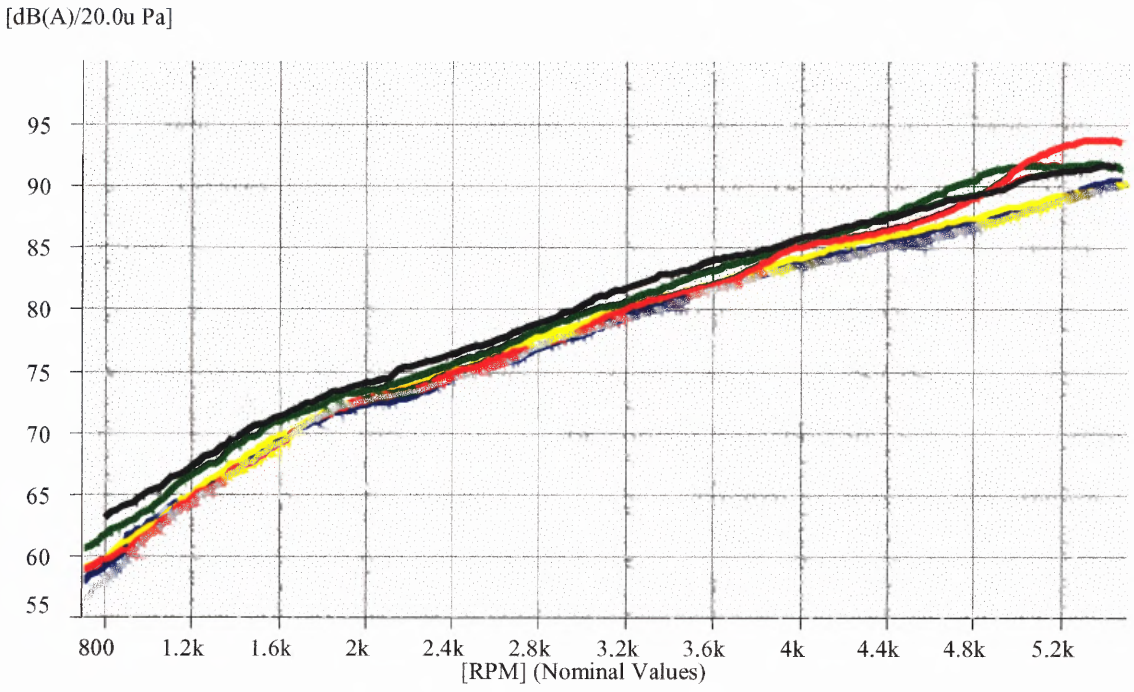

Figure 6.22 Overall level comparison – 45 degrees

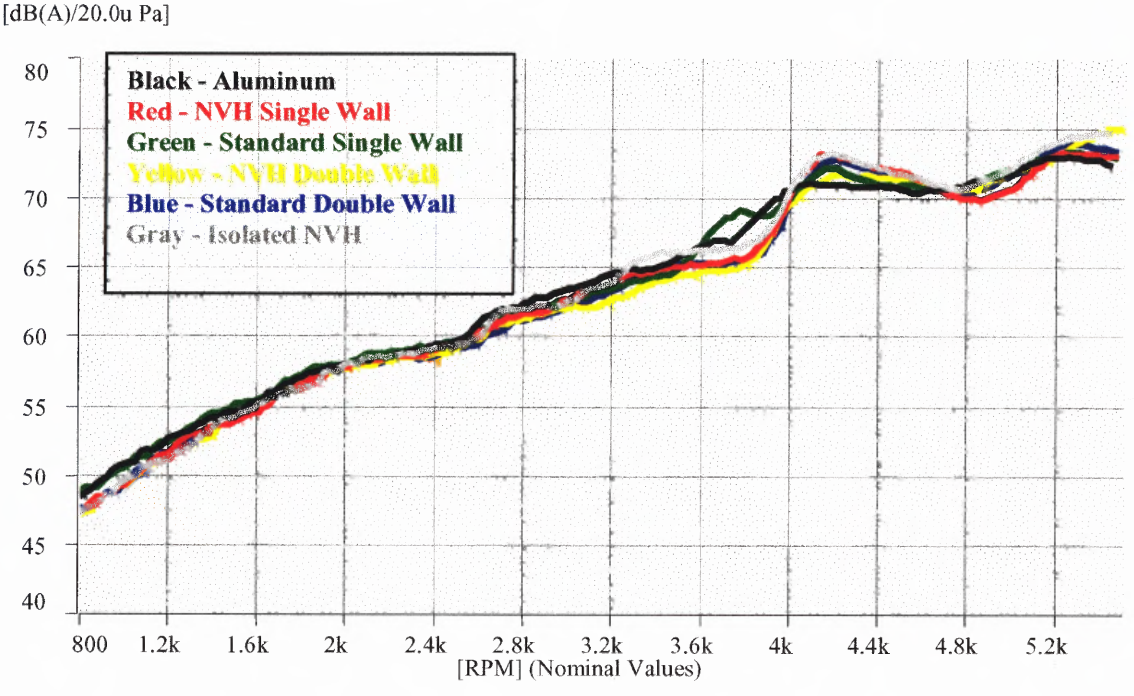

Figure 6.23 Overall level comparison - DRE

It was observed that the same physical phenomenon was driving the levels at the driver's ear. Again for the sake of brevity, only the overall levels are shown in Figure 6.23 above. Form this data; it was clear that the choice of manifold did not significantly influence the SPL at the driver's ear, except for one case. The aluminum manifold results in a definite reduction at the driver's ear.

6.3.3 Conclusion

The choice of material and construction of the manifold have a significant effect on the noise radiated from its top surface. The NVH material offers reduction in noise radiation when compared to the standard material in the single wall configuration. The standard material in the single wall configuration shows a reduction compared to the baseline aluminum manifold.

The NVH and standard materials show similar benefits in the double wall configuration. The double wall configuration virtually eliminates the dominant mode present in both single wall manifolds and aluminum manifold.

The isolated double wall manifold offers further reduction over the normal double wall construction due to an overall broadband reduction in noise. This offers insight into the importance of structural borne noise on the overall sound power of the manifold. Alterations to the manifolds are largely ineffective at reducing levels at the driver's ear in this testing configuration. A reduction in sound level is only accomplished when the contribution of a dominant source is reduced. Due to the large number of significant noise sources in a car, noise radiated by the intake manifold is considered non-dominant.

In a nutshell, the NVH material manifold shows reduction in the sound radiation level over the standard material and aluminum-based manifolds. This effect is consistent with the double wall configuration.

CHAPTER 7

GENERAL CONCLUSIONS

Acoustical characterization of polymer-based materials was presented for the steady state case of airborne sound transmission through infinite panels. It was shown that the acoustical characteristics of Nylon6 based resins could be evaluated using analytical sound transmission loss prediction techniques. This could be done best using flat panel or sheet geometry designated as barrier configurations in single and layered wall constructions. The infinite panel theory was assumed to simulate the finite case with theoretical manipulations. The formulation was presented for the classical infinite dimension case and was modified to approximate the finite size geometry within a diffuse sound field medium. A correlation weighting function was used in the calculation of the transmission coefficient for better approximation with measured data.

The layered panel case was assumed to be a special case of co-injection processed panels exhibiting fused layers at their interface. The sound transmission coefficient model for the layered case was formulated in terms of the impedance expressions for the latter specific configuration. The impinging sound wave was assumed to cause bending and extension deformations in the top and bottom layers, with lack of shear deformation in the core. The model devised for the single case was generalized to simulate the special case configuration sufficiently by adjusting the core density to represent a percentage of the skin layers' densities. This was done to represent the case in practice where chemical foaming agents are utilized during the co-injection process to vary the consistency of the core.

Analytically driven physical property determination for high STL established the link among properties at the macro and micro levels. Theoretical manipulation of factors affecting STL across the frequency range, could lead to an optimum set of parameters that would be backward integrated into the resin's matrix formulation stage.

An optimum noise control material was conceived with specific element variations to promote high STL capacity. Different levels of fillers and design configurations in-combination were also suggested for incremental performance. Patent protected concepts were recommended, as an option, for optimizing STL in the lower frequency regions. These included the use of distributed lumped masses in single layers, double layers with a range of air cavities thickness, and layered constructions with a variable percentage skin density in their core.

It was further suggested that computational techniques could be applied to analyze 3-D geometries and expand the theoretical validation, using the indirect baffled BEM approach or acoustic transparency techniques on simple and more complex shapes.

Employed sound transmission loss, sound intensity and sound radiation measurement techniques were described. NVH compounds were conceptualized into high sound transmission loss resin variations. Panels formed from these materials with balanced sets of properties were fabricated and used for validation. Theoretical predictions were confirmed. The noise reduction material showed measurable advantages in STL over standard materials. For layer and double wall configurations, it was observed that the double wall with air cavity exhibited positive results while the layered configuration with foamed cores did not offer a viable improvement. This confirmed the necessity to reduce voids within the cores in such constructions.

For the purpose of effective sound transmission reduction in vehicle environments, real components from simple to complex geometries were evaluated for sound transmission and sound radiation reduction. The performance of open systems such as engine covers is function of the level of flanking transmission during the measurement phase. The choice of materials and constructions of engine manifolds had a significant effect on the noise radiated from its top surface. The NVH material offered reduction in noise radiation when compared to the standard material in the single wall configuration. The NVH and standard materials showed similar benefits in the double wall configuration. However, the isolated double wall manifold offered further reduction over the normal double wall construction due to an overall broadband reduction in noise. This reinforced the importance of reducing flanking when acquiring measured data.

Based on the above, it was thus concluded that in practice, NVH criteria was achieved.

REFERENCES

1. L. Cremer, "Theorie der Shalldammung dunner Wande bei schragem Einfall," *Akustische Zeitschrift*, vol.7, pp. 81-102, 1942.

2. B. H. Sharp, "Prediction methods for the sound transmission of building elements," *Noise Cont. Engr.*, vol.11, pp. 53-63, 1978.

3. E. C. Sewell, "Transmission of reverberant sound through a single-leaf partition surrounded by an infinite rigid baffle," *J. Sound and Vib.*, vol.12, pp. 21-32, 1970.

4. Laboratory measurement of airborne sound insulation of building elements, *ISO 140-III,*USA, 1978.

5. R. E. Jones, "Field sound insulation of load-bearing sandwich panels for housing," *Noise Cont. Engr.*, vol.16, pp. 90-105, 1981.

6. L. E. Kinsler, A. R. Frey, A. P. Coppens, and J. V. Sanders, *Fundamentals of Acoustics*, John Wiley and Sons, New York, USA, 1982.

7. Determination of Sound Power Levels of Noise Sources Using Sound Intensity – Part 1: Measurement at Discrete Points, ISO 9614-1:1993 (E) Acoustics, *International Organization for Standardization*, Genève, Switzerland, 1993.

8. Y. T. Kim, H. C. Kim, S. S. Jung, M. J. Jho, and S. J. Suh, "Dependence of coincidence frequency in double-glazed window on glass thickness and interpane cavity," *Applied Acoustics*, vol. 63, pp. 927-936, 2002.

9. Laboratory measurement of the airborne sound barrier performance of automotive materials and assemblies, *SAE J1400*, May 1990.

10. Standard test method for the laboratory measurement of airborne sound transmission loss of building partitions, *American Society for Testing and Materials*, Philadelphia, PA, USA, ASTM E90-90, 1990.

11. J. R. Callister, A. R. George, and G. E. Freeman, "An empirical scheme to predict the sound transmission loss of single-thickness panels," *J. Sound and Vib.*, vol. 222(1), pp. 145-151, 1999.

12. F. Fahy, *Sound and Structural Vibration-Radiation, Transmission, and Response,* Academic Press In, pp. 143-163, 1994.

13. P. Saha, "Selection, Evaluation, and Measurements of Acoustical Materials for Vehicle Interior Noise Study," *SAE Professional Development Seminars Series*, pp. 103-109, 1997.

14. J. H. Kang, J. G. Ih, J. S. Kim, and H. S. Kim, "Prediction of sound transmission loss through multi-layered panels by using Gaussian distribution of directional incident energy," *J. Acoust. Soc. Am.*, vol.107(3), March 2000.

15. L. L. Beranek, *Noise Reduction*, McGraw-Hill, New York, USA, 1971.

16. J. Price, and M. J. Crocker, "Sound transmission through double panels using statistical energy analysism," *J. Acoust. Soc. Am.*, vol.47, pp. 683, 1970.

17. R. W. Guy, "The transmission of airborne sound through a finite panel, air gap, panel and cavity configuration – a steady state analysis," *Acoustica*, vol.49, pp. 323-333, 1981.

18. A. London, "Transmission of reverberant sound through double walls," *J. Acoust. Soc. Am.*, vol. 22, pp. 270-279, 1950.

19. K. A. Mulholland, H. D. Parbook, and A. Cummings, "The transmission loss of double panels," *J. Sound and Vib.*, vol. 6, pp. 324-334, 1967.

20. A. Cummings, and K. A. Mulholland, "The transmission loss of finite sized double panel in a random incidence sound field," *J. Sound and Vib.*, 8, 126-133, 1968.

21. L. E. Kinsler, A. R. Frey, A. B. Coppens, and J. V. Sanders, *Fundamentals of Acoustics*, J.Wiley and Sons, New York, USA, 1982.

22. A. D. Pierce, "Acoustics: An introduction to its physical principles and applications," *J. Acoust. Soc. Am.*, 1989.

23. A. D. Bruijn, "Influence of diffusivity on the transmission loss of a single-leaf wall," *J. Acoust. Soc. Am.*, vol. 47, pp. 667-675, 1970.

24. V. Hongisto, "Airborne sound insulation of wall structures – measurement and prediction methods," *Helsinki University of Technology, Laboratory of Acoustics and Audio Signal Processing*, Expo 2000, Report # 56.

25. J. S. Bolton, and Y. J. Kang, "Elastic porous materials for sound absorption and transmission control," *SAE, Noise & Vibration Conference Proceedings*, vol. 291, pp. 77-91, 1997.

26. A. J. B. Tadeu, and D. M. R. Mateus, "Sound transmission through single, double and triple glazing, Experimental evaluation," *Applied Acoustics*, vol. 62, pp. 307-325, 2001.

27. J. D. Quirt, "Sound transmission through windows I. single and double glazing," *J. Acoust. Soc. Am.*, vol. 72(3), pp. 834-844, 1982.

28. J. D. Quirt, "Sound transmission through windows II, Double and triple glazing," *J. Acoust. Soc. Am.*, vol. 74(2), pp. 534-542, August 1983.

29. R. E. Wentzel, and J. VanBuskirk, "A dissipative approach to vehicle sound abatement," Rieter Automotive North America, *Noise and Vibration Conference & Exposition*, Traverse City, MI, USA, Paper # 1999-01-1668, 1999.

30. R. E. Wentzel, and P. Saha, "Empirically predicting the sound transmission loss of double-wall sound barrier assemblies," *SAE Noise and Vibration Conference and Exposition*, Traverse City, MI, USA, Paper # 951268, 1995.

31. D. A. Welsh, and H. A. Evensen, "Vibrational and sound radiation properties of a double layered diesel engine gear cover," *SAE Noise and Vibration Conference Proceedings*, vol. 342, pp. 1-8, 1999.

32. A. H. Davis, "Reverberation equations for two adjacent rooms connected by an incompletely soundproof partition," *Phil. Mag.*, vol. 6(50), pp. 75-80, 1925.

33. E. Buckingham, "Theory and interpretation of experiments on the transmission of sound through partition walls," *Nat'l. Bur. Stand. Sci. Papers*, vol. 20, pp. 194-199, 1929.

34. A. London, "Tentative recommended practice for laboratory measurement of airborne-sound transmission loss of building floors and walls (ASTM E 90-50 Tentative)," *J. Acoust. Soc. Am.*, vol. 23, p. 686, 1951.

35. A. London, "Transmission of reverberant sound through double walls," *J. Res. Nat'l. Bur. Stand. (USA)*, vol. 44, pp. 77-88, 1959.

36. Testing of acoustics in buildings, Airborne and impact sound insulation, *Laboratory measurements of sound insulation of building elements*, DIN 52210, Part 3, 1987.

37. S. Gade, "Sound intensity – Part I: Theory," *Brüel & Kjaer Technical Review*, vol. 3, pp. 3-39, 1982.

38. J. A. Moore, "Sound transmission loss characteristics of three layer composite wall constructions," *Ph.D. thesis, Massachusetts Institute of Technology*, 1975.

39. R. E. Jones, "Intercomparisons of laboratory determinations of airborne sound transmission loss," J. Acoust. Soc. Am., vol. 66(1), pp. 148-164, July 1979.

40. O. V. Estorff, B. Tylkowski, and P. Scarth, "Sound radiation of two engine blocks by the BEM and the Rayleigh-Method," *2nd Worldwide SYSNOISE Users Meeting Proceedings*, III.4, Leuven, Belgium, 1995.

41. A. F. Seibert, "The BEM in acoustics – Physical insights and practical examples," *2nd Worldwide SYSNOISE Users Meeting Proceedings*, III.1, Leuven, Belgium, 1995.

42. N. Vlahopoulos, and S. T. Raveendra, "Formulation, implementation and validation of multiple connection and free edge constraints in an indirect boundary element formulation," *J. Sound and Vib.*, vol. 210(1), pp. 137-152, 1998.

43. S. T. Raveendra, N. Vlahopoulos, and A. Glaves, "An indirect boundary element formulation for multi-valued impedance simulation in structural acoustics," *Appl. Math. Modeling*, vol. 22, pp. 379-393, 1998.

44. J. P. Coyette, and K. R. Fyfe, "Solution of elasto-acoustic problems using a variational finite element/boundary element technique, *Numerical Techniques in Acoustic Radiation, Proceedings of Winter Annual Meeting of the ASME*, San Francisco, CA, USA, pp. 15-25, 1989.

45. C. Vallance, and N. Vlahopoulos, "The Prediction of Structural Noise Induced Vibration," *Sound and Vibration*, April 1996.

46. D. C. Smith, "Noise control design of vibrating structures using the boundary element Method," *Ms. Thesis, Purdue University*, 1988.

47. J. P. Coyette, "The use of finite element and boundary element models for predicting the vibro-acoustic behavior of layered structures," *Numerical Integration Technologies*, Ambachtenlaan 11a, B-3001, Leuven, Belgium, 1997.

48. J. P. Coyette, and J. L. Migeot, "An overview of boundary element approaches for acoustic modeling," *Internoise Conference Proceedings*, Leuven, Belgium, 1993.

49. *LMS/SYSNOISE Users' Manual*, Rev 5.3, LMS International, 1997.

50. A. F. Seybert, B. Soenarco, F. J. Rizzo, D. J. Shippy, "Application of the BIE method to sound radiation problem using an isoparametric element," *J. of Vib., Acoust., Stress, Reliab. Design*, vol. 106, pp. 414-419, 1984.

51. M. A. Biot, "Theory of propagation of elastic wave in a fluid-filled saturated porous solid I: Low frequency range; and II: Higher frequency range," *J. Acoust. Soc. Am.*, vol. 28, pp. 161-191, 1956.

52. M. A. Biot, "Generalized theory of acoustic propagation in porous dissipative media," *J. Acoust. Soc. Am.*, vol. 34, pp. 1254-1264, 1962.

53. S. T. Raveendra, S. Sureshkumar, and K. L. Hong, "Computational modeling of noise control materials," *Internoise Conference Proceedings*, Dearborn, MI, USA, Paper # 428, 2002.

54. K. Hong, M. VanRuiten, and S. T. Raveendra, "Computation of transmission loss and absorption coefficient of multi-layer absorbers with perforated facing," *Internoise Conference Proceedings*, Dearborn, MI, USA, Paper # N425, 2002.

55. Z. Zhang, and S. T. Raveendra, "Eigenfrequency extraction based on boundary element method," *Internoise Conference Proceedings*, Dearborn, MI, USA, Paper # N427, 2002.

56. C. F. McCulloch, L. Cremers, and P. Guisset, "Predictive models of transmission loss of panels with multi-layer treatment," *LMS Int.*, Pub. # 4.02/2094/A201, 01.00.

57. R. P. Shaw, and P. Bugl, "Transmission of plane waves through layered linear visco-elastic media," *J. Acoust. Soc. Am.*, vol. 46, pp. 649-654, 1969.

58. L. M. Brekhovskikh, *Waves in layered media*, Academic, New York, 1960.

59. J. Tillery, M. L. Szary, and M. Noras, "Maximize sound transmission loss through double wall system with optimized coupling," *SAE Noise & Vibration Conference and Exposition Proceedings*, vol. 309, pp. 127-130, 1997.

60. A. J. Pretlove, "Forced vibrations of a rectangular panel backed by a closed rectangular cavity," *J. Sound and Vib.*, vol. 3(3), pp. 252-261, 1966.

61. H. Y. Lai, S. Katragadda, J. Stuart-Bolton, and J. Alexander, "Layered fibrous treatments for sound absorption and sound transmission," *SAE Noise & Vibration Conference Proceedings*, vol. 309, pp. 1553-1560, 1997.

62. E. Homsi, "Acoustic characterization and optimization of sound transmission loss in polymer-based materials," *Internoise Conference Proceedings*, Dearborn, MI, USA, 2002, Paper # N418.

63. J. G. Ih, and J. H. Lee, "A prediction method for the sound transmission loss of finite double partitions at low-frequencies," *Internoise Conference Proceedings*, The Hague, The Netherlands, 2001.

64. A. Wolf, and E. Portal, "Requirements to noise reduction concepts and parts in future engine compartments," *SAE Conference Proceedings*, vol. SP 1515, pp. 7-12, , 2000.

65. A. Wolf, and N. Cvjeticanin, "Plastic component solutions for sound insulation and noise reduction in the engine compartment," *ASK Bauteileforum*, Spitzingsee, Germany, 1998.

66. J. A. Moore, and R. H. Lyon, "Sound transmission loss characteristics of sandwich panel constructions," *J. Acoust. Soc. Am.*, vol. 89(2), pp. 777-791, 1991.

67. Francis H.K. Chen, "The Challenges of Analytical Noise Prediction in the Automotive Industry," *Third Worldwide SYSNOISE Users' Conference Proceedings*, Troy, MI 1996.

68. K. Wyckaert, and H. Van der Auweraer, *Sound Quality: Perception, Analysis and Engineering*, LMS International Interleuvenlaan 68, 3001 Heverlee - Belgium.

69. W. W. Kraft, "Noise Attenuation for Polyamide Intake Manifold," *SAE Conference Proceedings*, Paper # 950232, Detroit, MI, 1995.

70. D. E. Winterborne, and R. J. Pearson, *Wave Action Methods for IC Engines*, Chapter 5, Society of Automotive Engineers, Inc., ISBN: 0-7680-0482-9, 1999.

71. E. Homsi, C. Lee, K. Hu, "Acoustic modeling and radiated noise prediction for plastic air-intake manifold," *SAE Noise and Vibration Conference Proceedings*, vol. 1, pp. 711-714, 2003.

72. Brüel and Kjær, *Noise Control-Principles and Practice*, Research Studies Press LTD, page 104, 1986.

73. L. E. Kinsler, A. R. Frey, A. B. Coppens, and J. V. Sanders, *Fundamental of Acoustics*, 3rd Edition, John Wiley & Sons, USA, pp. 110-111, 1982.

74. J. M. Crocker, and F. M. Kessler, *Noise and noise control*, vol. II. Boca Raton (FL): CRC Press, 1982.